9 The Crystal Chemistry of Beryllium

Frank C. Hawthorne and Danielle M.C. Huminicki

Department of Geological Sciences
University of Manitoba,
Winnipeg, Manitoba, Canada R3T 2N2
frank_hawthorne@umanitoba.ca

INTRODUCTION

Beryllium is not a very abundant element in the Earth, but, being an incompatible element in common rock-forming silicate minerals, it is susceptible to concentration *via* fractionation in geochemical processes. Moreover, its properties are such that Be does not tend to show extensive solid-solution with other elements, and hence usually forms minerals in which it is a discrete and essential constituent. Beryllium (atomic number 4) has the ground-state electronic structure [He]$2s^2$ and is the first of the group IIA elements of the periodic table (Be, Mg, Ca, Sr, Ba, Ra). The first (899 kJ/mol) and second (1757 kJ/mol) ionization enthalpies are sufficiently high that the total energy required to produce the Be^{2+} ion is greater than the compensating energy of the resulting ionic solid, even when the latter involves extremely electronegative elements. Hence bond formation involves covalent (rather than ionic) mechanisms. However, Be has only two electrons to contribute to covalent bonding involving four orbitals (s, p_x, p_y, p_z), resulting in Be being a strong Lewis acid (i.e., a strong electron-pair acceptor) with a high affinity for oxygen. The cation radius of Be^{2+} is 0.27 Å, (Shannon 1976) and Be is known only in tetrahedral coordination in minerals, although BeO_3 groups are known in synthetic compounds (e.g., $Ca_{12}Be_{18}O_{29}$, Y_2BeO_4 and $SrBe_3O_4$; Harris and Yakel 1966, 1967, 1969). The BeO_4 and SiO_4 groups have a marked tendency to polymerize in the solid state. Although $^{[4]}$Be (r = 0.27 Å) and $^{[4]}$Si (r = 0.26 Å) are very similar in size, solid solution between Be and Si is inhibited by the difference in formal charge of the two species (Be^{2+} vs. Si^{4+}).

CHEMICAL BONDING

We adopt a pragmatic approach to chemical bonding, using bond-valence theory (Brown 1981) and its developments (Hawthorne 1985, 1994, 1997) to consider structure topology and hierarchical classification of structure. We will use molecular-orbital theory to consider aspects of structural energetics, stereochemistry and spectroscopy of beryllium minerals. These approaches are not incompatible, as bond-valence theory can be considered as a simple form of molecular-orbital theory (Burdett and Hawthorne 1993; Hawthorne 1994).

STEREOCHEMISTRY OF $Be\varphi_4$ POLYHEDRA IN MINERALS

The variation of Be-φ (φ: O^{2-}, OH^-) distances and φ-Be-φ angles is of great interest for several reasons:

(1) mean bond-length and empirical cation and anion radii play a very important role in systematizing chemical and physical properties of crystals;

(2) variations in individual bond-lengths give insight into the stereochemical behavior of structures, particularly with regard to the factors affecting structure stability;

(3) there is a range of stereochemical variation beyond which a specific oxyanion or cation-coordination polyhedron is not stable; it is obviously of use to know this range, both for assessing the stability of hypothetical structures (calculated by DLS [Distance Least-Squares] refinement, Dempsey and Strens 1976; Baur 1977) and for assessing the accuracy of experimentally determined structures.

1529-6466/02/0050-0009$10.00 DOI:10.2138/rmg.2002.50.9

Here, we examine the variation in Be- φ distances in minerals and review previous work on polyhedral distortions in $Be\varphi_4$ tetrahedra. Data for 89 $Be\varphi_4$ tetrahedra were taken from 58 refined crystal structures with $R \leq 6.5\%$ and standard deviations of ≤0.005 Å on Be–φ bond-lengths; structural references are given in Appendix A.

Variation in <Be - φ> distances

The variation in <Be-φ> distances (< > denotes a mean value; in this case, of Be in tetrahedral coordination) is shown in Figure 1a. The grand <Be-φ> distance (i.e., the mean value of the <Be-φ> distances) is 1.633 Å, the minimum and maximum <Be-φ> distances are 1.598 and 1.661 Å, respectively (the 4 or more smallest and 2 or 3 largest values in Fig. 1a are considered unreliable), and the range of variation is 0.063 Å. Shannon (1976) lists the radius of $^{[4]}Be$ as 0.27 Å; assuming a mean anion-coordination number of 3.25 and taking the appropriate O/OH ratio, the sum of the constituent radii is 0.27 + 1.360 = 1.63 Å, in accord with the grand <Be-φ> distance of 1.633 Å. Brown and Shannon (1973) showed that variation in <M-O> distance correlates with bond-length distortion Δ (= Σ[l(o) - l(m)]/l(m); l(o) = observed bond-length, l(m) = mean bond-length) when the bond-valence curve of the constituent species shows a strong curvature, and when the range of distortion is large. There is no significant correlation between <Be-φ> and Δ; this is in accord with the bond-valence curve for Be-O given by Brown (1981).

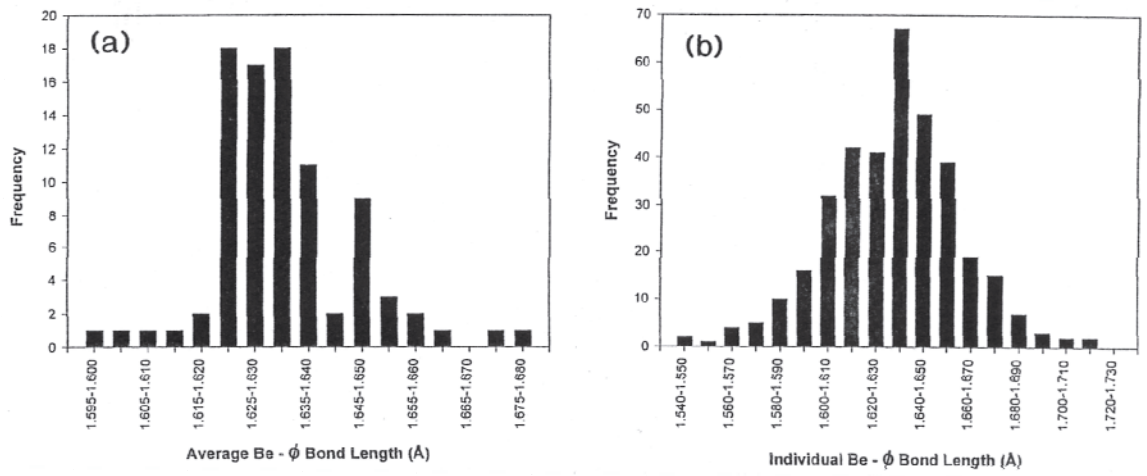

Figure 1. (a) Variation in average Be-O distance in minerals containing $Be\varphi_4$ tetrahedra; (b) variation in individual Be-O distance in minerals containing $Be\varphi_4$ tetrahedra.

Variation in Be - φ distances

The variation in individual Be-φ distances is shown in Figure 1b; the grand mean Be-φ distance is 1.633 Å. The minimum and maximum observed Be-φ distances are 1.545 and 1.714 Å, respectively, and the range of variation is 0.169 Å; the distribution is a skewed Gaussian. According to the bond-valence curve for Be (the universal curve for first-row elements) from Brown (1981), the range of variation in Be-φ bond-valence is 0.63-0.41 vu (valence units).

General polyhedral distortion in Be-bearing minerals

There is no general correlation between <Be-φ> and bond-length distortion. However, as pointed out by Griffen and Ribbe (1979), there are two ways in which polyhedra may distort (i.e., depart from their holosymmetric geometry): (1) the central cation may displace from its central position [bond-length distortion]; (2) the anions may displace from their ideal positions [edge-length distortion]; Griffen and Ribbe (1979) designate these two descriptions as BLDP (Bond-Length Distortion Parameter) and ELDP (Edge-Length

Distortion Parameter), respectively. Figure 2 shows the variation in both these parameters for the second-, third- and fourth-period (non-transition) elements in tetrahedral coordination. Some very general features of interest (Griffen and Ribbe 1979) are apparent from Figure 2:

(1) A BLDP value of zero only occurs for an ELDP value of zero; presuming that ELDP is a measure also of the O-T-O angle variation, this is in accord with the idea that variation in orbital hybridization (associated with variation in O-T-O angles) must accompany variation in bond-length.

(2) Large values of BLDP are associated with small values of ELDP, and vice versa. The variation in mean ELDP correlates very strongly with the grand mean tetrahedral-edge length for each period (Fig. 3).

Griffen and Ribbe (1979) suggested that the smaller the tetrahedrally coordinated cation, the more the tetrahedron of anions resists edge-length distortion because the anions are in contact, whereas the intrinsic size of the interstice is larger than the cation which can easily vary its cation-oxygen distances by 'rattling' within the tetrahedron.

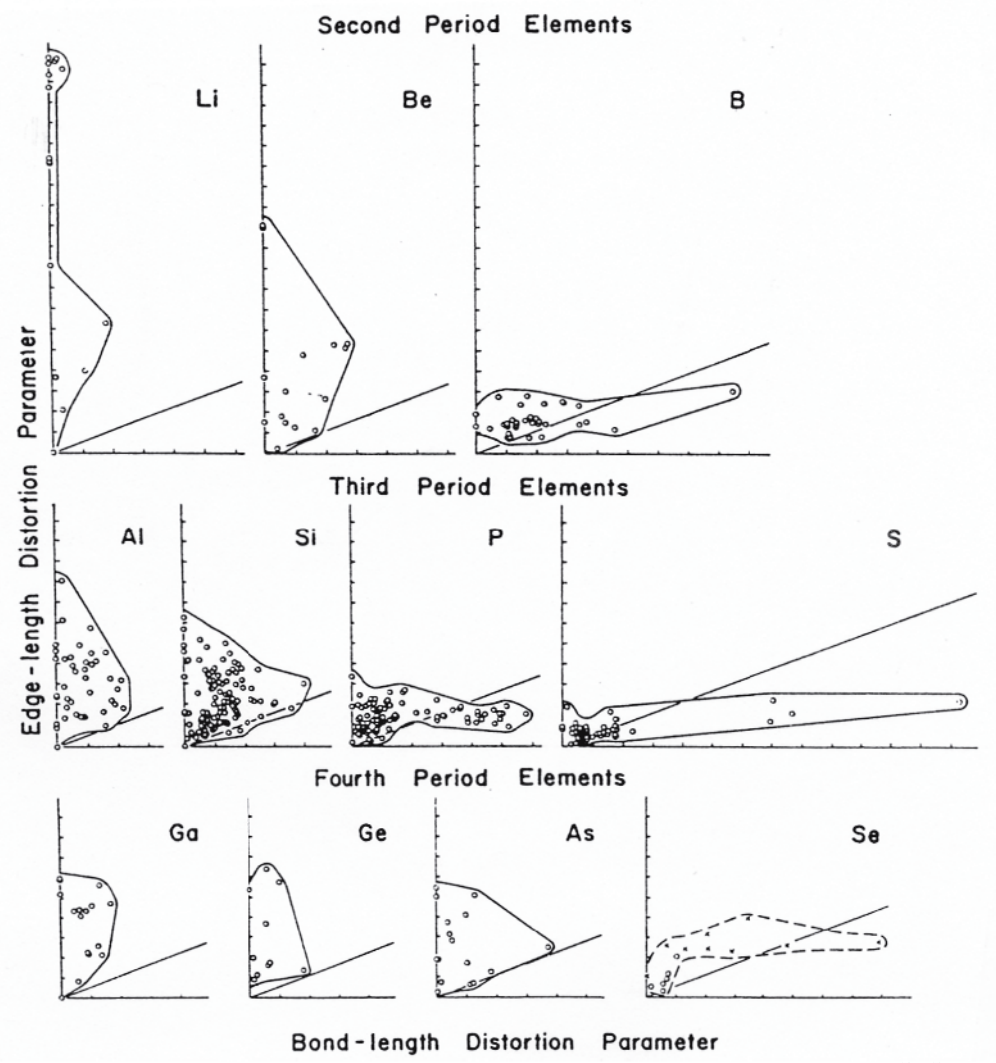

Figure 2. Variation in BLDP (Bond-Length Distortion Parameter) and ELDP (Edge-Length Distortion Parameter) for second-, third- and fourth-period non-transition elements in tetrahedral coordination by oxygen; after Griffen and Ribbe (1979).

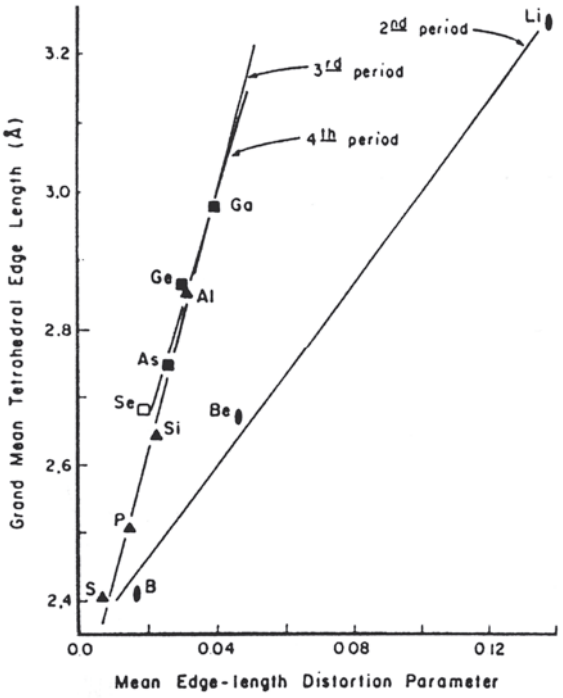

Figure 3. Variation in grand mean tetrahedral edge-length with mean ELDP for the second-, third- and fourth-period elements of the periodic table; after Griffen and Ribbe (1979).

MOLECULAR-ORBITAL STUDIES OF Beφ$_4$ POLYHEDRA

Molecular-orbital (MO) calculations have been used by theoretical chemists for many years, primarily to predict geometries, energetics and stabilities of molecules. MO methods are based on quantum mechanics, and range from empirical and semi-empirical methods, which include an experimentally determined component, to *ab-initio* methods, which include no experimentally determined parameters (see Tossell and Vaughan (1992) for an excellent summary of these methods). MO methods have been applied to the study of small molecules with considerable success, and available computational sophistication and power have permitted their application to mineralogically relevant problems for the past two decades (Gibbs 1982).

Beryllium-oxygen structures have been the topic of a small number of MO calculations, and are ideal in this regard due to the relatively small number of electrons involved in a BeO4 polyhedron. To date, most MO calculations for these structures have been done using molecular clusters which are designed to be an approximation of local conditions within a crystal structure. These clusters are only an approximation of the *local* environment in a structure, and many long-range effects in a periodic structure are ignored by such calculations. The first MO calculations for Be structures involved *ab-initio* MO methods applied to small clusters that modeled both individual Bej 4 polyhedra and larger clusters, allowing the study of such structural aspects as Be-O-Si bond-angles. The most rigorous approach is an *ab-initio* periodic Hartree-Fock MO calculation that includes the entire crystal structure (with appropriate boundary conditions). These calculations are computationally very demanding, and have been restricted to a small number of minerals; crystal *ab-initio* MO calculations have been done for BeO, the synthetic analogue of bromellite (Lichanot et al. 1992, Lichanot and Rerat 1993). MO calculations have provided the energetics and geometries of clusters, have given insight into the Be-O chemical bond, the molecular-orbital structures of BeO4 polyhedra, and have contributed significantly to the interpretation of various spectra of Be minerals.

Prediction of equilibrium geometries

MO calculations have often been used as an aid in understanding the geometry of Beφ$_4$

polyhedra, and MO arguments have frequently been used in explaining observed stereochemical variations in minerals.

Beφ4 groups. Schlenker et al. (1978) examined the geometry of bond-bending and bond-stretching in BeO_4^{6-} clusters using extended-Hückel calculations. Molecular-orbital theory predicts that the bond-overlap population for a $^{[4]}$T-O bond should be related to $\langle O\text{-}T\text{-}O\rangle_3$, the average of the three O-T-O angles involving the bond. Figure 4a shows the variation in bond-overlap population with the average of the O-T-O angles common to the bond for the BeO^{6-}_4 groups, calculated for a series of idealized polyhedra with C_{2v} and C_{3v} point symmetries. This suggests that the Be-O bond-lengths should be inversely related to $\langle O\text{-}^{[N]}Be\text{-}O\rangle_{N-1}$, and Figure 4b shows that this is the case. There is more scatter in the trend of Figure 4b than is present in the results of the calculations in Figure 4a; however, the latter data are derived from molecules, whereas the observed stereochemical data come from crystal structures in which the polyhedra are in various strained configurations.

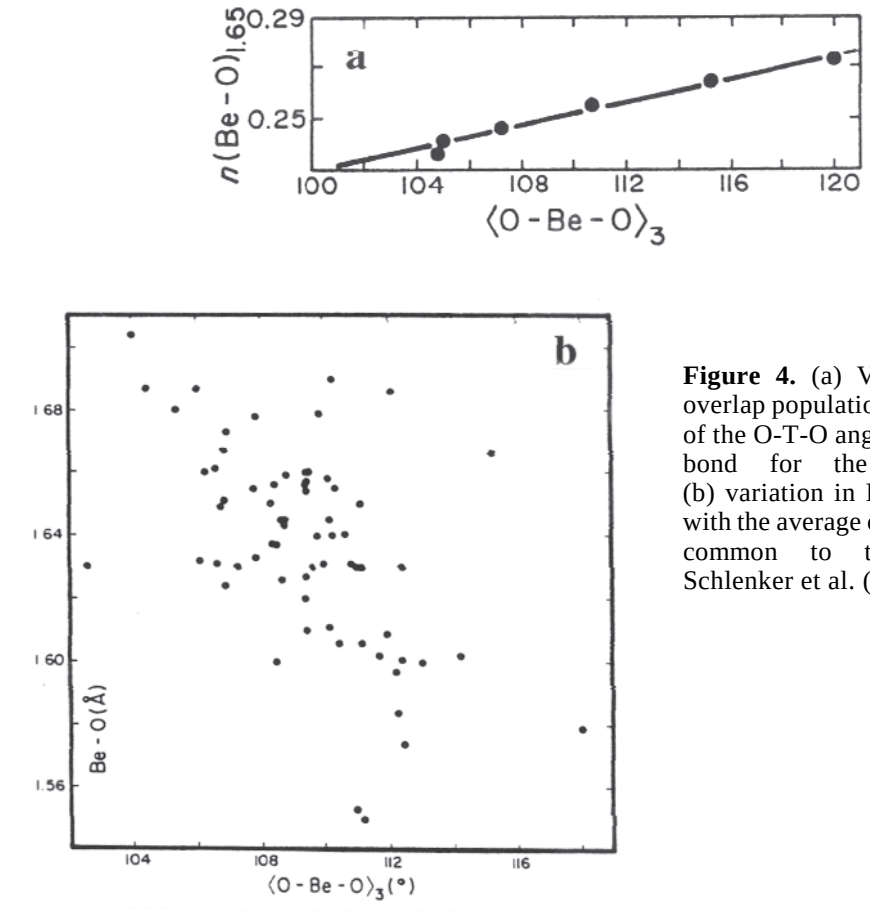

Figure 4. (a) Variation in bond-overlap population with the average of the O-T-O angles common to the bond for the $Be\varphi_4^{6-}$ group; (b) variation in Be-φ bond-lengths with the average of the φ-T-φ angles common to the bond; after Schlenker et al. (1978).

Gupta et al. (1981) reported SCF-HF (Self-Consistent Field Hartree-Fock) calculations on the $Be(OH)_4^{2-}$ tetrahedron, and observed that it is important to have a low cluster-charge in order to reproduce experimental bond-lengths. A minimal basis-set, STO-3G (Slater-Type Orbitals expanded by three Gaussians; Tossell and Vaughan (1992) give a readable summary of MO methods), reproduces experimental distances quite closely for $Be(OH)O_4^-$ polyhedra: Be-φ (exp) = 1.64, Be-φ (calc) = 1.63 Å.

The Be-O-Si linkage. In many minerals, the $Be\varphi_4$ tetrahedron polymerizes with SiO_4 tetrahedra, and hence the Be-O-Si linkage is of great interest. Tossell and Gibbs (1978)

showed that Be-O-Si linkages produce a range of Be-O-Si bond-angles from ~114-138° with a maximum frequency at ~129° (see also Ganguli 1979). Downs and Gibbs (1981) reported HF calculations done using a STO-3G basis set on $BeSi(OH)_7$ and H_6BeSiO_7, both of which contain the Be-O-Si linkage. In $BeSi(OH)_7$, the bridging oxygen is formally overbonded (with an incident Pauling bond-strength sum of 2.5 vu), whereas in H_6BeSiO_7, the bridging oxygen is formally underbonded (with an incident Pauling-bond-strength sum of 1.5 vu). The optimized geometries for the two clusters (Fig. 5) show long Be-O and Si-O bonds for the overbonded bridging anion (Fig. 5a) and short Be-O and Si-O bonds for the underbonded bridging anion (Fig. 5b), as expected. The actual values of the bond-lengths are not truly representative of the local arrangement as incident bond-valence sums calculated from the values of Brown (1981) give values at the bridging anion of 1.40 (ignoring H) and 1.66 vu, respectively. Obviously the O-H bond-length used (as fixed in the optimization) is too short for the actual local arrangement in Figure 5a, and the bridging anion in Figure 5b requires another coordinating cation. Nevertheless, the Be-O-Si angles of 129° and 131° are close to the grand mean observed value reported by Tossell and Gibbs (1978).

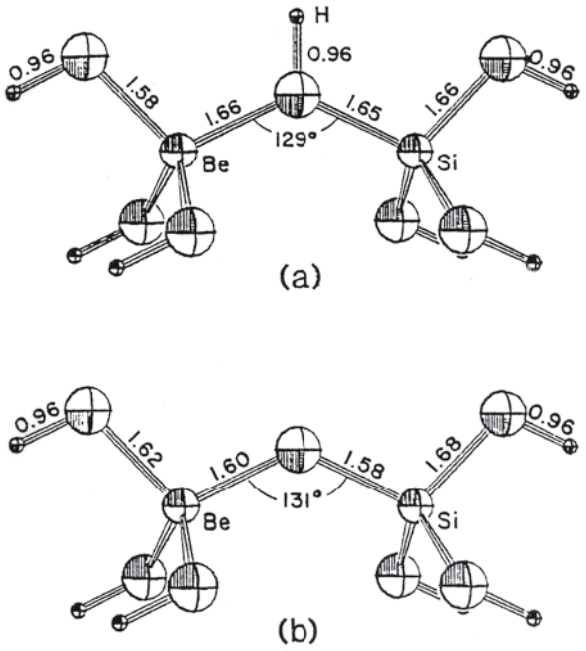

Figure 5. Optimized geometries for (a) $BeSi(OH)_7$ and (b) H_6BeSiO_7, calculated using a minimal STO-3G basis set. Large spheres = O, small spheres = H, with O-Be-O = O-Si-O = 109.47° (fixed) and O–H = 0.960 Å (fixed). After Downs and Gibbs (1981).

Downs and Gibbs (1981) also examined the energetics of bond bending for these two clusters (Fig. 6a) and showed that the Boltzmann distribution curve for the energies of $BeSi(OH)_7$ (i.e., $\exp[-\Delta E(\angle\text{Be-O-Si})/kT]$, where T = 300 K) are in accord with the distribution of Be-O-Si angles in beryllosilicates (Fig. 6b). Similar results were reported by Geisinger et al. (1985).

Lichanot et al. (1992) and Lichanot and Rerat (1993) examined the structure and properties of bromellite using the *ab-initio* method in the Hartree-Fock approximation with an all-electron basis set and periodic boundary conditions to model the complete crystal structure. The crystallographic parameters are in fairly close agreement (Table 2, below); note that the experimental values have been extrapolated to 0 K using the thermal-expansion coefficient $2.66 \times 10^{-5}\ K^{-1}$ for *a* and *c*, and $1.5 \times 10^{-6}\ K^{-1}$ for *u* (Hazen and Finger 1986). The calculated elastic constants are compared with experimental values in Table 1. The experimental values of Sirota et al. (1992) were adjusted to 0 K using the model of Garber and Granato (1975a,b). The agreement is quite close for the diagonal components of the elastic tensor, but the discrepancies for the off-diagonal elements are large: C_{12} 24%, C_{13}

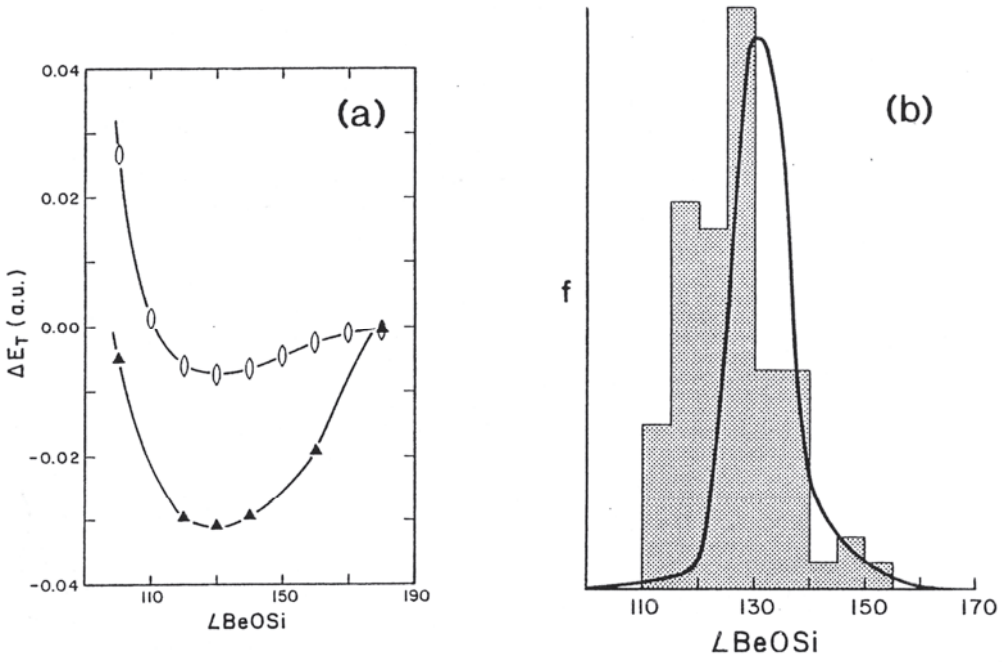

Figure 6. (a) Potential-energy curves, ΔE_T = E(180°) - (∠Be-O-Si), as a function of Be-O-Si angle in $BeSi(OH)_7$ (triangles) and H_6BeSiO_7 (lozenges) with bond lengths fixed at the optimized values; (b) histogram of Be-O-Si angles in beryllosilicates with the Boltzmann distribution curve for energies of $BeSi(OH)_7$. After Downs and Gibbs (1981).

48%, although we note that some of the uncorrected experimental values are much closer to the calculated values than the 'corrected' experimental values. This range in accuracy of the calculated values is not surprising; there are usually problems calculating off-diagonal tensor components from theoretical models, a problem that may relate to the difficulty of dealing with non-central forces.

Deformation electron-density maps

A deformation electron-density map is obtained by subtracting the electron density associated with spherically symmetrical free atoms from the total electron-density of the cluster. In such maps, a positive electron-density indicates that the electron density in this region is increased due to bonding effects, whereas a negative electron-density occurs where the electron density has been depleted by bonding effects. Such maps show the location of chemical bonds and lone-pair electrons, and can be obtained from experiment, from first-principles calculations, or from a combination of experiment and calculation. Gupta et al. (1981) used the HF MO descriptions of the electronic wavefunctions to calculate deformation-electron-density maps for $Be(OH)O_4^{2-}$ clusters. Despite ambiguities in the definition of reference state, there is a depletion of charge at the central Be atom, charge transfer to oxygen, concentration of charge density on the oxygen lone-pair region, and an increase in charge in the T-O and O-H bond regions. Downs and Gibbs (1987) obtained experimental deformation-density maps for phenakite, and showed that there are accumulations of deformation density associated with Be-O and Si-O bonds, and that short bonds show greater accumulations of deformation density than long bonds.

Interpretation of spectroscopic data

MO methods provide the molecular-orbital structure of atom clusters, and hence are of considerable use in the interpretation of many types of spectra for minerals and glasses.

Orbital energies. Many forms of spectroscopy involve the absorption and/or emission of energy as a result of transitions of the experimental system from one energetic state to another. The assignment and interpretation of such titative (or semi-quantitative) understanding of the energy levels of the system. In general, a knowledge of the molecular-orbital structure of the system provides this understanding, either directly when the transitions involve electrons, or indirectly *via* calculation of a physical parameter (e.g., the EFG: Electric-Field Gradient) that affects other (e.g., nuclear) spectral transitions.

Vaughan and Tossell (1973) calculated the orbital energies for BeO_4^{6-} using the CNDO/2 (Complete Neglect of Differential Overlap) method (Tossell and Vaughan 1992), and obtained results that are in accord with the OK_α X-ray emission spectrum of BeO (Fig. 7); note that peak B in Figure 7 is thought to be a reflectivity spike from the analyzing crystal used in the measurement of the spectrum (Liefeld et al. 1970).

Table 1. Physical properties of bromellite calculated with the 'crystal' Hartree-Fock method (1), (2).

	(1)	*(2)*	*Experimental*
a (Å)	2.680	2.697	2.675
c	4.336	4.361	4.344
c/*a*	1.618	1.617	1.624
u	0.3798	0.3791	0.3765
*K	251	244	210
C_{11}	-	526	518/461/470
C_{12}	-	110	144/127/168
C_{13}	-	92	176/88/119
C_{33}	-	556	516/492/494
C_{44}	-	148	152/148/153
C_{66}	-	-	274/167/152

(1) Lichanot et al. (1992); (2) Lichanot and Rerat (1993)
*K = bulk modulus in GPa; C_{ij} = elastic constants, three sets of experimental values are shown: Sirota et al. (1992), Cline et al. (1967) and Bentle (1966).

BERYLLIUM MINERALS AND THE IONIC MODEL

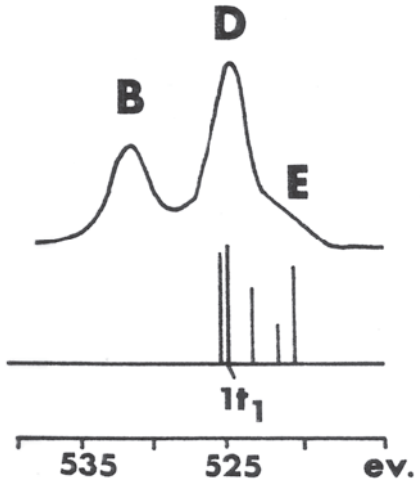

Figure 7. The OK_α spectrum of BeO (after Koster 1971); the posi-tions and relative intensities of the predicted X-ray emission peaks are shown below; after Vaughan and Tossell (1973).

In the *ionic model*, a crystal structure is considered as an array of spheres that bear the formal charges of the ions constituting the crystal. Originally, the energy of the crystal was then calculated as the sum of the 'electrostatic' interactions over the whole crystal plus the sum of the short-range repulsive interactions (usually represented as an exponential or inverse-power function) (Pauling 1929; O'Keeffe 1981). This model is *empirical* in that it requires experimental observations (i.e., interatomic distances), in addition to universal constants, as input to the calculations. Moreover, it shows only semi-quantitative agreement with even the most ionic materials.

Developments of the ionic approach in the last 30 years have greatly increased its rigor and power. The key development was the proof of a universal functional relation between the potential energy (total ground-state energy) and the electron density of an array of atoms. This provided the impetus to develop *ab-initio* models that need no experimental input apart from the universal constants. A model widely used in mineralogy is the *Modified Electron Gas* (MEG) model

of Gordon and Kim (1972). This model defines the ionic-limit electron density at any point in a crystal as the sum of the electron densities from the component free-ions at their sites in the structure; these latter electron densities result from quantum-mechanical calculations for the individual free-ions. For such models, the free oxide-ion (O^{2-}) wave-function is not stable; however, it can be stabilized by placing it in a potential well produced by a shell of surrounding positive charge (Watson 1958). Such a shell can be fixed, the *rigid-ion* model of Cohen and Gordon (1976), or can include spherical-charge relaxation, e.g., the *Potential Induced Breathing* (PIB) model of Boyer et al. (1985).

Table 2. Calculated (MEG method) and experimental properties for BeO (from Tossell 1980).

[cn]		*+2*	*+1*	*Experimental*
[4]	Be-O (Å)	1.7	1.84	1.64
	ΔH (kcal mol^{-1})	-212	-89	-142
	B (megbars)	-	2.58	2.2
[6]	Be-O (Å)	1.79	1.99	-
	ΔH (kcal mol^{-1})	-232	-73	-

Table 3. Physical properties* of bromellite calculated with the PIB model (after Cohen et al. 1987).

Property	*PIB*	*Experimental*
Volume ($Å^3$)	29.24	27.6
c/a	1.58	1.62
z (Be)	0.385	0.378
K (GPa)	186	210
K′	3.72	5.1
Murnaghan fit range	-10 to -47	
Max. error in P	0.08	
*E*2 (cm^{-1})	333 [0.31]	338 [0.03]
*A*1 (TO)	555 [1.54]	682 [1.57]
*E*1 (TO)	637 [1.59]	723 [1.52]
*E*2	645 [1.68]	682 [1.73]
*A*1 (LO)	1347 [0.78]	1095 [0.92]
*E*1 (LO)	1383 [0.84]	1097 -
C_{11} (Gpa)	371	518/461/470
C_{12}	108	144/127/168
C_{13}	90	176/88/119
C_{33}	361	516/492/494
C_{44}	132	152/148/153
C_{66}	131	274/167/152

* K = bulk modulus; K′ = derivative of K; *E* and *A* = Raman frequencies (Jephcoat et al. 1986; Arguello et al. 1969), values in [ ] are associated Grüneisen parameters; C_{ij} = elastic constants, three sets of experimental values are shown: Sirota et al. (1992), Cline et al. (1967) and Bentle (1966).

Tossell (1980) examined several mineralogically important oxides, including BeO, from the viewpoint of the *Modified Electron Gas* (MEG) model. He used shells of +2 and +1 charge, respectively, to stabilize the free-oxide (O^{2-}) wave-function in his calculations, and in addition, a free unstabilized wave-function. The results for BeO are summarized in Table 2. The experimental heat of formation lies between the values calculated for the +2 and +1 stabilized-ion models, somewhat closer to the latter results. This result is in accord with the fact that the +1 stabilized-ion model predicts the correct coordination-number ([4]) for BeO (whereas the +2 stabilized-ion model predicts [6] to be more stable than [4]). The calculated bulk modulus for BeO is somewhat larger than the experimental value. The measure of agreement for BeO is less than that obtained for the alkali halides but greater than that obtained for ZnO, SiO_2 and TiO_2, suggesting that the deviation between calculated and observed properties is a measure of the degree of covalency in the metal-oxygen bonds.

Cohen et al. (1987) examined several oxide minerals, including bromellite, using the *Potential Induced Breathing* (PIB) model; the results for bromellite are given in Table 3. For the zero-pressure structure and equation of state, the agreement with experiment is reasonably good and much improved over rigid-ion models. BeO is calculated to be stable in the wurtzite arrangement (i.e., bromellite) at zero pressure, in agreement with observation. The agreement for the calculated and observed elastic constants is reasonable (Table 3), as is the agreement between the calculated and observed Raman frequencies and Gruneisen parameters.

HIERARCHICAL ORGANIZATION OF CRYSTAL STRUCTURES

Ideally, the physical, chemical and paragenetic characteristics of a mineral should arise as natural consequences of its crystal structure and the interaction of that structure with the environment in which it occurs. Hence an adequate structural hierarchy of minerals should provide an epistemological basis for the interpretation of the role of minerals in Earth processes. We have not yet reached this stage for any major class of minerals, but significant advances have been made. For example, Bragg (1930) classified the major rock-forming silicate minerals according to the geometry of polymerization of $(Si,Al)O_4$ tetrahedra, and this scheme was extended by Zoltai (1960) and Liebau (1985); it is notable that the scheme parallels Bowen's reaction series (Bowen 1928) for silicate minerals in igneous rocks. Much additional insight can be derived from such structural hierarchies, particularly with regard to controls on bond topology (Hawthorne 1983a, 1994) and mineral paragenesis (Moore 1965, 1973; Hawthorne 1984; Hawthorne et al. 1987).

Hawthorne (1983a) proposed that structures be ordered or classified according to the polymerization of those cation coordination polyhedra with higher bond-valences. Higher bond-valence polyhedra polymerize to form *homo-* or *heteropolyhedral clusters* that constitute the *fundamental building block (FBB)* of the structure. The *FBB* is repeated, often polymerized, by translational symmetry operators to form the *structural unit*, a complex (usually anionic) polyhedral array (not necessarily connected) the excess charge of which is balanced by the presence of *interstitial* species (usually large low-valence cations) (Hawthorne 1985). The possible modes of cluster polymerization are obviously (1) unconnected polyhedra; (2) finite clusters; (3) infinite chains; (4) infinite sheets; (5) infinite frameworks.

POLYMERIZATION OF $Be\varphi_4$ AND OTHER $T\varphi_4$ TETRAHEDRA

Bond valence is a measure of the strength of a chemical bond, and, in a coordination polyhedron, can be approximated by the formal valence divided by the coordination number. Thus, in a BeO_4 group, the mean bond-valence is $2/4 = 0.5$ vu. The valence-sum rule (Brown 1981) states that the sum of the bond valences incident at an atom is equal to the magnitude

of the formal valence of that atom. Thus any oxygen atom linked to the central Be cation receives only ~0.50 vu from the Be^{3+} cation, and hence must receive ~1.50 vu from other coordinating cations. In most oxysalt structures, the coordination number of oxygen is most commonly [3] or [4]. This being the case, the *average* bond-valence incident at the oxygen atom bonded to one Be cation is ~0.50 vu for the other three cation-oxygen bonds. There are three general ways in which this bond-valence requirement may be satisfied:

(1) the oxygen atom is bonded to three additional Be atoms to produce [4]-coordination by $^{[4]}$Be, with an incident bond-valence at the oxygen atom of $4 \times 0.50 = 2.00$ vu; this is the case in bromellite: BeO.

(2) the oxygen atom is bonded to an additional Be atom and one H atom to produce an ideal incident bond-valence arrangement of $2 \times 0.50 + 1.00 = 2.00$ vu. This idealized situation is somewhat perturbed by the presence of hydrogen bonds, which provide an additional ~0.20 vu to the anion, with a concomitant lessening of the strength of the O(donor)-H bond: $2 \times 0.50 + 0.20 + 0.80 = 2.00$ vu. This is the case in behoite and clinobehoite, $Be(OH)_2$.

(3) the oxygen atom bonds to a [4]-coordinated high-valence cation (S^{6+}, As^{5+}, P, Si, Al) to produce a tetrahedral polymerization; this is the most common structural arrangement in the Be minerals. This mechanism can involve

   (a) solely a tetrahedral framework, e.g., phenakite: Be_2SiO_4;

   (b) a tetrahedral framework with interstitial cations, e.g., anhydrous beryl: $Be_3Al_2Si_6O_{18} = Al_3[Be_3Si_6O_{18}]$;

   (c) discontinuous polymerization of tetrahedra linked by interstitial cations, e.g., gugiaite: $Ca_2[BeSi_2O_7]$;

   (d) a combination of (b) and (c) with (2), e.g., väyrynenite: $Mn[Be(PO_4)OH]$.

Thus most Be minerals consist of $Be\varphi_4$ tetrahedra polymerizing with other $T\varphi_4$ tetrahedra, and hence we will organize their structures on this basis.

A STRUCTURAL HIERARCHY FOR BERYLLIUM MINERALS

In accord with the above discussion, Be minerals are classified into five distinct groups according to the polymerization of $T\varphi_4$ tetrahedra (T = Be, Zn, B, Al, Si, As, P, S) in the crystal structure:

(1) unconnected tetrahedra (Table 4);

(2) finite clusters of tetrahedra (Table 4);

(3) infinite chains of tetrahedra (Table 5, below);

(4) infinite sheets of tetrahedra (Table 6, below);

(5) infinite frameworks of tetrahedra (Table 7, below).

Within each class, structures are arranged in terms of increasing bond-valence within the constituent tetrahedra. Detailed chemical and crystallographic information, together with references, are given in Appendix A.

The structure diagrams presented here generally have the following shading pattern:

- BeO_4 tetrahedra are shaded with small crosses;
- SiO_4 tetrahedra are shaded with a random-dot pattern;
- PO_4 tetrahedra are shaded with broken lines;
- $M^{2+}O_4$ octahedra are shaded with orthogonal trellis;
- $M^{3+}O_6$ octahedra are shaded with lines.

Table 4. Beryllium minerals based on isolated $Be\varphi_4$ groups and finite $T\varphi_4$ clusters.

Mineral	*Interstitials*	*Figure*
	Isolated tetrahedra	
Chrysoberyl	$^{[6]}$Al	-
Magnesiotaaffeite-6*N*′3*S* [1]	$^{[6]}$Al	8a,b,c
Magnesiotaaffeite-2*N*′2*S* [2]	$^{[6]}$Al	8a,b,c
	Finite cluster	
Gainesite	Zr, Na, K	9a,b

[1]previously known as musgravite-18*R*. [2]previously known as taaffeite-8*H*.

Isolated $T\varphi_4$ groups

Chrysoberyl, $Al_2[BeO_4]$, is isostructural with forsterite, $Mg_2[SiO_4]$, a member of the olivine group (structure not shown). The Be atom occupies the tetrahedron analogous to the SiO_4 group in forsterite, and Al occupies the octahedrally coordinated M1 and M2 sites. The overall structure is a close-packed array of O anions with Al and Be occupying the interstices. The bond valences are uniform and fairly strong, $^{[4]}$Be–O = $^{[6]}$Al-O ≅ 0.50 vu, and hence the structure has no cleavage and is hard (Mohs hardness = 8.5).

Magnesiotaaffeite-6*N*′3*S* (formerly musgravite-18*R*), $MgAl_5[BeMgAlO_{12}]$, the isostructural **ferrotaaffeite-6*N*′3*S*** (formerly pehrmanite-18*R*), $Fe^{2+}Al_5[BeFe^{2+}AlO_{12}]$, and **magnesiotaaffeite-2*N*′2*S*** (formerly taaffeite-8*H*), $MgAl_7[BeMg_2AlO_{16}]$, are all close-packed structures that are regarded as members of a *polysomatic series* (Armbruster 2001) or *polytypoids*. The structure of magnesiotaaffeite-6*N*′3*S* consists of an 18-layer repeat of O atoms in the sequence (BACACBACBCBACBABAC; *hhcccc*). There are three types of polyhedral layers in the structure: (1) an interrupted sheet of edge-sharing octahedra (Fig. 8a, shown with BeO_4 tetrahedra from an adjacent layer) that is topologically the same as the octahedral sheet in dioctahedral sheet-silicates (e.g., kaolinite); this is called the O sheet; (2) a layer of one octahedron and two tetrahedra; each MgO_6 octahedra links to three adjacent BeO_4 tetrahedra by corner-sharing to form a continuous polyhedral sheet (Fig. 8b); the additional tetrahedra within this layer, denoted T_1' by Nuber and Schmetzer (1983), occur in the interstices of the T_1' sheet (as shown in Fig. 8a) but are actually attached to the O sheet; (3) a layer of one AlO_6 octahedron and two MgO_4 tetrahedra, the T_2 layer, that topologically resembles the T_1' layer. These layers stack along the *c*-axis (Fig. 8c) in the sequence (O-T_1'-O-T_1'–O-T_2-O-T_1'-O-T_1'-O-T_2-O-T_1'-O-T_1'-O-T_2). The structure of magnesiotaaffeite-2*N*′2*S* consists of an 8-layer repeat of O-atoms in the sequence (BCABCBAC; *hccc*). As with magnesiotaaffeite-6*N*′3*S*, the structure consists of O, T_1' and T_2 layers, again stacked along the *c*-axis, but now in the sequence (O-T_2-O-T_1'-O-T_2-O-T_1').

Armbruster (2001) has shown that minerals of the högbomite, nigerite and taaffeite groups form polysomatic series involving spinel (*S*) and nolanite (*N*) or modified nolanite (*N*′) modules. For the Be minerals, the root name *taaffeite* is used, together with a prefix that denotes the composition of the spinel module: $MgAl_2O_4$ = *magnesio*; $FeAl_2O_4$ = *ferro*. The various polysomes are characterized by a hyphenated suffix that indicates the numbers of nolanite (*N*), modified nolanite (*N*′) and spinel (*S*) modules.

As with chrysoberyl, the bond valences are uniform and fairly strong, and it is notable that both chrysoberyl and magnesiotaaffeite-6*N*′3*S* can form rare and expensive gemstones.

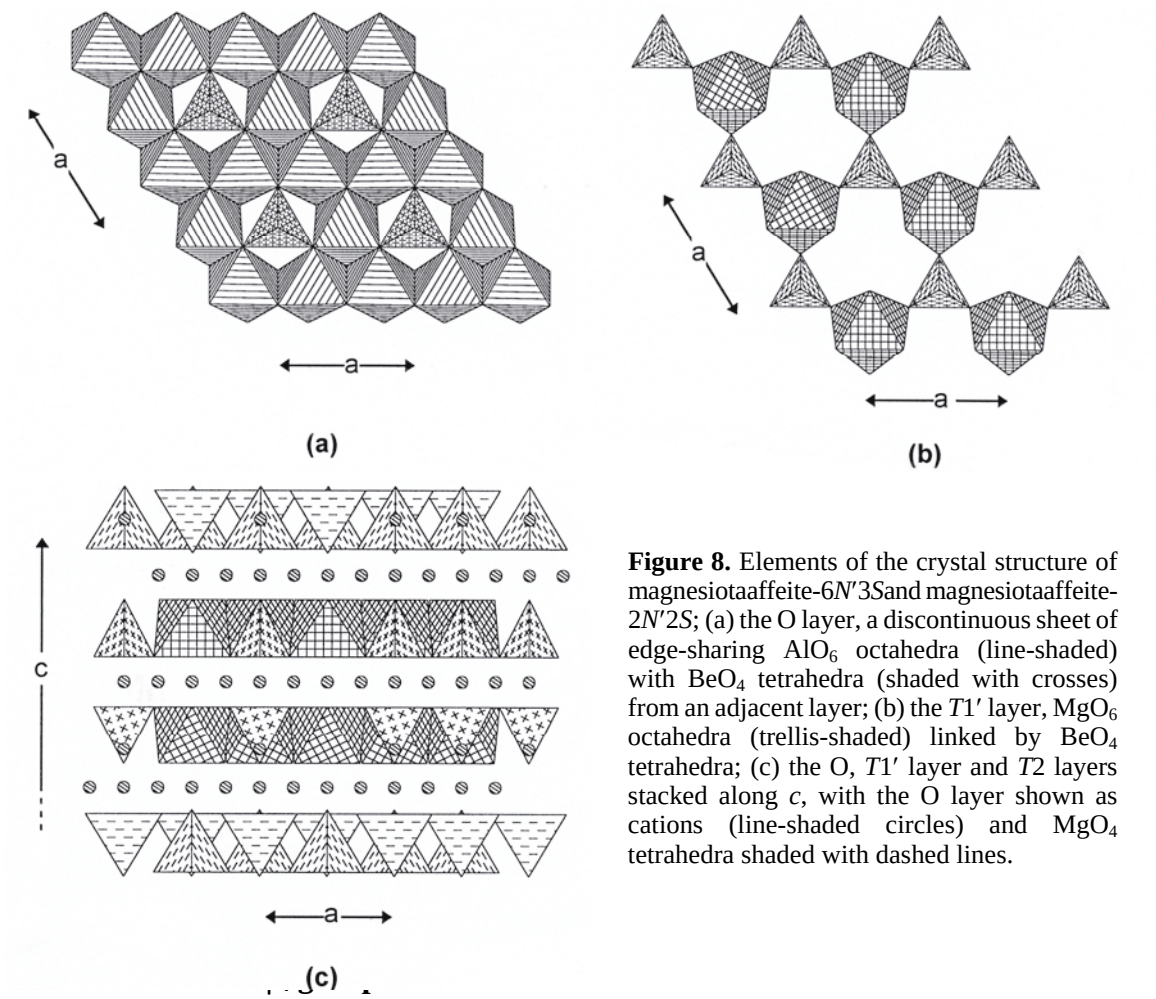

Figure 8. Elements of the crystal structure of magnesiotaaffeite-6*N*′3*S* and magnesiotaaffeite-2*N*′2*S*; (a) the O layer, a discontinuous sheet of edge-sharing AlO_6 octahedra (line-shaded) with BeO_4 tetrahedra (shaded with crosses) from an adjacent layer; (b) the *T*1′ layer, MgO_6 octahedra (trellis-shaded) linked by BeO_4 tetrahedra; (c) the O, *T*1′ layer and *T*2 layers stacked along *c*, with the O layer shown as cations (line-shaded circles) and MgO_4 tetrahedra shaded with dashed lines.

Gainesite, $Na_2Zr_2[Be(PO_4)_4](H_2O)_{1.5}$, is the only finite-cluster structure known so far among the Be minerals. A BeO_4 tetrahedron links to four PO_4 tetrahedra to form the pentameric cluster $[BeP_4O_{16}]$ (Fig. 9a). These clusters are linked into a continuous framework through ZrO_6 octahedra (Fig. 9b) topologically identical to the $[Si_5O_{16}]$ cluster in *zunyite*, $Al_{13}O_4[Si_5O_{16}](OH)_{18}Cl$. Note that the Be and P sites in the gainesite structure are only half-occupied, and in the tetrahedral-octahedral framework, tetrahedral clusters alternate with cavities occupied by interstitial Na atoms.

Infinite chains of $T\varphi_4$ tetrahedra

The minerals in this class can be divided into two broad groups based on the (bond valence) linkage involved in the infinite chains: (1) structures with Be-Si (and Si-Si) linkages; (2) structures with Be-P (or Be-As) linkages. Minerals of this class are listed in Table 5. It is interesting to note that those structures in the first group have no or only minor H-bonding, whereas the minerals of the second group have extensive H-bonding; the reasons for this are not yet apparent.

Chains involving Be-Si linkages.

"**Makarochkinite**," $Ca(Fe^{2+}{}_4Fe^{3+}Ti^{4+}O_2[(BeAlSi_4)O_{18}]$, contains decorated chains of BeO_4, SiO_4 and $(Si,Al)O_4$ tetrahedra; the basic chain resembles a pyroxenoid-like TO_3 chain consisting of alternating dimers of $(Be_{0.5}Si_{0.5})O_4$ tetrahedra and $(Si_{0.75}Al_{0.25})O_4$ tetrahedra,

,

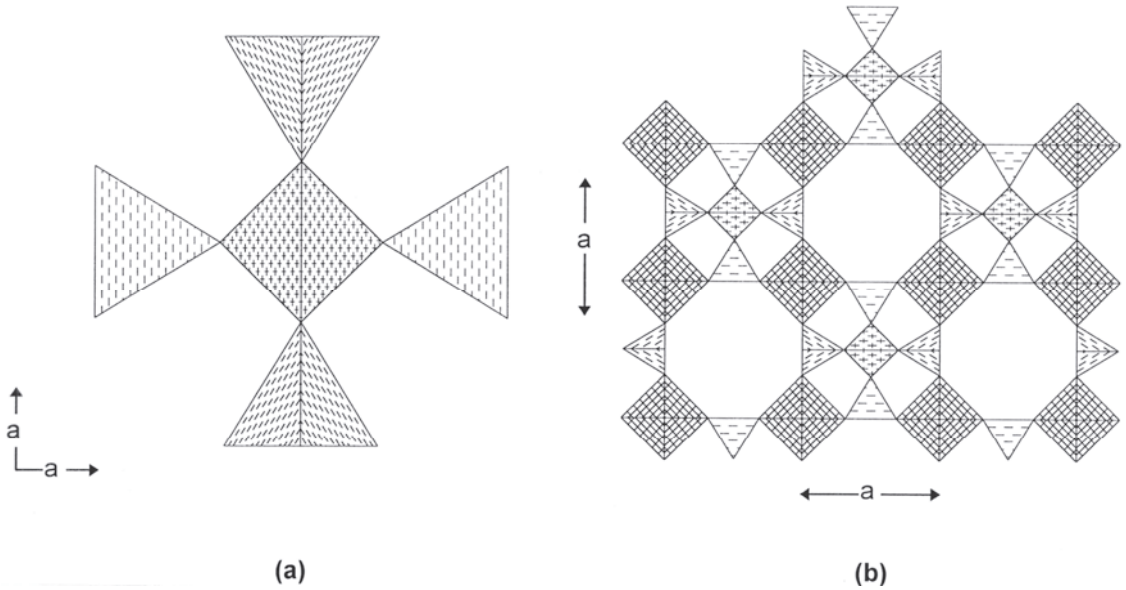

Figure 9. The crystal structure of gainesite. (a) The $[BeP_4O_{16}]$ pentamer that is the finite tetrahedron cluster in gainesite. (b) The tetrahedral-octahedral framework in gainesite; ZrO_6 octahedra are line-shaded.

Table 5. Beryllium minerals based on chains of $T\varphi_4$ tetrahedra.

Mineral	*Linkage*	*Interstitials*	*Figure*
"Makarochkinite"	Be-Si-Si-Al	$^{[6]}$[Ti,Mg,Fe]	10a,b
Khmaralite	Be-Si-Si-Al	$^{[6]}$[Mg,Fe^{2+},Al]	10c,d
Sverigeite	Be-Be-Si-Si	$^{[6]}$Sn + $^{[6]}Mn^{2+}$	11a,b,c
Joesmithite	Be-Si-Si	$^{[6]}$[Mg,Fe^{2+},Al] + $^{[8]}$Ca + Pb	11d
Surinamite	Be-Si-Si	$^{[6]}$[Mg,Al] + O	12a,b
Euclase	Be-Si	$^{[6]}$Al + H-bonding	13a,b
Bearsite	Be-As	H-bonding	14a,b
Moraesite	Be-P	H-bonding	14c,d
Fransoletite	Be-P	H-bonding	15a,b
Parafransoletite	Be-P	Ca + H-bonding	15a,b
Väyrynenite	Be-P	$^{[6]}Mn^{2+}$+ H-bonding	13c,d
Roscherite	Be-P	$^{[6]}$Al + Ca + H-bonding	15c,d

and it is decorated with side-groups of SiO_4 tetrahedra attached to each of the $(Be_{0.5}Si_{0.5})O_4$ tetrahedra. These chains extend along the *a*-axis (Fig. 10a), forming layers of tetrahedra orthogonal to [011] (Fig. 10b). The layers of tetrahedra are linked by ribbons of edge-sharing $Fe^{2+}O_6$ and $Fe^{3+}O_6$ octahedra (with minor substitution of Ti^{4+} and Mg), and between these ribbons in the layer of octahedra are interstitial sites containing [7]-coordinated Ca (with minor substitution of Na).

"Makarochkinite" has not been approved as a new mineral by the Commission on New Minerals and Mineral Names of the International Mineralogical Association. However, it is

a Be-bearing structure of the aenigmatite type, and it is included here on this basis. There are two additional Be-bearing minerals with the aenigmatite structure, **høgtuvaite** and **welshite**, but the crystal structures of these minerals have not yet been refined. Grauch et al. (1994) state that "makarochkinite" is identical to høgtuvaite; this issue will be discussed later.

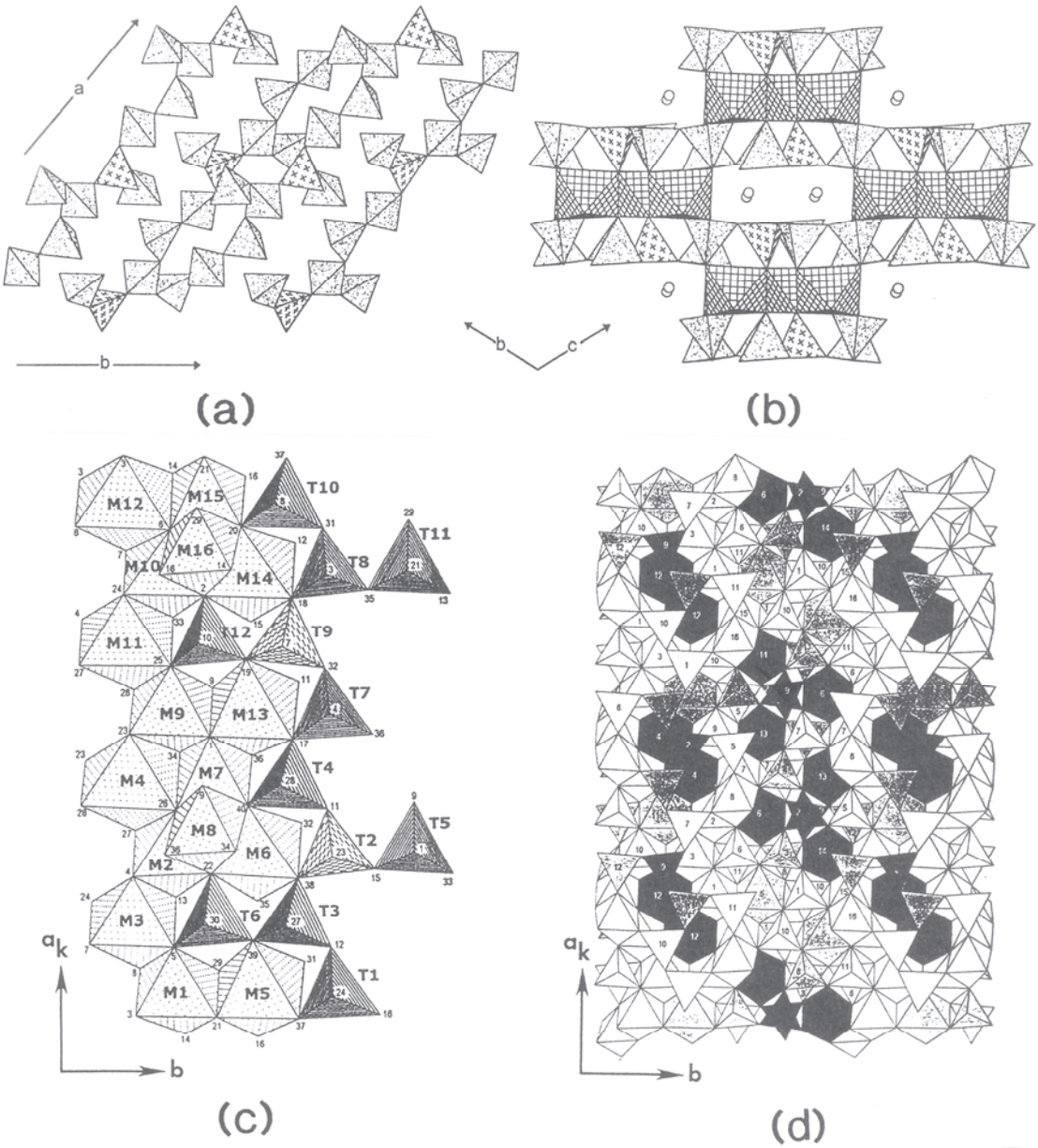

Figure 10. The crystal structures of "makarochkinite" and khmaralite; (a) "makarochkinite" projected onto (001); note the chains of BeO_4 and SiO_4 tetrahedra extending parallel to the *a*-axis; (b) "makarochkinite" projected onto (100); circles in (b) represent interstitial Ca atoms; (c) khmaralite projected onto (001); Be is concentrated in the *T*2 and *T*9 tetrahedra; (d) khmaralite projected onto (001); black, grey and white tetrahedra are enriched in Be, Si and Al, respectively. Used by permission of the Mineralogical Society of America, from Barbier et al. (1999), *American Mineralogist*, Vol. 84, Figs. 4 and 5, pp. 1656-57.

Khmaralite, $Mg_7Al_9O_4[Al_6Be_{1.5}Si_{4.5}O_{36}]$, is a close-packed Be-bearing silicate mineral that is closely related to sapphirine. It was originally noted by Grew (1981) as a beryllian sapphirine, and later reported as a new mineral by Barbier et al. (1999). The structure consists of open-branched chains of tetrahedra (Fig. 10c) that are occupied by Be, Al and Si. Some *T* sites are extensively disordered, whereas others are fairly ordered, and Be is dominant at the *T*2 and *T*9 sites. These chains combine with edge-sharing octahedra to form a dense-packed structure (Fig. 10d). The superstructure in khmaralite corresponds to a doubling of the *a* axis in monoclinic sapphirine-2*M* (in the $P2_1/c$ setting).

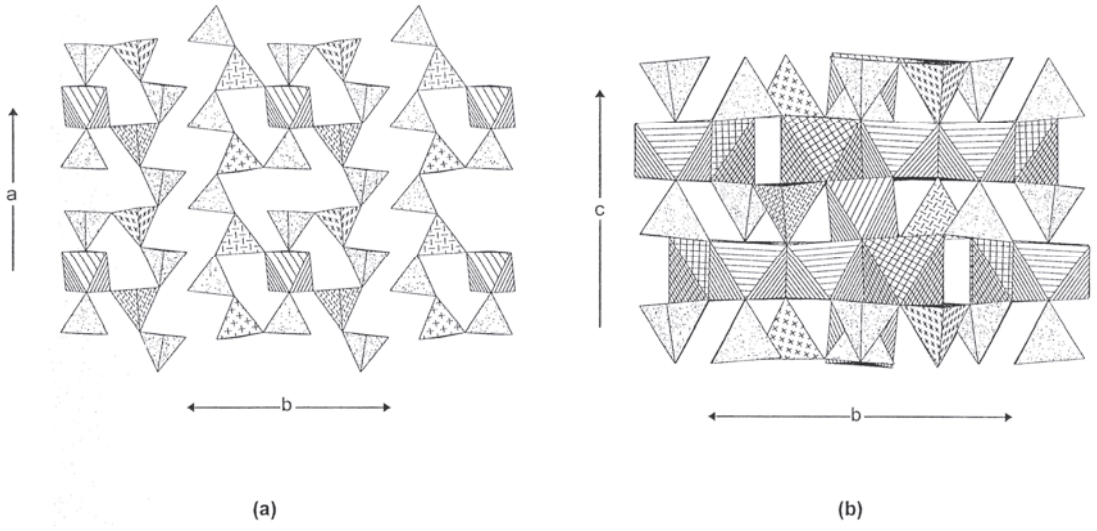

Figure 11. The crystal structure of surinamite; (a) projected onto (001); note the chains of BeO_4, AlO_4 341 (dash-shaded) and SiO_4 tetrahedra extending in the *a*-direction; (b) projected onto (100).

Surinamite, $(Mg,Fe^{2+})_3Al_3O[BeAlSi_3O_{15}]$, consists of $T\varphi_3$ chains of BeO_4, AlO_4 and SiO_4 tetrahedra extending parallel to *a* and decorated by SiO_4 tetrahedra every four tetrahedra along its length (Fig. 11a). Adjacent chains are linked through single AlO_6 octahedra to form ribbons that define a dominantly tetrahedral layer. These layers are interleaved with discontinuous layers of edge-sharing $(Mg,Fe^{2+})O_6$ and AlO_6 octahedra (Fig. 11b). As with the other chains considered above, the BeO_4 tetrahedron is three-connected to other tetrahedra. The structure of surinamite is related to that of sapphirine (Moore and Araki 1983; Christy and Putnis 1988).

Sverigeite, Na $(Mn^{2+},Mg)_2Sn^{4+}[Be_2Si_3O_{12}(OH)]$, has complex chains of corner-sharing $[Be_2SiO_8(OH)]$ three-membered rings and $[Be_2Si_2O_{11}(OH)]$ four-membered rings extending parallel to the *a*-axis (Fig. 12a). These chains are cross-linked in the *b*-direction by SnO_6 octahedra (Fig. 12a) and by $[(Mn^{2+},Mg)_2O_{10}]$ dimers (Fig. 12b). Viewed down the *b*-axis (Fig. 12c), the SnO_6 octahedra form a body-centered array, and the interstitial Na atoms occur between octahedra adjacent in the *c*-direction. The coordination around the Na atom is somewhat unusual with four short bonds (2.43 Å) in a square-planar arrangement and four long bonds (3.07 Å).

Joesmithite, ideally $Pb^{2+}Ca_2(Mg_3Fe^{3+}_2)[(Si_6Be_2)O_{22}](OH)_2$, is a novel amphibole with Be ordered at the *T*2 tetrahedron of the normal *C*2/*m* amphibole structure (Hawthorne 1983b). Double $[T_8O_{22}]$ chains of tetrahedra extend along the *c*-axis (Fig. 12d), linking ribbons of edge-sharing $(Mg,Fe^{2+})O_6$ and $(Mg,Fe^{3+})O_6$ octahedra that also extend along *c*. Occupying the [8]-coordinated M4 sites is Ca, and Pb^{2+} occupies the *A* cavity between the back-to-back chains of tetrahedra. The Pb^{2+} atom is displaced toward the Be site, bonding strongly to the chain-bridging anions involving the BeO_4 tetrahedron and also producing a

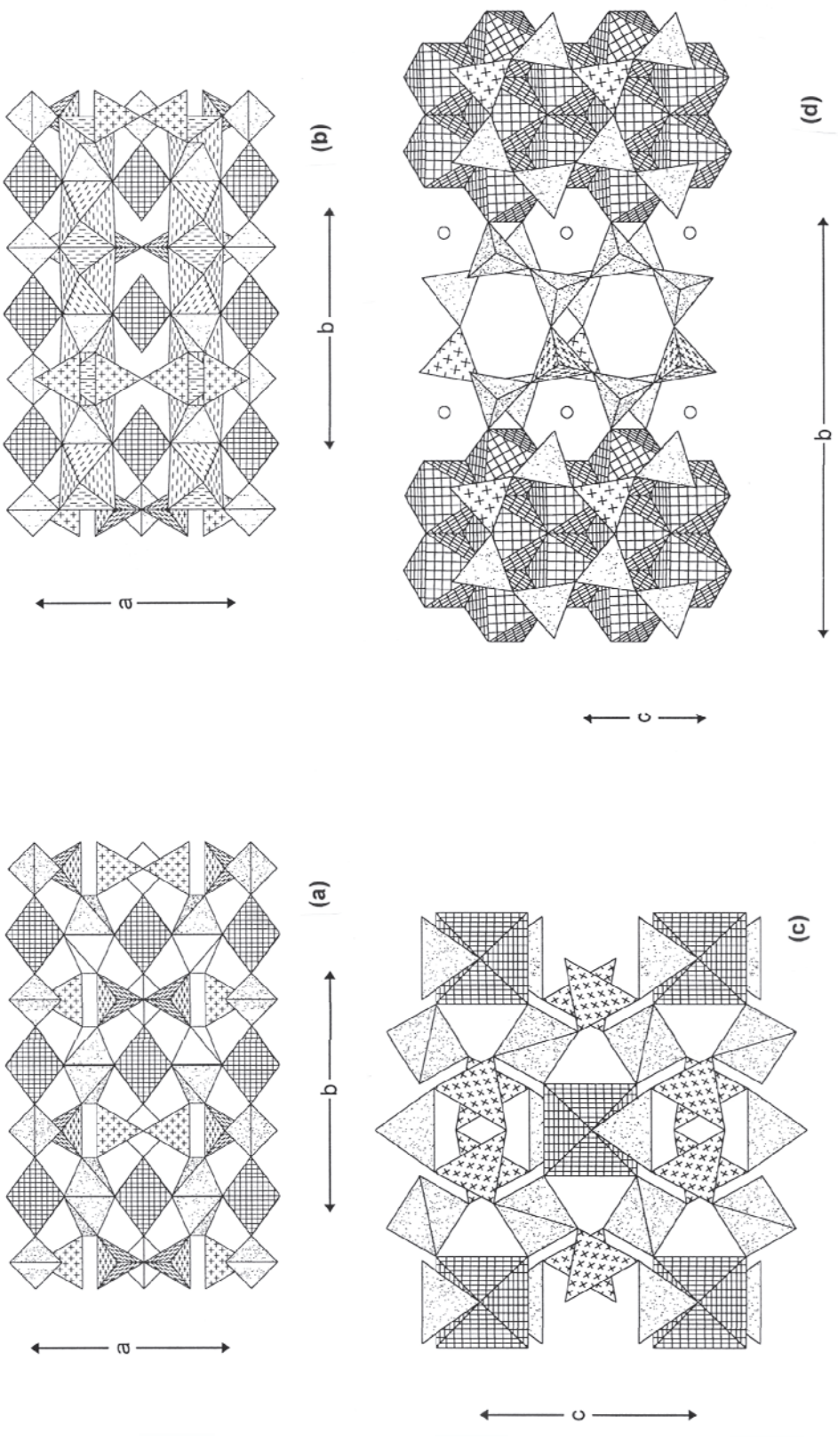

Figure 12. The crystal structures of sverigeite and joesmithite; (a) sverigeite projected onto (001); note the complex chains of corner-sharing $[Be_2SiO_8(OH)]$ three-membered rings and $[Be_2Si_2O_4(OH)]$ four-membered rings extending along the *a*-direction; the SnO_6 octahedron is trellis-shaded; note that the SiO_4 tetrahedra do *not* share edges; the $[(Mn^{2+},Mg)_2O_{10}]$ dimers are omitted for clarity; (b) sverigeite projected onto (001); note the dimers of MnO_6 octahedra (dash-line shaded); (c) sverigeite projected down *b*; (d) joesmithite projected onto (100); unshaded circles are Ca.

local stereochemistry that satisfies the spatial requirements for stereoactive lone-pair behavior for Pb^{2+} (Hawthorne 1983b; Moore et al. 1993).

Euclase, $Al[BeSiO_4(OH)]$, with minor substitution of F for (OH), contains chains of BeO_4 and SiO_4 tetrahedra extending in the *a*-direction (Fig. 13a): BeO_4 tetrahedra link by corner-sharing to form a (fully rotated) pyroxene-like TO_3 chain that is decorated on both sides to form a ribbon in which the BeO_4 tetrahedra are three-connected to SiO_4 tetrahedra and the SiO_4 tetrahedra are two-connected to BeO_4 tetrahedra. In addition, the anion bridging the BeO_4 tetrahedra also belongs to an SiO_4 group. The ribbon-like chains of tetrahedra are arranged in modulated sheets parallel to {001} and linked by edge-sharing pyroxene-like chains of AlO_6 octahedra (Fig. 13b).

Chains involving Be-P and Be-As linkages.

Bearsite, $[Be_2(AsO_4)(OH)](H_2O)_4$, is made up of chains of BeO_4 and AsO_4 tetrahedra. Two BeO_4 and one AsO_4 tetrahedra alternate along the length of a simple TO_3 chain; two of these chains meld *via* sharing corners such that the BeO_4 tetrahedra are three-connected and the AsO_4 tetrahedron is four-connected. The resultant ribbons extend in the *a*-direction (Fig. 14a). The ribbons form a face-centered array when viewed down [100] (Fig. 14b), and the resultant tunnels between the ribbons are filled with interstitial H_2O groups that are held in the structure purely by H-bonding.

Moraesite, $[Be_2(PO_4)(OH)](H_2O)_4$, has a structure extremely similar to that of bearsite, as might be expected by the similarity of the chemical formulae, unit-cell dimensions and space groups (*C*2/*c* vs. $P2_1/a$; see Appendix A). $[Be_2(PO_4)(OH)]$ ribbons extend along the *c*-direction (Fig. 14c), and are topologically identical to the $[Be_2(AsO_4)(OH)]$ chains in bearsite (Fig. 14a). The ribbons form a face-centered array in moraesite (Fig. 14d) similar to that in bearsite (Fig. 14b). The difference between the two structures seems to arise from the slight difference in placement of the H_2O groups within the channels (compare Figs. 14b and 14d).

Fransoletite and **parafransoletite** are dimorphs which have the composition $Ca_3[Be_2(PO_4)_2(PO_3\{OH\})_2](H_2O)_4$. The principal motif in each structure is a complex chain of tetrahedra consisting of four-membered rings of alternating BeO_4 and PO_4 tetrahedra that linked through common BeO_4 tetrahedra; these chains extend in the *a*-direction (Fig. 15a). Viewed end-on (Fig. 15b), the chains form a square array and are linked by [6]- and [7]-coordinated Ca atoms that form sheets parallel to {001}; further interchain linkage occurs through H-bonding involving H_2O groups. The fransoletite and parafransoletite structures differ only in the relative placement of the octahedrally coordinated Ca atom and the disposition of adjacent chains along their length (Kampf 1992).

Väyrynenite, $Mn^{2+}[Be(PO_4)(OH)]$, contains chains of BeO_4 and PO_4 tetrahedra extending in the *a*-direction (Fig. 13c): BeO_4 tetrahedra link by corner-sharing to form a pyroxenoid-like TO_3 chain that is decorated on both sides by PO_4 tetrahedra to form a ribbon in which the BeO_4 tetrahedra are four-connected and the PO_4 tetrahedra are two-connected. These ribbon-like chains are linked by edge-sharing pyroxene-like chains of $Mn^{2+}O_6$ octahedra that also extend parallel to the *a*-axis. The resulting structural arrangement consists of modulated sheets of tetrahedra and octahedra (Fig. 13d) that are similar (Mrose and Appleman 1962) to the analogous sheets in euclase (Fig. 13a).

Roscherite and **zanazziite** are composed of very convoluted chains of $Be\varphi_4$ and PO_4 tetrahedra extending in the [101] direction (Fig. 15c; note that in this view, the two chains appear to join at a mirror plane parallel to their length; however, the plane in question is a glide plane and the two chains do not join at this plane, they are displaced in the *c*-direction). The chain consists of four-membered rings of alternating $Be\varphi_4$ and PO_4 tetrahedra linked through PO_4 tetrahedra that are not members of these rings (Fig. 15c). These chains are linked by $(Al,\square)O_6$ and $(Mg,Fe^{2+})O_6$ octahedra that form edge-sharing chains parallel to

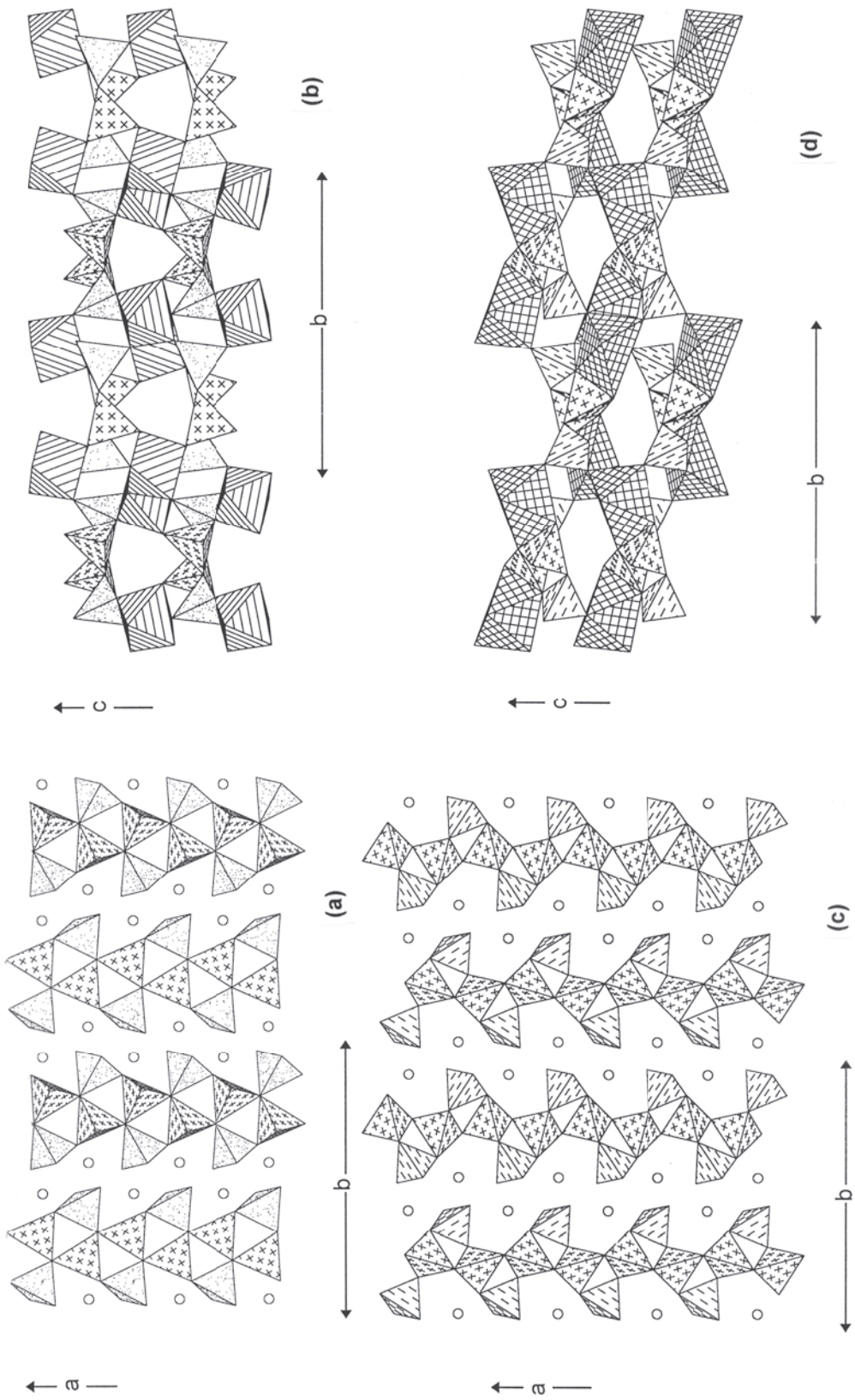

Figure 13. The crystal structures of euclase and väyrynenite; (a) euclase projected onto (001); note the chains of BeO_4 and SiO_4 tetrahedra extending in the *a*-direction; Al atoms are shown as circles; (b) euclase projected onto (100); AlO_6 octahedra are line-shaded; (c) väyrynenite projected onto (001); chains of BeO_4 and PO_4 tetrahedra extend in the *a*-direction; circles are Al atoms; (d) väyrynenite projected onto (100); note the similarity of euclase and väyrynenite in this view (although the chains of tetrahedra are topologically distinct).

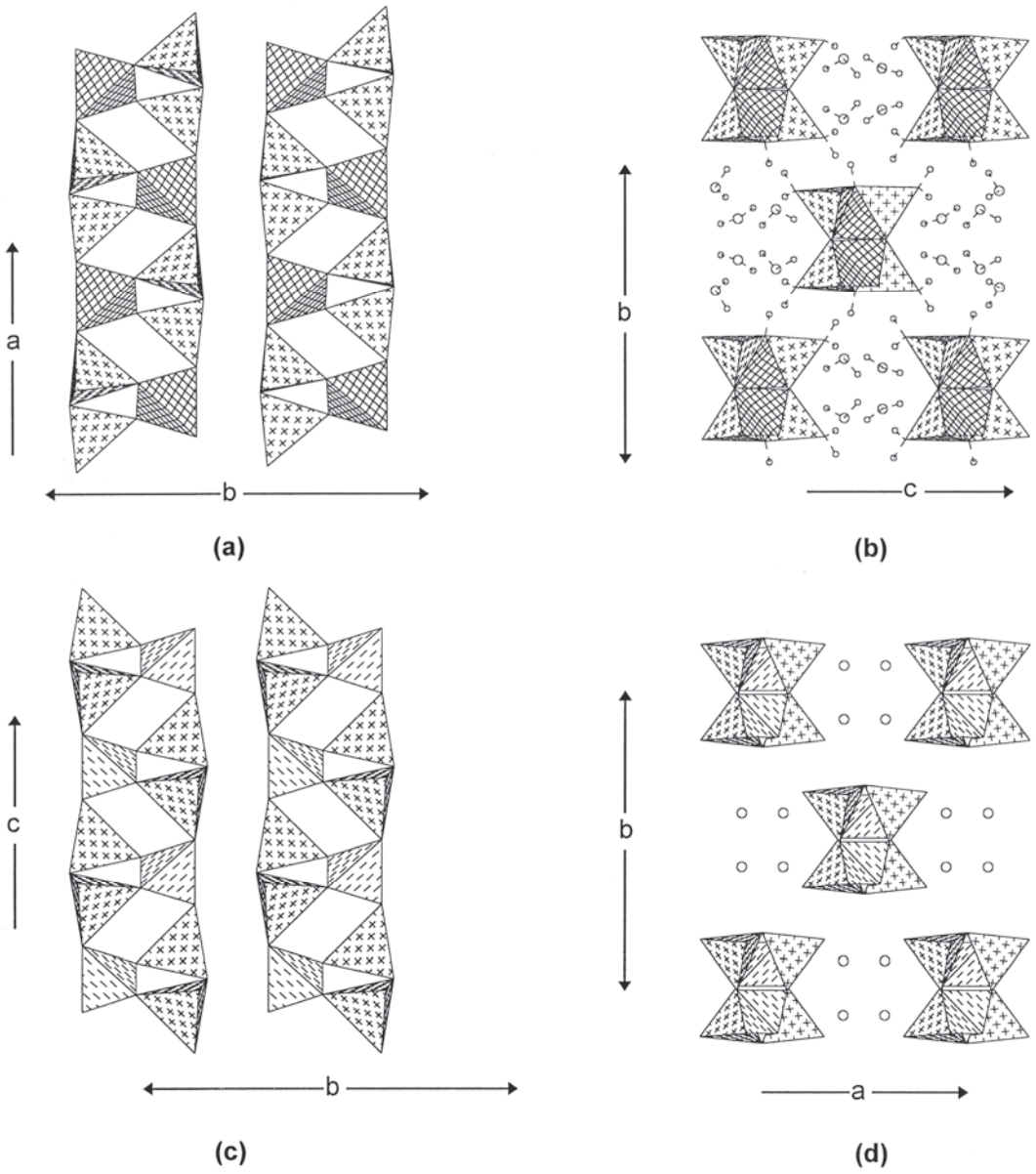

Figure 14. The crystal structures of bearsite and moraesite; (a) bearsite projected onto (001); AsO_4 tetrahedra are trellis-shaded; note the chains of tetrahedra extending along *a*; (b) bearsite projected onto (100); H_2O groups are indicated as unshaded circles; (c) moraesite projected onto (100); the chains of tetrahedra extending along *a* are topologically identical to the chains in bearsite (Fig. 14a); (d) moraesite projected onto (001); H_2O groups are shown as unshaded circles.

[110] and [1$\bar{1}$0]; the octahedral chains link to each other in the [001] direction by sharing *trans* vertices (Fig. 15d). The resultant octahedral-tetrahedral framework is strengthened by [7]-coordinated Ca occupying the interstices.

The structure and composition of these minerals is not completely understood. Roscherite (Slavík 1914) is the Mn^{2+}-dominant species and zanazziite (Leavens et al. 1990) is the Mg-dominant species. Lindberg (1958) also reports an Fe^{2+}-dominant species from the Sapucaia pegmatite, Minas Gerais, that is currently unnamed. The situation is complicated by the fact that the original crystal-structure determination of roscherite (Fanfani et al. 1975) was done on a crystal of what was later determined to be zanazziite with the ideal end-

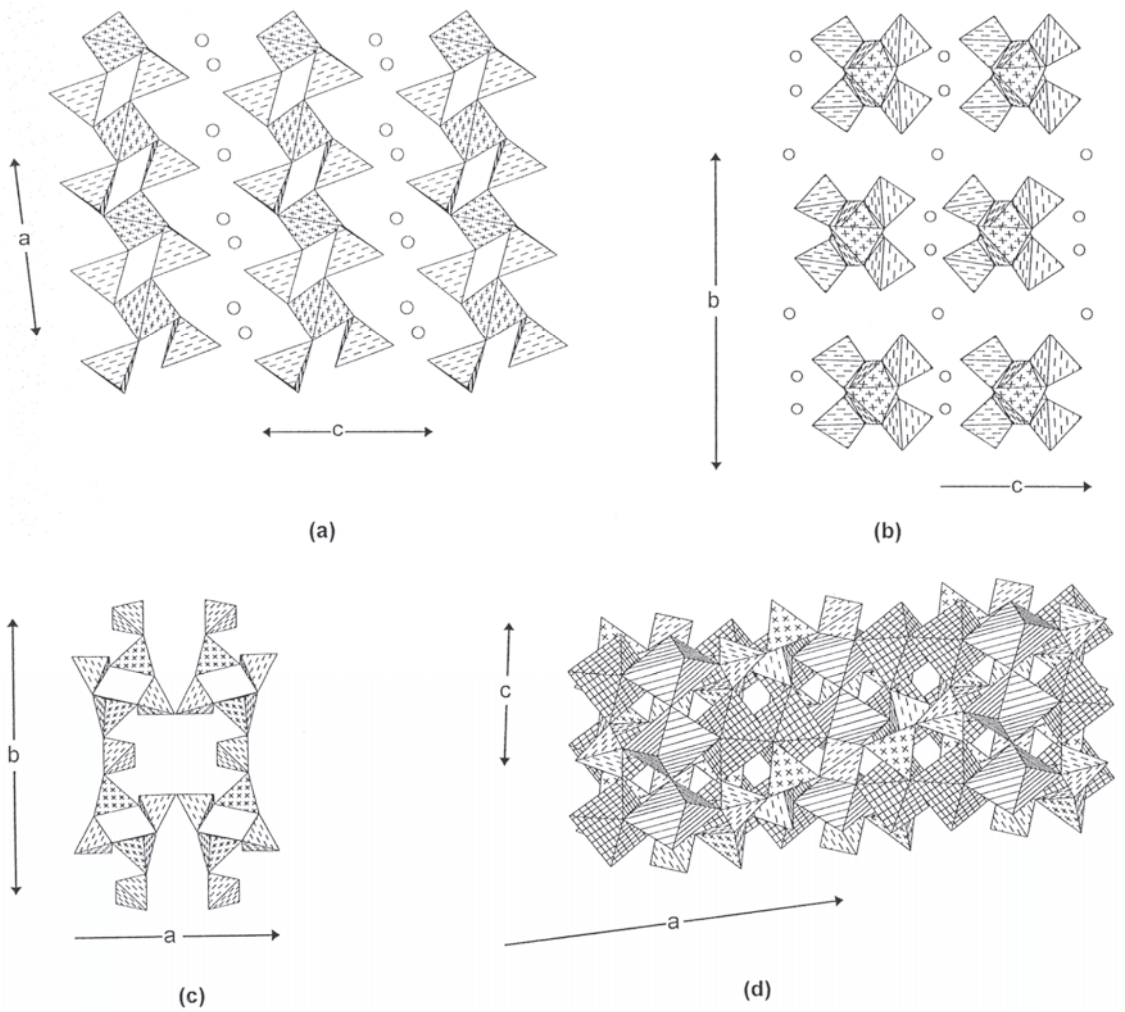

Figure 15. The crystal structure of fransoletite and roscherite; (a) fransoletite projected onto (010); circles are Mn^{2+} atoms; chains of BeO_4 and PO_4 tetrahedra extend along *a*; (b) fransoletite projected onto (100), a view in which the chains are seen end-on; (c) the structural unit in roscherite projected onto (001); chains of BeO_4 and PO_4 tetrahedra extend along *b*; note that the PO_4 tetrahedra in the center of the figure do *not* share a common anion, but are separated in the *c*-direction; (d) roscherite projected onto (010); note that the trivalent octahedra (trellis-shaded) are only two-thirds occupied (by Al); Ca atoms are omitted for clarity.

member formula $Ca_2Mg_4(Al_{0.67}\square_{0.33})_2[Be_4(PO_4)_6(OH)_6](H_2O)_4$. Fanfani et al. (1977) report a triclinic structure for roscherite that is Mn^{2+} dominant, i.e., roscherite with the ideal end-member formula $Ca_2Mn^{2+}{}_4(Fe^{3+}{}_{0.67}\square_{0.33})(\square)[Be_4(PO_4)_6(OH)_4(H_2O)_2](H_2O)_4$. Note that the trivalent-cation content ($Al_{1.33}$ vs. $Fe^{3+}{}_{0.67}$) and type are different in the two species, and electroneutrality is maintained by replacement of OH by H_2O: $Fe^{3+} + \square$ (vacancy) + 3 $H_2O \rightarrow Al^{3+}{}_2 + 3$ OH. Whether the monoclinic $\rightarrow$ triclinic transition is caused by the $Mn^{2+} \rightarrow Mg$ replacement or by the reaction noted above is not yet known.

Infinite sheets of $T\varphi_4$ tetrahedra

The minerals in this class can be divided into three broad groups (Table 6) based on the bond-valences of the linkages involved in the infinite sheets: (1) structures with Be-Be linkages; (2) structures with Be-B linkages; (3) structures with Be-Si (and Si-Si) linkages; (4) structures with Be-As and Be-P linkages.

Table 6. Beryllium minerals based on sheets of $T\varphi_4$ tetrahedra.

Mineral	*Linkage*	*Interstitials*	*Figure*
Clinobehoite	Be-Be	H-bonding	16a,b
Berborite-1T	Be-B	H-bonding	17a
Berborite-2T	Be-B	H-bonding	17b
Berborite-2H	Be-B	H-bonding	17c
Gugiaite	Be-Si-Si	$^{[8]}$Ca	-
Meliphanite	Be-Si-Si	$^{[8]}$Ca, Na	-
Leucophanite	Be-Si-Si	$^{[8]}$Ca	18a,b
Jeffreyite	Be-Si-Si	$^{[8]}$Ca, Na	-
Gadolinite-(Ce)	Be-Si-Si	Ce, Fe^{2+}	-
Gadolinite-(Y)	Be-Si-Si	Y, Fe^{2+}	-
"Hingganite-(Y)"	Be-Si-Si	Y	18c,d
Hingganite-(Yb)	Be-Si-Si	Yb	18c,d
"Calcybeborosilite"	Be-Si-Si	Ca,Y	-
Minasgeraisite-(Y)	Be-Si-Si	Ca, Y	-
Semenovite	Be-Si-Si	Ca, Y Fe^{2+}, Na + H-bonding	19a,b
Aminoffite	Be-Si-Si	$^{[8]}$Ca + H-bonding	20a,b
Harstigite	Be-Si-Si	$^{[6]}$Mn + H-bonding	20c,d
Samfowlerite	Be-Si-Si-Zn	Ca, $^{[6]}$Mn + H-bonding	21a,b
Bityite	Be-Si-Si-Al	Ca, Al + H-bonding	-
Sorensenite	Be-Si-Si	Na, $^{[6]}$Sn + H-bonding	21c,d
Bergslagite	Be-As	$^{[8]}$Ca	22a,b
Herderite	Be-P	$^{[8]}$Ca + H-bonding	22c,d
Hydroxylherderite	Be-P	$^{[8]}$Ca + H-bonding	22c,d
Uralolite	Be-P	Ca	23a,b
Ehrleite	Be-P	$^{[6]}$Zn + H-bonding	23c,d
Asbecasite	Be-As, Be-Si, Si-Si	$^{[6]}$[Ti,Sn]	24a,b,c,d

Sheets involving Be-Be linkages.

Clinobehoite, $[Be(OH)_2]$, consists of $Be(OH)_4$ tetrahedra linked into sheets by sharing vertices. $Be\varphi_4$ tetrahedra share corners to form $[Be\varphi_3]$ chains that resemble almost fully rotated pyroxene chains that extend in the *b*-direction (Fig. 16a) and are cross-linked into a thick slab by other corner-linked $Be\varphi_4$ tetrahedra. When the sheets are seen edge-on (Fig. 16b), stacked along the *a*-direction, it can be seen that the cross-linking $Be\varphi_4$ tetrahedra share vertices and form undulating chains along *b*. The sheets are held together solely by H-bonding.

Sheets involving Be-B linkages.

Berborite, $[Be_2\{BO_3(OH)\}](H_2O)$, has three polytypes, designated 1*T*, 2*T* and 2*H* by Giuseppetti et al. (1990). All three structures consist of sheets of corner-sharing BeO_4

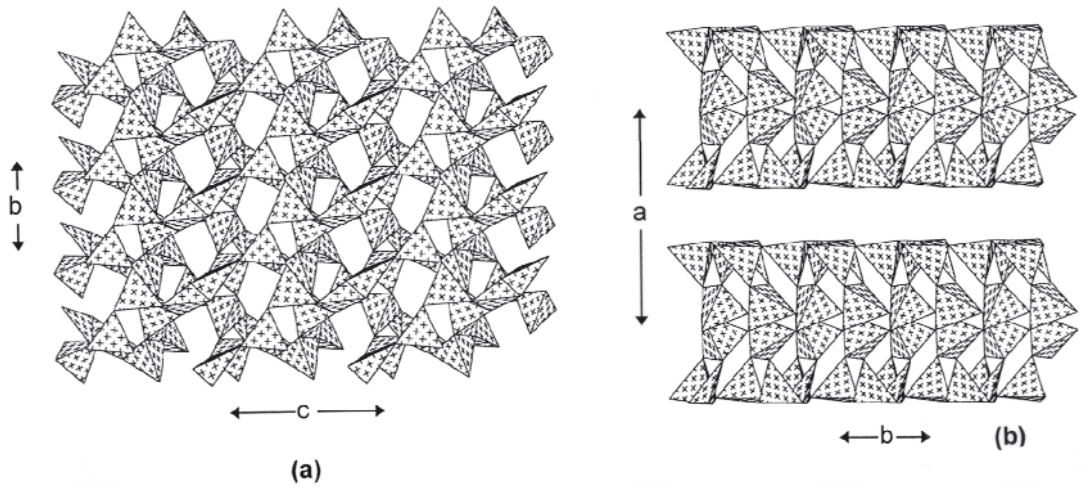

Figure 16. The crystal structure of clinobehoite: (a) projected onto (100); chains of $Be(OH)_4$ tetrahedra (fully rotated pyroxene-like conformation) are cross linked with $Be(OH)_4$ tetrahedra to form sheets parallel to (100); (b) projected onto (001), showing two sheets stacked along *a*; cf. Figures 25a and 25b for behoite.

tetrahedra and BO_3 triangles, and the sheets are identical in all three polymorphs; the structures differ in the relative positioning of adjacent layers in each polytype. The unit cell has a dimer of $Be\varphi_4$ tetrahedra surrounded by BO_3 triangles (Fig. 17a), such that the structure in the {001} plane is a 6_3 net of corner-connected $Be\varphi_4$ tetrahedra with each hexagonal hole containing a BO_3 triangle such that the polyhedra define a 3^6 net with adjacent BeO_4 tetrahedra pointing in opposite directions along *c*; this layer is the first layer in all the polytypes. In berborite-1*T*, the layers shown in Figure 17a are linked by a rather disordered arrangement of H-bonding involving the OH and H_2O groups. In berborite-2*T*, the structure consists of alternations of the layers shown in Figures 17a and 17b, again linked by H-bonding. In berborite-2*H*, the structure consists of alternations of the layers shown in Figures 17a and 17c. It is to be emphasized that the layers shown in Figure 17 are identical; their differing appearance results from different orientation and placement with regard to the unit cell. This general building principle for berborite polytypes indicates that other polytypes are (at least geometrically) possible.

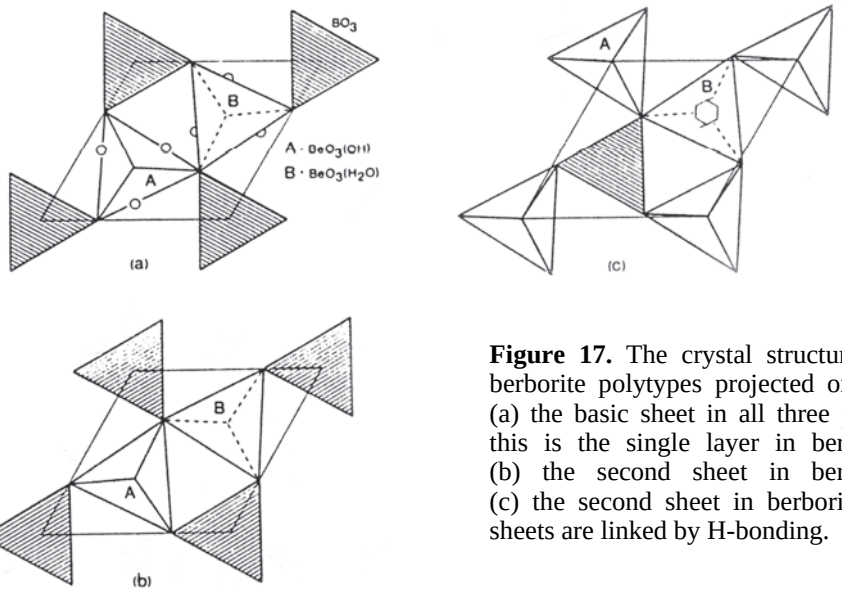

Figure 17. The crystal structures of the berborite polytypes projected onto (001); (a) the basic sheet in all three polytypes; this is the single layer in berborite-1*T*; (b) the second sheet in berborite-2*T*; (c) the second sheet in berborite-2*H*; all sheets are linked by H-bonding.

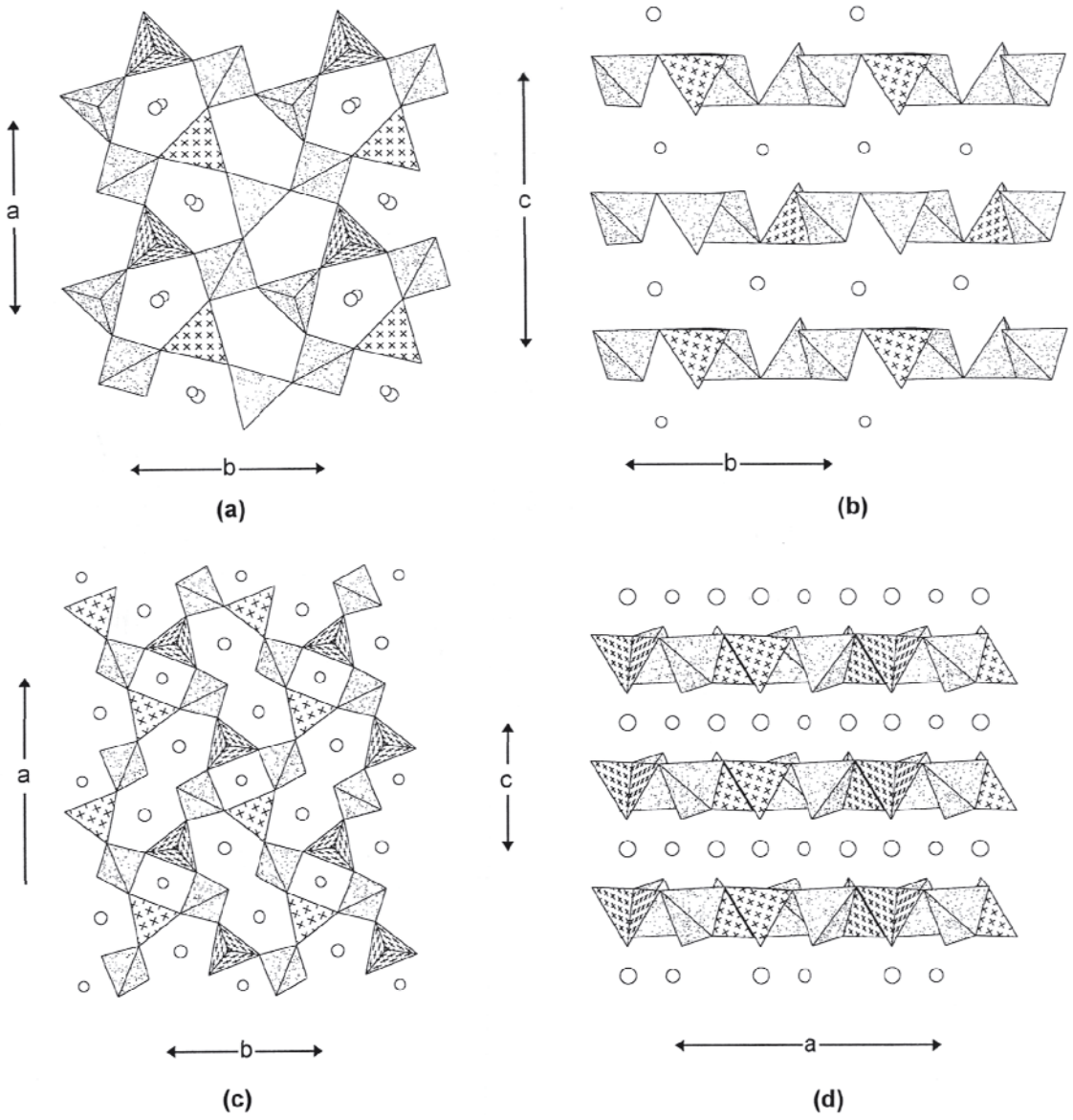

Figure 18. The crystal structures of leucophanite and hingganite-(Yb); (a) leucophanite projected onto (001); BeO_4 and SiO_4 tetrahedra occupy the vertices of a $(5^3_2 5^4_1)$ two-dimensional net; (b) leucophanite projected onto (100); large circles are Na, small circles are Ca; (c) hingganite-(Yb) projected onto (001); large circles are Y, small circles are □ (vacancies) which are filled in other minerals of the gadolinite group; (d) hingganite-(Yb) projected onto (010).

Sheets involving Be-Si linkages.

Gugiaite, $Ca_2[BeSi_2O_7]$,
meliphanite, $(Ca,Na)_2[Be(Si,Al)_2O_6(O,OH,F)]$,
leucophanite, $(Ca,Na)_2[Be(Si,Al)_2O_6(O,F)]$, and
jeffreyite, $(Ca,Na)_2[(Be,Al)Si_2(O,OH)_7]$,

all have structures topologically related (identical sheets) to that of *melilite*, $(Ca,Na)_2(Al,Mg)(Si,Al)_2O_7$. The structure of leucophanite is shown in Figures 18a and 18b. BeO_4 and SiO_4 tetrahedra occur at the vertices of a two-dimensional net (Fig. 18a) in which half of the SiO_4 tetrahedra are four-connected and the rest of the tetrahedra are

three-connected. These sheets are stacked in the *c*-direction and are linked by [8]-coordinated interstitial cations (Fig. 18b). In leucophanite, the interstitial Ca and Na atoms are ordered into different sheets (Fig. 18b) as a result of the orthorhombic symmetry of this particular mineral. In gugiaite, Ca occupies all layers between the sheets, and gugiaite is tetragonal. In meliphanite, Ca and Na are disordered, and meliphanite also has tetragonal symmetry. Although the structure of jeffreyite is not known, it must consist of a derivative of the gugiaite arrangement with ordered replacement of some Be by Al. Rare-earth elements may substitute for Ca in leucophanite, and Cannillo et al. (1992) showed that REE-bearing leucophanite is actually triclinic; thus the structure described by Cannillo et al. (1992) is actually that of an unnamed new mineral.

Gadolinite-(Ce), $Ce_2Fe^{2+}[Be_2Si_2O_{10}]$,
gadolinite-(Y), $Y_2Fe^{2+}[Be_2Si_2O_{10}]$,
hingganite-(Yb), $Yb_2\square[Be_2Si_2O_8(OH)_2]$,
"**hingganite-(Y)**," $Y_2\square[Be_2Si_2O_8(OH)_2]$,
"**calcybeborosilite**," $CaY\square[BeBSi_2O_8(OH)_2]$, and
minasgeraisite-(Y), $CaY_2[Be_2Si_2O_{10}]$

all belong to the *gadolinite group.* The basic unit of the sheet is a four-membered ring of two BeO_4 and two SiO_4 tetrahedra in the sequence [Be-Si-Be-Si]. These rings link by sharing tetrahedral vertices to generate eight-membered rings of alternating BeO_4 and SiO_4 tetrahedra (Fig. 18c). These sheets stack in the *c*-direction (Fig. 18d) and are linked by [8]-coordinated rare-earth cations and [6]-coordinated Fe^{2+}. The different minerals have the same (topological) structural unit and differ in the interstitial species linking the sheets together. "Hingganite-(Y)" is referred to in the literature (Ximen and Peng 1985; Peterson et al. 1994) but is not yet an accredited mineral species. The crystal structure (Ximen and Peng 1985) shows it to be isostructural with hingganite-(Yb).

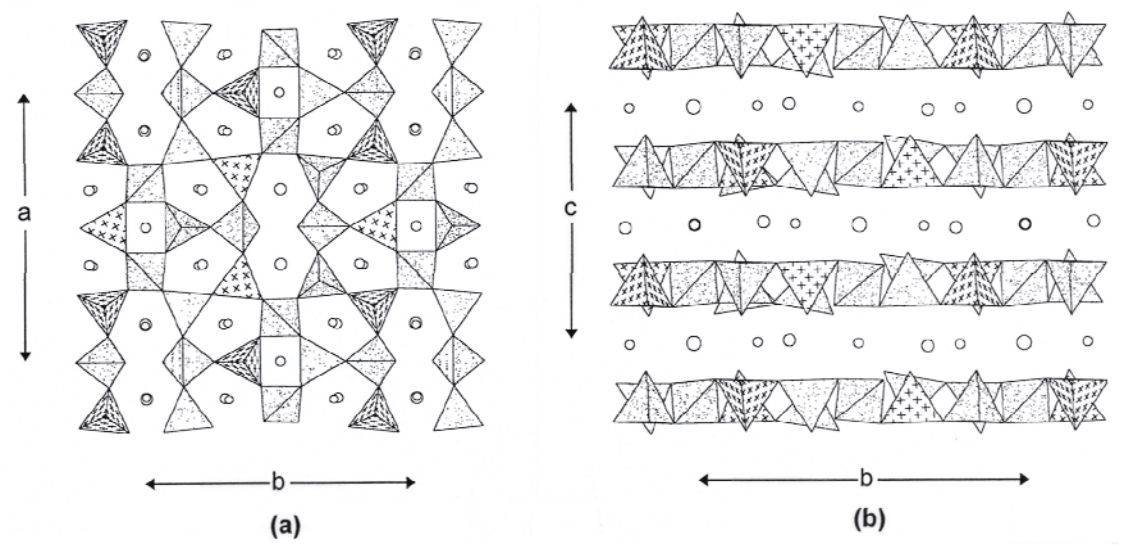

Figure 19. The crystal structure of semenovite; (a) projected onto (001); $Be\varphi_4$ and $Si\varphi_4$ tetrahedra occur at the vertices of a two-dimensional net; large circles are RE, small circles are (Ca,Na); (b) projected onto (100); Fe atoms are omitted for clarity.

Semenovite, $(RE)_2Fe^{2+}Na_{0-2}(Ca,Na)_8[Be_6Si_{14}O_{40}(OH)_4F_4]$, has ordered $Be\varphi_4$ and $Si\varphi_4$ tetrahedra occurring at the vertices of a two-dimensional net (Fig. 19a). In the structure refinement of Mazzi et al. (1979), the Be and Si occupancies are partly disordered

(either 80:20 or 20:80); however, in view of the pervasive twinning present, it is possible that this partial disorder is not correct (Mazzi et al. 1979). For simplicity, we have assumed complete Be-Si order here. There are two distinct $Be\varphi_4$ tetrahedra, both of which are three-connected within the sheet, and five distinct $Si\varphi_4$ tetrahedra, one of which is four-connected and four of which are three-connected. The $Be\varphi_4$ tetrahedra involve one F and one OH group, respectively, and there is also one acid-silicate group, $SiO_3(OH)$. There is one four-membered ring consisting of one $Be\varphi_4$ and three SiO_4 tetrahedra that links to its translational equivalent along *a* through an eight-membered ring with the sequence (Si-Si-Si-Si-Si-Be-Si-Be). These chains meld in the *b*-direction by sharing vertices with adjacent chains that are displaced *a*/2 in the *a*-direction, giving rise to intermediate chains of corner-sharing five-membered rings with the sequences (Si-Si-Si-Si-Be) and (Si-Be-Si-Si-Be). These sheets stack in the *c*-direction and are linked by layers of interstitial cations (Fig. 19b), [6]-coordinated Fe^{2+}, [8]-coordinated RE, [8]-coordinated Ca and [8]-coordinated Na.

The $[Be_6Si_{14}O_{40}F_4]$ sheet in semenovite (Fig. 19a) is topologically the same as the $[Be_4Si_6O_{22}(OH)_2]$ sheet in harstigite (Fig. 20c). This equivalence is not immediately apparent from the chemical formula of the sheets, but may be seen if we write both

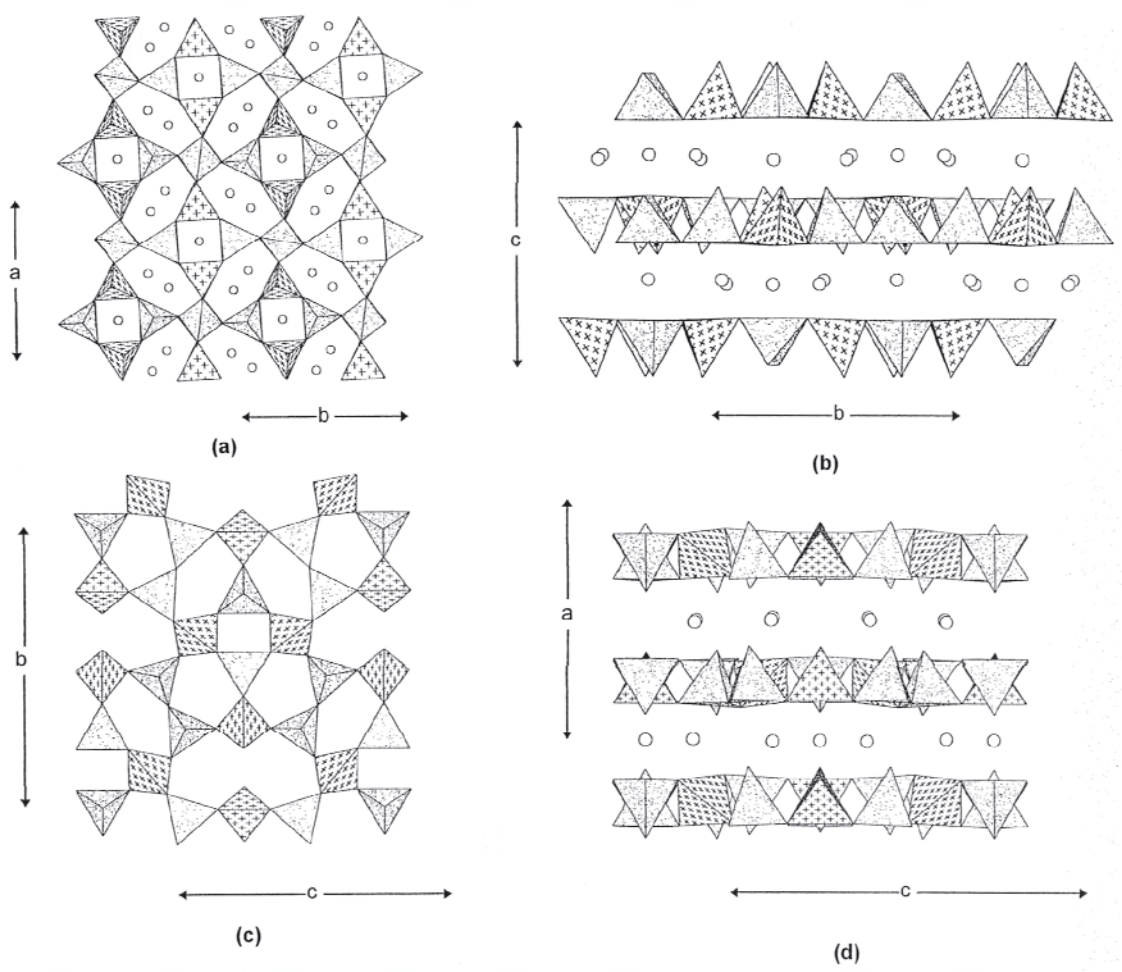

Figure 20. The crystal structures of aminoffite and harstigite; (a) aminoffite projected onto (001); $Be\varphi_4$ and SiO_4 tetrahedra occur at the vertices of a two-dimensional net; unshaded circles are Ca; (b) aminoffite projected onto (100); (c) the structural unit of harstigite projected onto (100); $Be\varphi_4$ and SiO_4 tetrahedra occur at the vertices of a net; (d) harstigite projected onto (010); circles are Ca and Mn atoms.

sheets as $[T_{20}O_{40}(OH)_4\varphi_4]$ where T = Be + Si and φ = O, F. The cell dimensions of both minerals are very close (Appendix A). However, comparison of Figures 20c and 19a shows that the pattern of ordering of Be and Si differs between the two structures. This is in accord with the different chemical compositions and space groups: $[Be_6Si_{14}O_{40}(OH)_4F_4]$, *Pmnn*, and $[Be_4Si_6O_{22}(OH)_2]$, *Pnam*.

Aminoffite, $Ca_2[Be_2Si_3O_{10}(OH)_2]$, consists of $Be\varphi_4$ and SiO_4 tetrahedra arranged at the vertices of a two-dimensional net; the resultant sheet is linked in the *c*-direction by [7]-coordinated interstitial Ca. Four-membered rings of alternating $Be\varphi_4$ and SiO_4 tetrahedra are linked by additional SiO_4 tetrahedra (Fig. 20a). The tetrahedra of the ring are three-connected, the linking SiO_4 tetrahedra are four-connected, and the tetrahedra in adjacent four-membered rings point in opposite directions (i.e., along +*c* or -*c*). Sheets are stacked along *c* (Fig. 20b) where they are linked by layers of interstitial Ca.

Harstigite, $Ca_6Mn^{2+}[Be_4Si_6O_{22}(OH)_2]$, contains four-membered rings of alternating $Be\varphi_4$ and SiO_4 tetrahedra, as does aminoffite, but their linkage is far more complicated in the latter mineral. In harstigite, the tetrahedra occur at the vertices of a two-dimensional net (Fig. 20c). There are two distinct $Be\varphi_4$ tetrahedra, one of which is four-connected and the other of which is three-connected. The SiO_4 tetrahedra of the four-membered ring are three-connected to $Be\varphi_4$ tetrahedra; the other two SiO_4 groups of the five-membered rings form a pyro-group $[Si_2O_7]$ which links to $Be\varphi_4$ tetrahedra (Fig. 20c). The sheets are stacked along the *a*-direction (Fig. 20d) and linked by layers of [7]- and [8]-coordinated Ca and [6]-coordinated Mn^{2+} atoms.

Samfowlerite, $Ca_{14}Mn^{2+}{}_3[(Be_7Zn)Zn_2Si_{14}O_{52}(OH)_6]$, contains $Be\varphi_4$, SiO_4 and $Zn\varphi_4$ (broken-line shaded in Fig. 21a) tetrahedra arranged at the vertices of a two-dimensional net (Fig. 21a). Eight-membered rings of tetrahedra (Zn-Si-Be-Si-Zn-Si-Be-Si) link through four-membered (Be-Si-Be-Si) and five-membered rings to form the net; there are two types of five-membered rings: (Zn-Si-Si-Zn-Si) and (Be-Si-Be-Si-Si). These sheets (Fig. 21b) are linked by layers of [6]-coordinated Mn^{2+} and [8]-coordinated Ca atoms. Site-occupancy refinement showed some Be Zn solid-solution in one of the tetrahedra. Rouse et al. (1994) raise the possibility that samfowlerite consists of domains of ordered arrangements of Zn and Be, but they have no evidence for this.

Bityite, $CaLiAl_2[BeAlSi_2O_{10}](OH)_2$, is a brittle mica, with Ca at the interlayer site. In the tetrahedral $[T_4O_{10}]$ sheet, there is almost complete ordering of (Al,Si) and Be, and the symmetry of the overall atomic arrangement is reduced from *C*2/*c* to *Cc*. There is also complete ordering between Al and (Li,□) over the octahedral sites. It seems probable that coupling of these two ordering patterns is induced by local bond-valence requirements.

Sorensenite, $Na_4Sn^{4+}[Be_2Si_6O_{18}](H_2O)_2$, contains BeO_4 and SiO_4 tetrahedra linked into a sheet in which the BeO_4 tetrahedra are four-connected and the SiO_4 tetrahedra are three-connected. Pairs of BeO_4 tetrahedra share an edge to form a $[Be_2O_6]$ group (Fig. 21c) that links to six SiO_4 tetrahedra, forming a $[Be_2Si_6O_{22}]$ cluster that also occurs in the structures of eudidymite (Fig. 34a, below) and epididymite (Fig. 34d, below). These clusters link in the *b* and *c* crystallographic directions by sharing tetrahedral corners. In the (100) plane (Fig. 21c), the clusters occur at the vertices of a centered plane orthogonal lattice with large interstices that contain octahedrally coordinated Sn^{4+} cations and [8]-coordinated Na that link the sheets in the [100] direction (Fig. 21d).

Sheets involving Be-P and Be-As linkages.

Bergslagite, $Ca[Be(AsO_4)(OH)]$,
hydroxylherderite, $Ca[Be(PO_4)(OH)]$ and

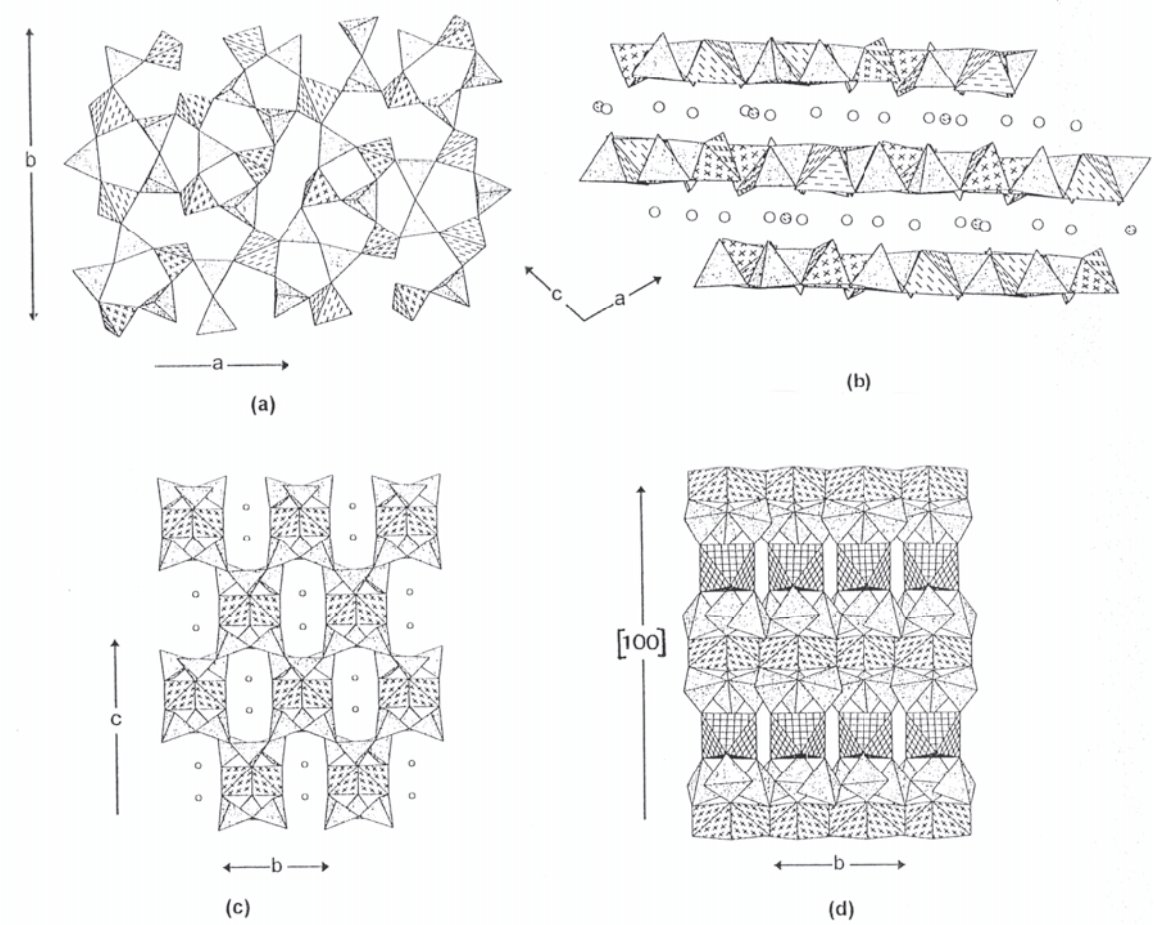

Figure 21. The crystal structures of samfowlerite and sorensenite; (a) the structural unit of samfowlerite projected onto (001); Beφ$_4$ and SiO_4 tetrahedra occur at the vertices of a two-dimensional net; (b) the structural unit of samfowlerite projected onto (010), with interstitial Ca (unshaded circles) and Mn (shaded circles); (c) sorensenite projected onto (100); edge-sharing [$Be_2\varphi_6$] dimers link to triplets of SiO_4 tetrahedra to form clusters that share corners to form thick sheets; Sn are shown as small circles; (d) sorensenite projected onto (001); thick sheets are cross-linked by [6]-coordinated Sn^{4+} and Na (omitted).

herderite, Ca[Be(PO_4)F],

are isostructural, although the structures of the first two were reported in different orientations: $P2_1/c$ and $P2_1/a$, respectively. The sheet unit consists of Beφ$_4$ and $T^{5+}O_4$ tetrahedra at the vertices of a two-dimensional net (Figs. 22a,c). Four-membered rings of alternating Beφ$_4$ and $T^{5+}O_4$ tetrahedra link directly by sharing vertices between Beφ$_4$ and $T^{5+}O_4$ tetrahedra; thus the sheet can be considered to be constructed from chains of four-membered rings that extend in the [011] and [$01\bar{1}$] directions in bergslagite (Fig. 22a) and in the [110] and [$1\bar{1}0$] directions in herderite (Fig. 22c). These sheets stack in the *a*-direction in bergslagite (Fig. 22b) and the *c*-direction in herderite (Fig. 22d) and are linked by layers of [8]-coordinated Ca atoms. Note that the structure reported by Lager and Gibbs (1974) seems to have been done on hydroxylherderite rather than herderite.

Uralolite, $Ca_2[Be_4P_3O_{12}(OH)_3](H_2O)_5$, contains Beφ$_4$ and PO_4 tetrahedra linked into a sheet (Fig. 23a). Eight-membered rings of tetrahedra (P-Be-P-Be-P-Be-P-Be) link through common PO_4 groups to form chains that extend along [101]. These chains link in the (010) plane via sharing of tetrahedral vertices, forming three-membered (Be-Be-Be and Be-Be-P) and four-membered (Be-Be-Be-P) rings. Interstitial [7]-coordinated Ca

atoms lie within the eight-membered rings (in projection). The layers stack along the *b*-direction (Fig. 23b) and are linked by Ca atoms (circles) and H-bonding; in this view, the three- and four-membered rings are easily seen.

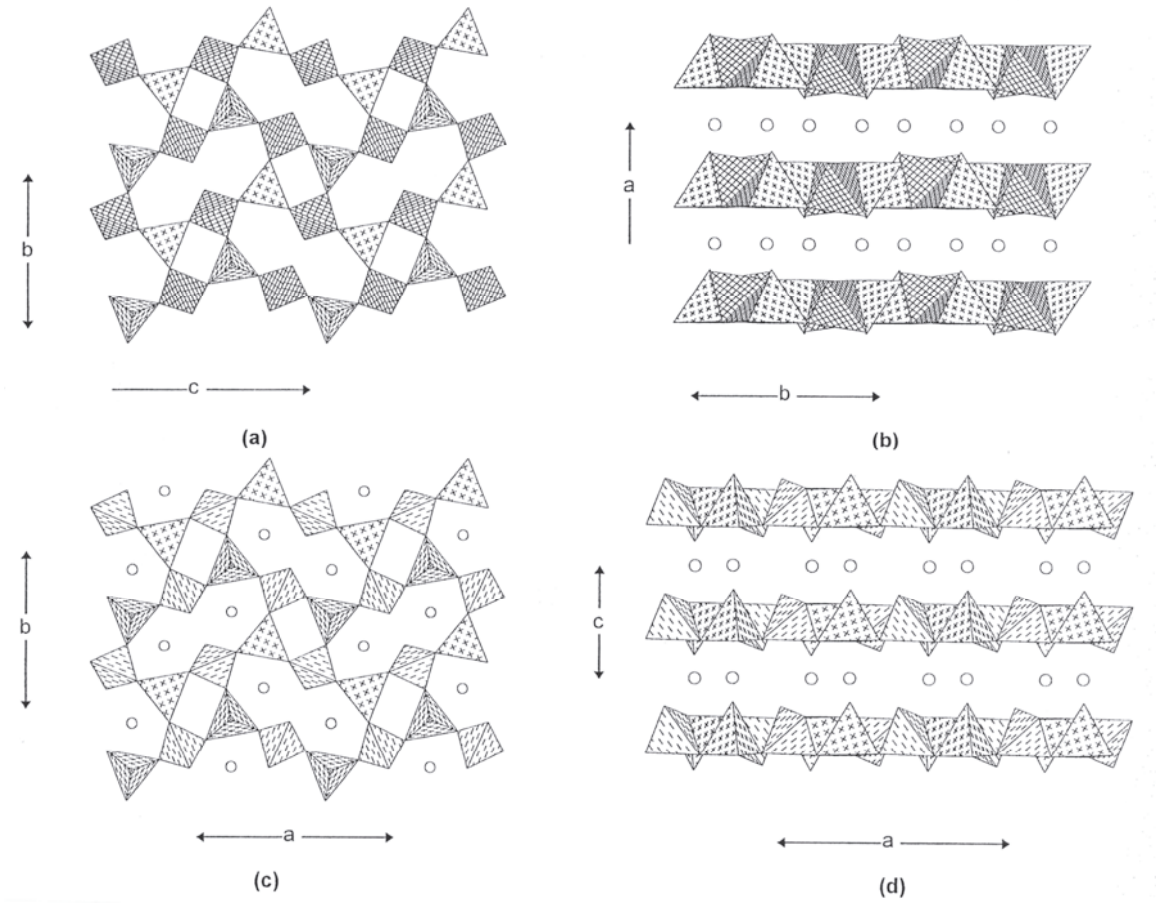

Figure 22. The crystal structures of bergslagite and herderite; (a) bergslagite projected onto (100); BeO_4 and AsO_4 (trellis-shaded) tetrahedra occur at the vertices of a net; (b) bergslagite projected onto (001); circles are Ca atoms; (c) herderite projected onto (100); BeO_4 and PO_4 tetrahedra lie at the vertices of a net; (c) herderite projected onto (010); circles are Ca atoms.

Ehrleite, $Ca_2[BeZn(PO_4)_2(PO_3\{OH\})](H_2O)_4$, has a very complicated sheet of tetrahedra, both from topological and chemical viewpoints. There is one distinct BeO_4 tetrahedron and this links to four $P\varphi_4$ groups (Fig. 23a); similarly, there is one ZnO_4 tetrahedron and this links to four $P\varphi_4$ groups. However, the $P\varphi_4$ groups link only to three or two other tetrahedra. Four-membered rings of alternating BeO_4 and PO_4 tetrahedra link through common BeO_4 tetrahedra to form chains in the *a*-direction (Fig. 23a). These chains are linked in the *c*-direction by four-membered rings of alternating ZnO_4 and PO_4 tetrahedra to form additional four-membered rings (Zn-P-Be-P). The result is an open sheet, parallel to (010), with buckled twelve-membered rings (Fig. 23a) into which project the H atoms of the acid-phosphate groups. These sheets stack along the *b*-direction (Fig. 23b) and are linked together by [7]-coordinated and [8]-coordinated interstitial Ca atoms.

Asbecasite, $Ca_3Ti^{4+}[Be_2Si_2As^{3+}{}_6O_{20}]$ contains BeO_4 and SiO_4 tetrahedra and $As^{3+}O_3$ triangular pyramids linked into thick sheets (or slabs) parallel to (001). The slab of tetrahedra and triangular pyramids consists of two sheets that meld in the *c*-direction; one

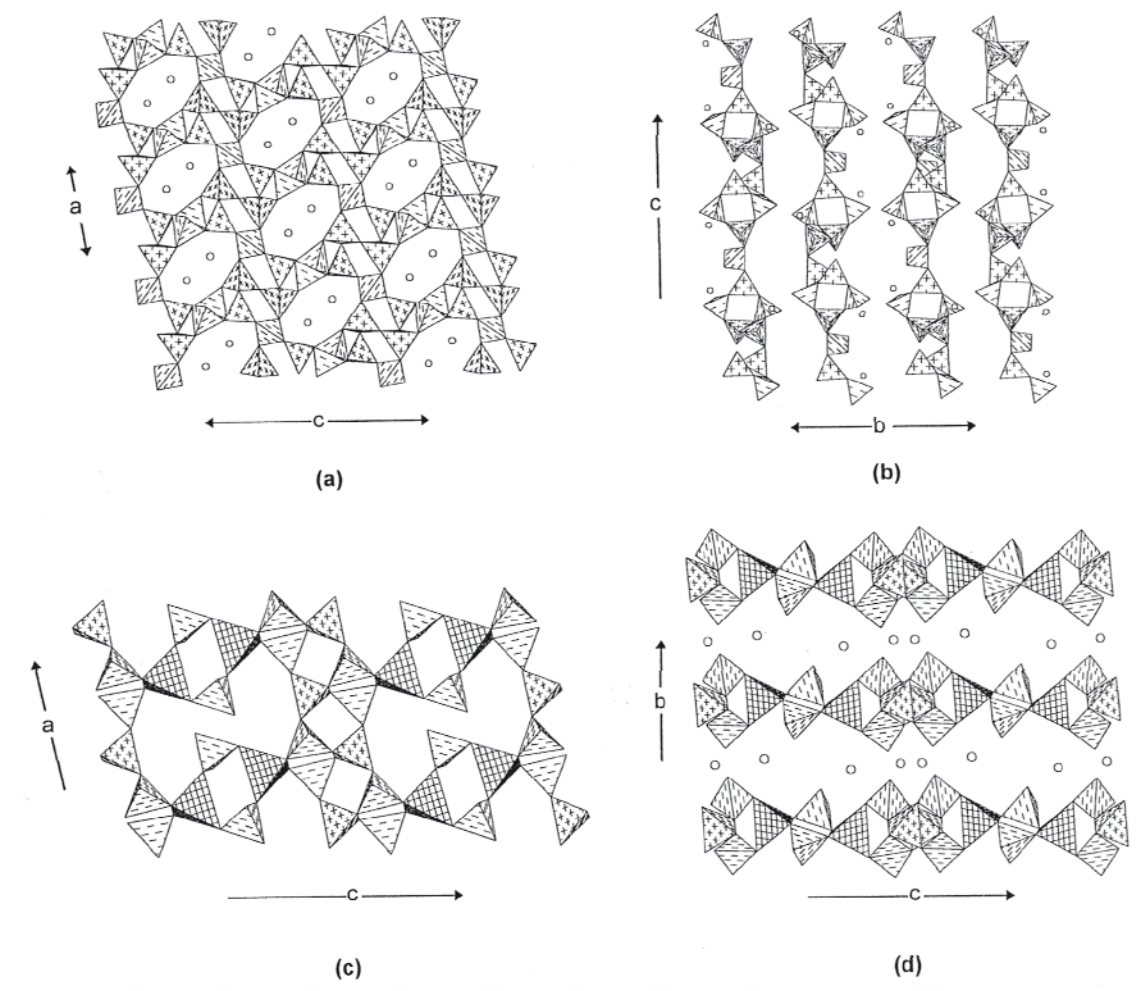

Figure 23. The crystal structures of uralolite and ehrleite; (a) uralolite projected onto (010); circles are Ca atoms; (b) uralolite projected onto (100); (c) the structural unit in ehrleite projected onto (010); BeO_4, PO_4 and ZnO_4 (trellis-shaded) tetrahedra share corners to form a sheet; (d) ehrleite projected onto (100); circles are Ca atoms.

sheet is illustrated in Figure 24a. Each tetrahedron is linked to three triangular pyramids in the plane of the sheet, and each triangular pyramid links to two tetrahedra; the result is a rather irregular-looking sheet. However, Figure 24b shows the same sheet with the $Ti^{4+}O_6$ octahedra inserted; the result is a simple 6^3 net of tetrahedra/triangles/octahedra. Hence the asbecasite sheet is simply a 6^3 net of corner-sharing tetrahedra/triangles with1/6 of the vertices omitted. Two of these layers fuse *via* linkage of BeO_4 and SiO_4 tetrahedra (Fig. 24d) to produce a thick slab that is the structural unit in asbecasite. These slabs stack in the *c*-direction and are interleaved with sheets of edge- and corner-sharing $(Ti,Sn)O_6$ octahedra and CaO_8 polyhedra (Fig. 24c).

Infinite frameworks of $T\varphi_4$ tetrahedra

The minerals of this class can be divided into seven broad groups (Table 7) based on the linkages involved in the framework: (1) structures with Be-Be linkages; (2) structures with Be-B linkages; (3) structures with Be-Be/Li-Si linkages; (4) structures with Be-Si linkages; (5) structures with Be-Si-Si-Al linkages; (6) structures with Be-Si-Si linkages; (7) structures with Be-P linkages. As with the other classes, structures with weaker *T-T* linkages *usually* have fewer interstitial cations

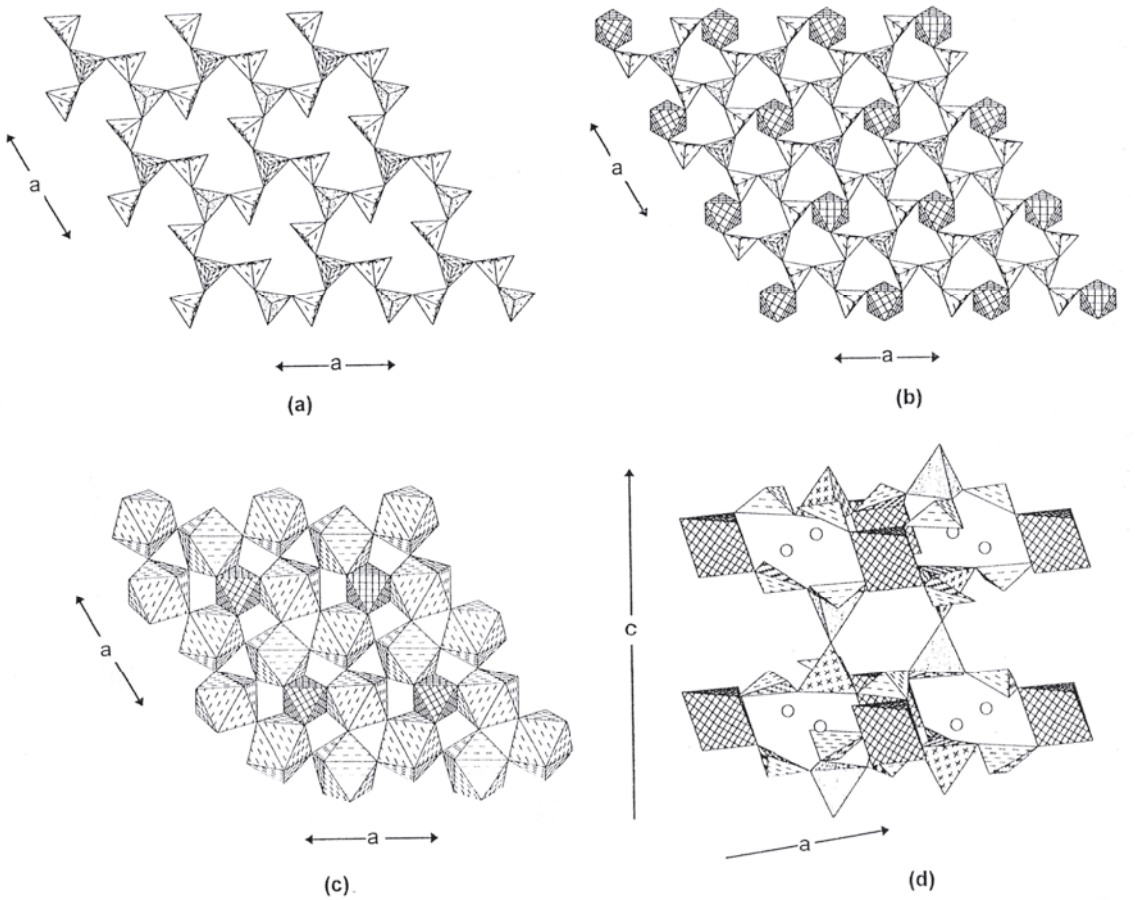

Figure 24. The crystal structure of asbecasite; (a) the sheet of BeO_4 and SiO_4 tetrahedra and $As^{3+}O_3$ triangular pyramids projected down [001]; (b) the same sheet as in (a) together with $Ti^{4+}O_6$ octahedra, showing that each polyhedron occurs at the vertices of a 6^3 net; (c) the sheet of $Ti^{4+}O_6$ octahedra and CaO_8 polyhedra projected down [001]; (d) perspective view of the way in which the sheets of tetrahedra and triangles meld to form slabs that link in the [001] direction through $Ti^{4+}O_6$ octahedra and interstitial Ca (unshaded circles); dashed triangular pyramids: $As^{3+}O_3$ groups; trellis-shaded octahedra: $Ti^{4+}O_6$ groups; broken-line-shaded polyhedra: CaO_8 groups.

(a result of the electroneutrality principle), although individual structures occur that do not follow this trend (e.g., swedenborgite).

Frameworks involving Be-Be linkages.

Behoite, $[Be(OH)_2]$, consists of a simple framework of $Be\varphi_4$ tetrahedra that is closely related to the arrangement of tetrahedra in β-cristobalite. Viewed in the *a*-direction (Fig. 25a), the structure consists of BeO_4 tetrahedra at the vertices of a 6^3 net, forming six-membered rings of tetrahedra. Note that, although some tetrahedra appear to share edges, this is not the case; careful inspection of Figure 25a shows that the apparent common edge of the two tetrahedra actually inclines in opposing directions in each tetrahedron. Viewed in the *b*-direction (Fig. 25b), the tetrahedra occur at the vertices of a 4^4 net. The resultant framework is strengthened by H-bonding between the OH anions of adjacent tetrahedra in the structure.

Bromellite, [BeO] is chemically the simplest of the beryllium minerals. Viewed down [001] (Fig. 25c), BeO_4 tetrahedra occur at the vertices of a 3^6 net, forming three-

Table 7. Beryllium minerals based on frameworks of $T\varphi_4$tetrahedra.

Mineral	*Linkage*	*Interstitials*	*Figure*
Behoite	Be - Be	H-bonding	25a,b
Bromellite	Be - Be	-	25c,d
Swedenborgite	Be-Be	$^{[6]}Sb^{5+}$, Na	26a,b
Hambergite	Be-Be-B	H-bonding	27a,b
Rhodizite	Be-B	$^{[6]}$Al, K + H-bonding	27c,d
Liberite	Be-Si-Li	Li	-
Phenakite	Be-Be-Si	-	28a,b
Hsianghualite	Be-Si	Ca, Li	29a
Trimerite	Be-Si	$^{[6]}$Mn, Ca	29b,c
Danalite	Be-Si	$^{[6]}$Fe	29d,e
Genthelvite	Be-Si	$^{[6]}$Zn	29d,e
Helvite	Be-Si	$^{[6]}$Mn	29d,e
Tugtupite	Be-Si-Si-Al	Na	30a
Bavenite	Be-Si-Si-Al	Ca + H-bonding	30b,c
Roggianite	Be-Si-Si-Al	Ca + H-bonding	31a,b
Lovdarite	Be-Si-Si	Na, K + H-bonding	32a,b,c
Bertrandite	Be-Si-Si	H-bonding	33a,b
Chkalovite	Be-Si-Si	Na	33c,d
Eudidymite	Be-Si-Si	Na + H-bonding	34a,b
Epididymite	Be-Si-Si	Na + H-bonding	34c,d
Leifite	Be-Si-Si	Na + H-bonding	35a,b
Milarite	Be-Si-Si	Ca, Na, K + H-bonding	35c,d
Odintsovite	Be-Si-Si	Ca, Ti, Na, K	35e,f
Barylite	Be-Si-Si	Ba	36a,b
Chiavennite	Be-Si-Si	$^{[6]}$Mn, Ca + H-bonding	36c,d
Beryl	Be-Si-Si	$^{[6]}$Al	36e,f
Bazzite	Be-Si-Si	$^{[6]}$Sc	36e,f
Stoppaniite	Be-Si-Si	$^{[6]}Fe^{3+}$	36e,f
Beryllonite	Be-P	Na	37a,b
Tiptopite	Be-P	K, Na, Li	38a,b
Pahasapaite	Be-P	Ca, Li	38c
Weinebeneite	Be-P	Ca + H-bonding	39a,b
Hurlbutite	Be-P	Ca	39c,d
Babephite	Be-P	Ba	40a,b

membered rings of tetrahedra. With only Be and O in the structure, the bond-valence requirements of the anion have to be satisfied solely by Be. As Be-O ≅ 0.50 vu, this requires that each O anion be linked to four Be atoms. Hence bromellite differs from the most of the tetrahedral frameworks in that each tetrahedral vertex has to link to four tetrahedra, rather than two tetrahedra as is usually the case in these framework structures. Viewed along [100] (Fig. 25d), we see a similar view: tetrahedra at the vertices of a 3^6 net.

Swedenborgite, $NaSb^{5+}[Be_4O_7]$, is an extremely elegant structure, and much can be said about its architecture solely based on the chemical composition. The principal high-

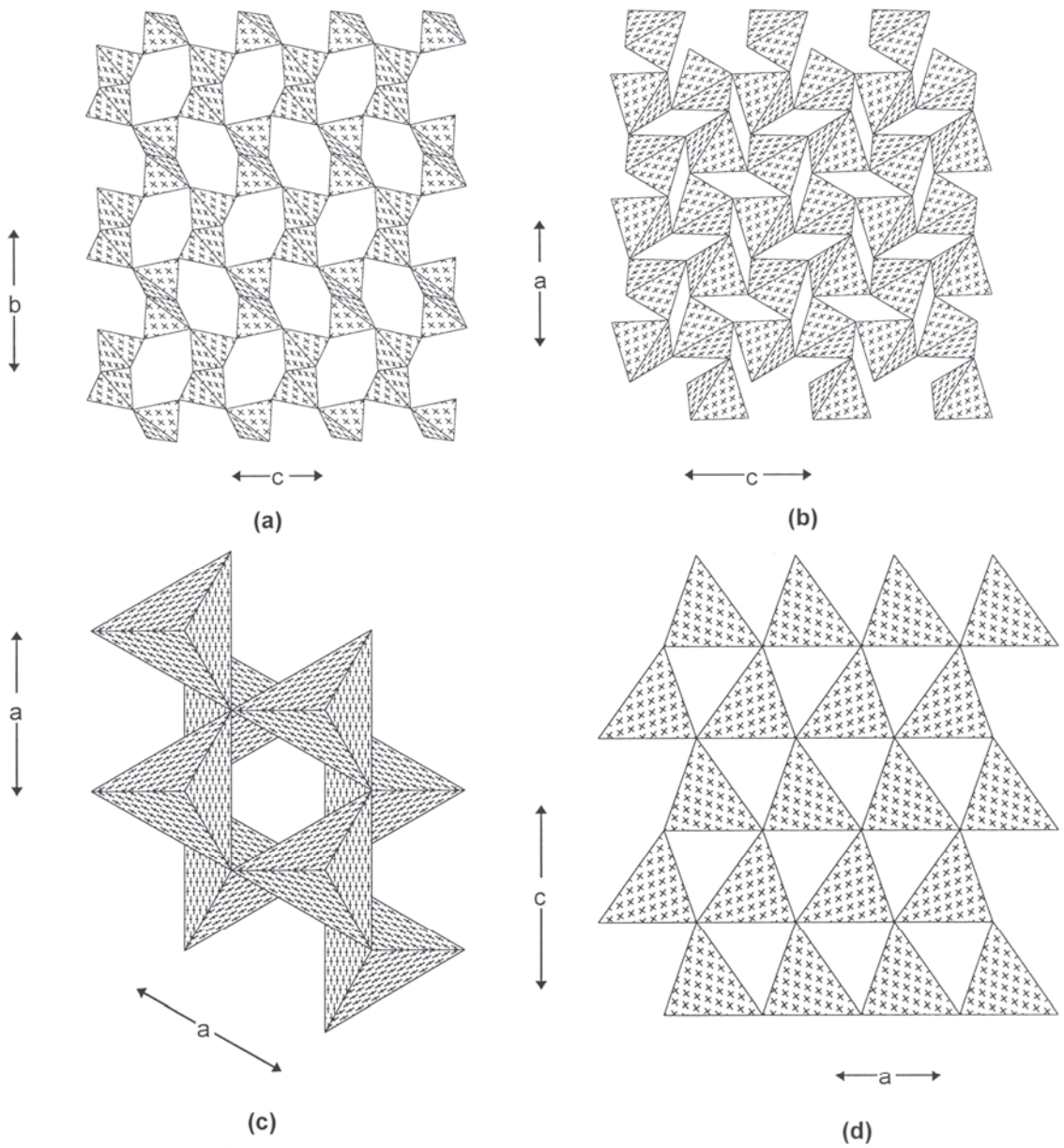

Figure 25. The crystal structures of behoite and bromellite; (a) behoite projected onto (100), a framework of corner-sharing $Be(OH)_4$ tetrahedra; the tetrahedra do *not* share an edge (they overlap in projection but are skewed in three dimensions); tetrahedra lie at the vertices of a 6^3 net; (b) behoite projected onto (010), with $Be(OH)_4$ tetrahedra lying at the vertices of a 4^4 net; (c) bromellite projected onto (001); BeO_4 tetrahedra lie at the vertices of a 3^6 net; (d) bromellite projected onto (010); BeO_4 tetrahedra lie at the vertices of a 3^6 net.

valence cation, Sb^{5+}, is usually [6]-coordinated. Presuming that this is the case in swedenborgite, this leaves an O atom whose bond-valence requirements must be satisfied by bonding to Be and Na only. The simplest way for this to occur is for one O anion to bond to four Be atoms, i.e., as in a fragment of the structure of bromellite (Fig. 25c). The resulting structure then requires linking of equal numbers of $[Be_4O_{13}]$ and (SbO_6) groups. An obvious way to arrange these motifs (because of their shape) is at the vertices of a plane hexagonal net, in which each motif is surrounded by three of the other motif.

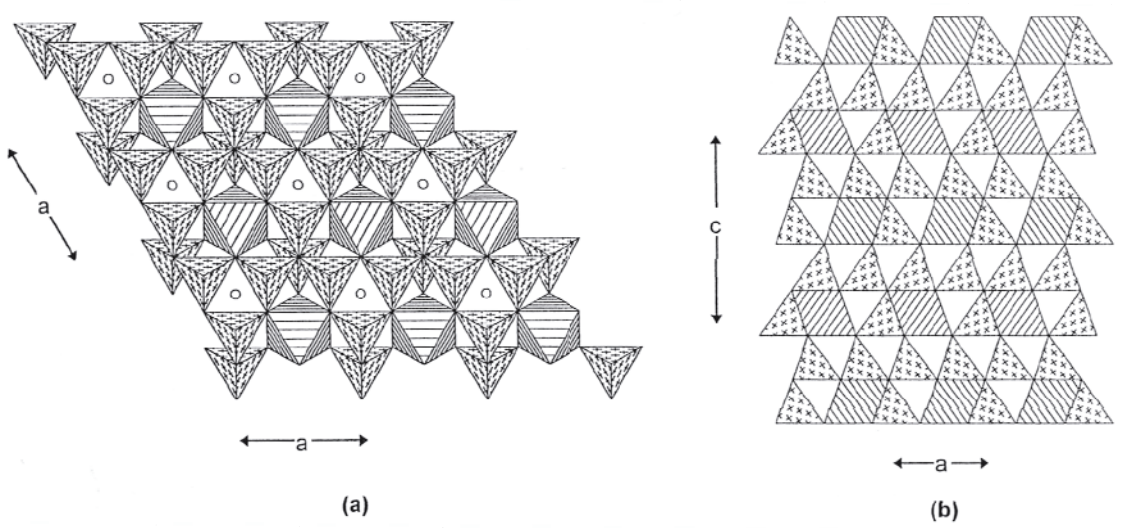

Figure 26. The crystal structure of swedenborgite; (a) projected onto (001); a framework of $[Be_4O_{13}]$ clusters, linked by sharing corners, with interstitial $^{[6]}Sb$; circles are Na atoms; (b) projected onto (010).

Linking the tetrahedral-octahedral vertices produces the stoichiometry $Sb[Be_4O_7]$ and the arrangement shown in Figure 26a, with Na atoms occupying the interstices. These layers link directly by sharing tetrahedral vertices (Fig. 26b) to form the overall framework.

Frameworks involving Be - B linkages.

Hambergite, $[Be_2(BO_3)(OH)]$, consists of a framework of $Be\varphi_4$ tetrahedra and $Be\varphi_3$ triangles. The Be:B ratio of 2:1 requires that the structure consist of $[Be_2O_7]$ dimers linked by (BO_3) triangles. This linkage can be envisaged as convoluted chains extending in the *b*-direction (Fig. 27a, in which only alternate chains are shown for clarity). The overall framework (Fig. 27b) is quite densely packed as the O atoms need to be [3]-coordinated in order to satisfy their bond-valence requirements: $O\text{-}^{[4]}Be \quad 2 + O\text{-}^{[3]}B = 0.50 \times 2 + 1.00 = 2.00$ vu.

Rhodizite, $KAl_4[Be_4(B_{11}Be)O_{28}]$, and **londonite**, $CsAl_4[Be_4(B_{11}Be)O_{28}]$, also have framework-vertex coordination-numbers somewhat higher than 2.0, as is apparent from the framework formula: $[T_{16}O_{28}]$ or $[TO_{1.75}]$. In projecting down *c* (Fig. 27c), the tetrahedra form an interrupted checkerboard pattern with K and Cs occupying the vacant squares. Viewed along [011] (Fig. 27d), the tetrahedra occupy vertices of a 3^6 net in projection, with octahedrally coordinated Al occupying the interstices. The AlO_6 octahedra occur as tetramers of the form $[Al_4O_{16}]$ in which each octahedron shares an edge with the other three octahedra to form a compact cluster with a tetrahedral cavity at the center.

Frameworks involving Be-Be/Li-Si linkages.

The structure of **liberite**, $Li_2[Be(SiO_4)]$, has been solved, but there is an error in the parameters reported, and the structure should be re-examined.

Phenakite, $[Be_2(SiO_4)]$, consists of a framework of BeO_4 and SiO_4 tetrahedra with a very interesting ordering pattern of chemically different tetrahedra over the vertices of a highly connected three-dimensional net. Both the chemical formula and the local bond-valence requirements indicate that some of the anions must be more than two-connected. Viewed down the *c*-direction (Fig. 28a), the structure consists of six-membered rings of tetrahedra connected in the (001) plane by four-membered rings of tetrahedra. One-third

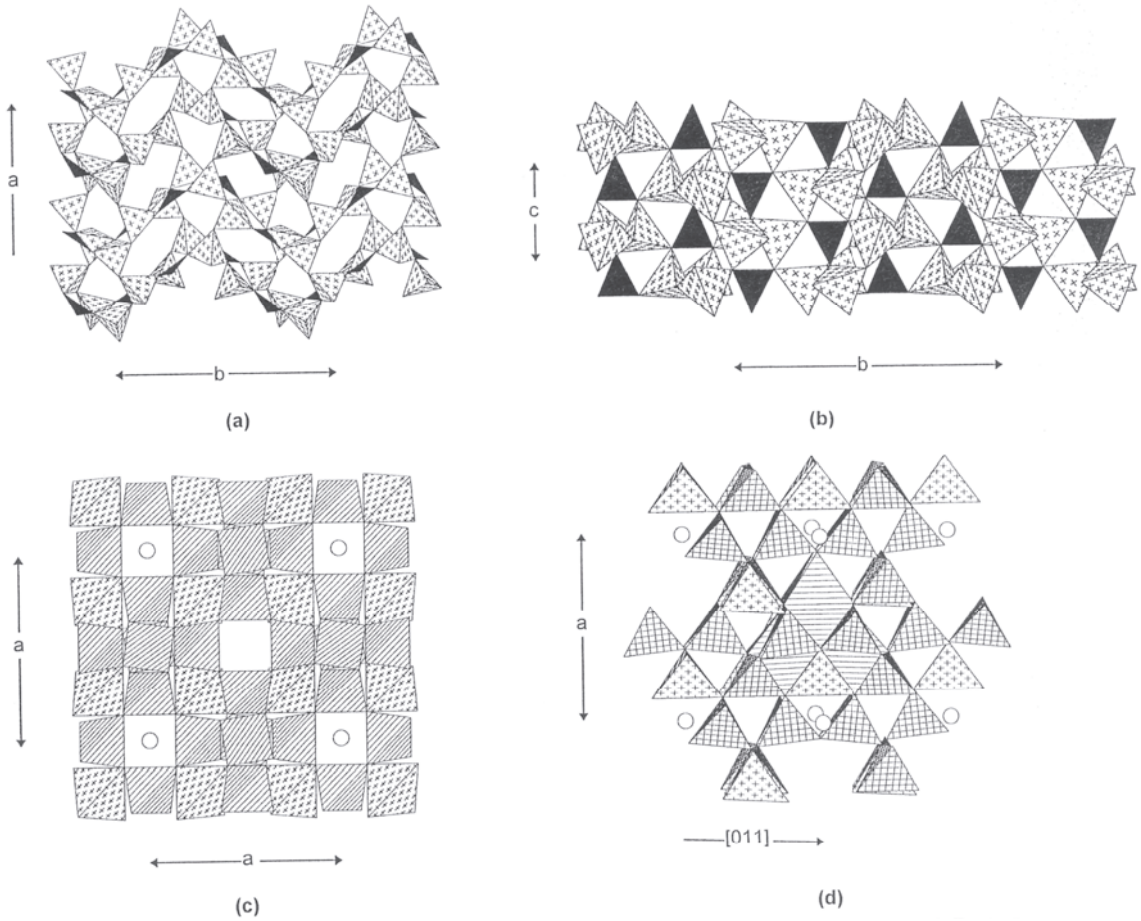

Figure 27. The crystal structures of hambergite and rhodizite; (a) hambergite projected onto (001); black triangles are $B\varphi_3$ groups; (b) hambergite projected onto (100); (c) rhodizite projected onto (001); circles are K atoms; (d) rhodizite projected onto [011]; BO_4 tetrahedra are trellis-shaded.

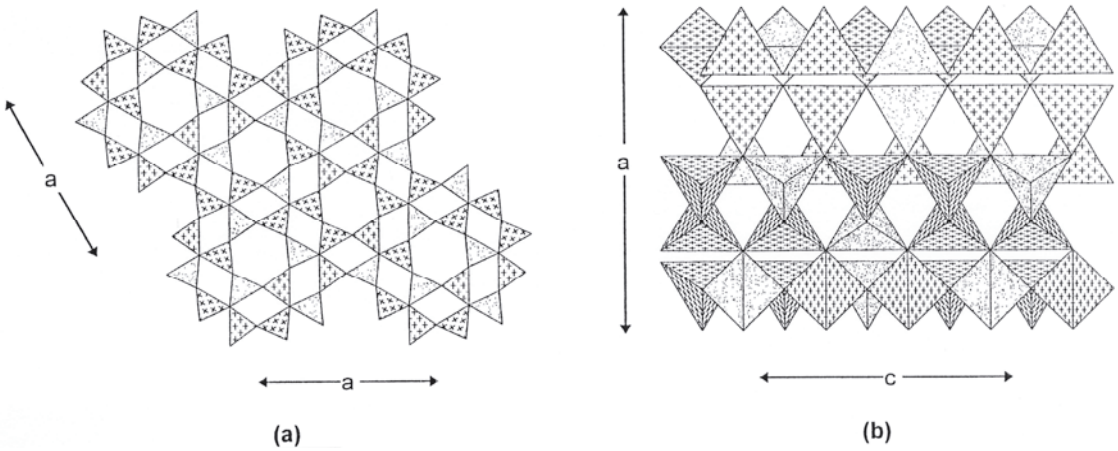

Figure 28. The crystal structure of phenakite; (a) projected onto (001); (b) projected onto (010).

of the six-membered rings consist solely of BeO_4 tetrahedra and two thirds consists of alternating BeO_4 and SiO_4 tetrahedra, giving a Be:Si ratio of 2:1. The connecting four-membered rings are of two different types: when they connect $[Be_6O_{18}]$ and $[Be_3Si_3O_{18}]$ rings, they consist of three BeO_4 tetrahedra and one SiO_4 tetrahedron; when they connect two $[Be_3Si_3O_{18}]$ rings, they consist of two BeO_4 tetrahedra and two SiO_4 tetrahedra. However, another way to look at the structure derives from considering the mineral stoichiometry and the bond-valence requirements at the anions. The simplest way in which the bond-valence requirements can be satisfied at the anions is for them to bond to two Be and one Si atoms: $2 \times 0.50 + 1.00 = 2.00$ vu. If the resulting $[Be_2SiO_{10}]^{12-}$ clusters are placed at the vertices of a plane hexagonal net such that the tetrahedra connect with each other, the structure shown in Figure 28a results. The nets of Figure 28a are stacked along the *c*-direction such that chains of tetrahedra are formed (Fig. 28b) with the sequence Be-Be-Si. The resulting structure has continuous hexagonal channels parallel to the *c*-direction.

Frameworks involving Be-Si linkages.

Hsianghualite, $Ca_3Li_2[Be_3Si_3O_{12}]F_2$, forms a framework of alternating BeO_4 and SiO_4 tetrahedra (Fig. 29a). Prominent four-membered rings of BeO_4 and SiO_4 tetrahedra are cross-linked to other four-membered rings by tetrahedra that are constituents of other four-membered rings. The result is a four-connected framework (Fig. 29a) that is very similar to the aluminosilicate framework in analcite (Mazzi and Galli 1978).

Trimerite, $CaMn^{2+}{}_2[Be(SiO_4)]_3$, consists of an ordered framework of four-connected BeO_4 and SiO_4 tetrahedra. Viewed in the *b*-direction, the tetrahedra occur at the vertices of a 6^3 net (Fig. 29b) and point up (*u*) or down (*d*) the *b* direction in the following sequence: [*uddudu*]. These sheets stack in the *b*-direction (Fig. 29c), linking through corner-sharing of tetrahedra from adjacent sheets at $y \sim 0$ and 1/2. Nine-coordinated Ca and [6]-coordinated Mn^{2+} occupy the interstices in the framework. Of particular interest is the octahedrally coordinated Mn^{2+} which occurs in face-sharing dimers. Trimerite is topologically isostructural with beryllonite, $Na[Be(PO_4)]$. In the latter structure, there are three independent Na sites as compared to one Ca site and two Mn sites in trimerite. In beryllonite, NaO_6 octahedra share faces, similar to the MnO_6 octahedra in trimerite.

Danalite, $Fe^{2+}{}_8S_2[Be_6Si_6O_{24}]$,

genthelvite, $Zn_8S_2[Be_6Si_6O_{24}]$ and

helvite, $Mn^{2+}{}_8S_2[Be_6Si_6O_{24}]$, are isostructural minerals of the *helvite* group with a framework similar to that of the minerals of the sodalite group. Four-membered alternating rings of BeO_4 and SiO_4 tetrahedra link to six-membered rings of alternating BeO_4 and SiO_4 tetrahedra (Fig. 29d). There are two interstitial species in danalite, Fe^{2+} and S^{2-}. The Fe^{2+} is four-coordinated by three O atoms and one S atom to form a distorted tetrahedron (which can also be described as an elongated triangular pyramid). The S^{2-} atom is coordinated by four Fe^{2+} atoms, and hence four distorted FeO_2S tetrahedra share a single vertex (S) (Fig. 29e).

Frameworks involving Be-Si-Si-Al linkages.

Tugtupite, $Na_8[Be_2Al_2Si_8O_{24}]Cl_2$, is isostructural with sodalite, $Na_8[Al_6Si_6O_{24}]Cl_2$. Four-membered rings of BeO_4, SiO_4 (2) and AlO_4 tetrahedra link to six-membered rings of tetrahedra (Fig. 30a). Within the four-membered rings, the linkage [Be-Si-Al-Si] does not involve Si-Si linkages. The situation in the six-membered rings is different, as there are two Si-Si linkages involved [Be-Si-Si-Al-Si-Si]. The framework charge is neutralized by [5]-coordinated Na which bonds to the interstitial Cl atom.

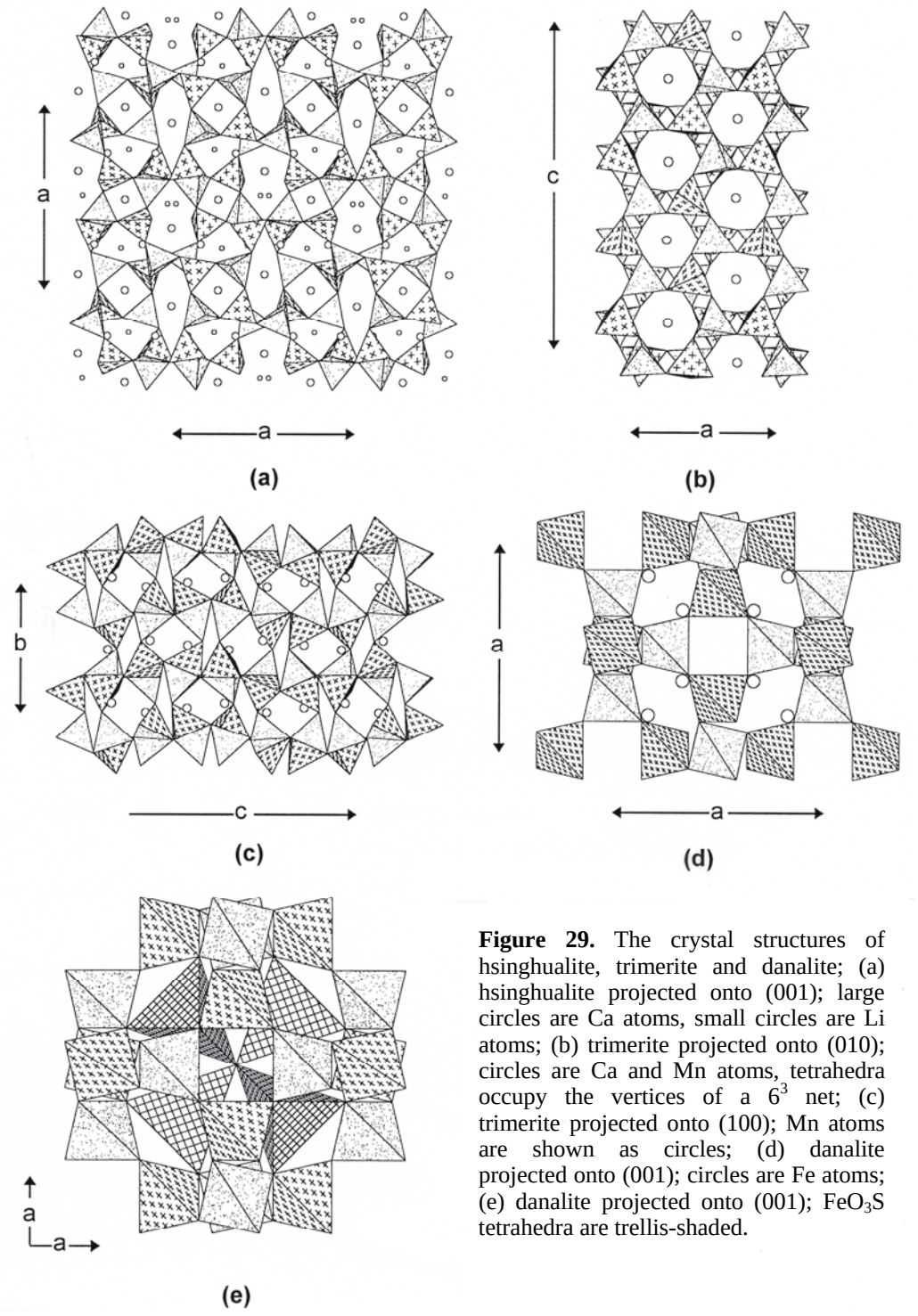

Figure 29. The crystal structures of hsinghualite, trimerite and danalite; (a) hsinghualite projected onto (001); large circles are Ca atoms, small circles are Li atoms; (b) trimerite projected onto (010); circles are Ca and Mn atoms, tetrahedra occupy the vertices of a 6^3 net; (c) trimerite projected onto (100); Mn atoms are shown as circles; (d) danalite projected onto (001); circles are Fe atoms; (e) danalite projected onto (001); FeO_3S tetrahedra are trellis-shaded.

Bavenite, $Ca_4[Be_2Al_2Si_9O_{26}(OH)_2]$, contains four-membered rings of SiO_4 and AlO_4 tetrahedra [Al-Si-Al-Si] linked through six-membered rings of SiO_4 tetrahedra to form chains that extend along the *a*-direction. Adjacent chains are linked through linear BeO_4-SiO_4-BeO_4 groups, forming two types of six-membered rings between the chains: [Be-Si-Si-Al-Si-Si] and [Be-Si-Si-Be-Si-Si]. These sheets stack in the *b*-direction, as shown in Figure 30c, with AlO_4 tetrahedra as the linking elements between the sheets. This arrangement results in large cavities that contain the [7]-coordinated interstitial

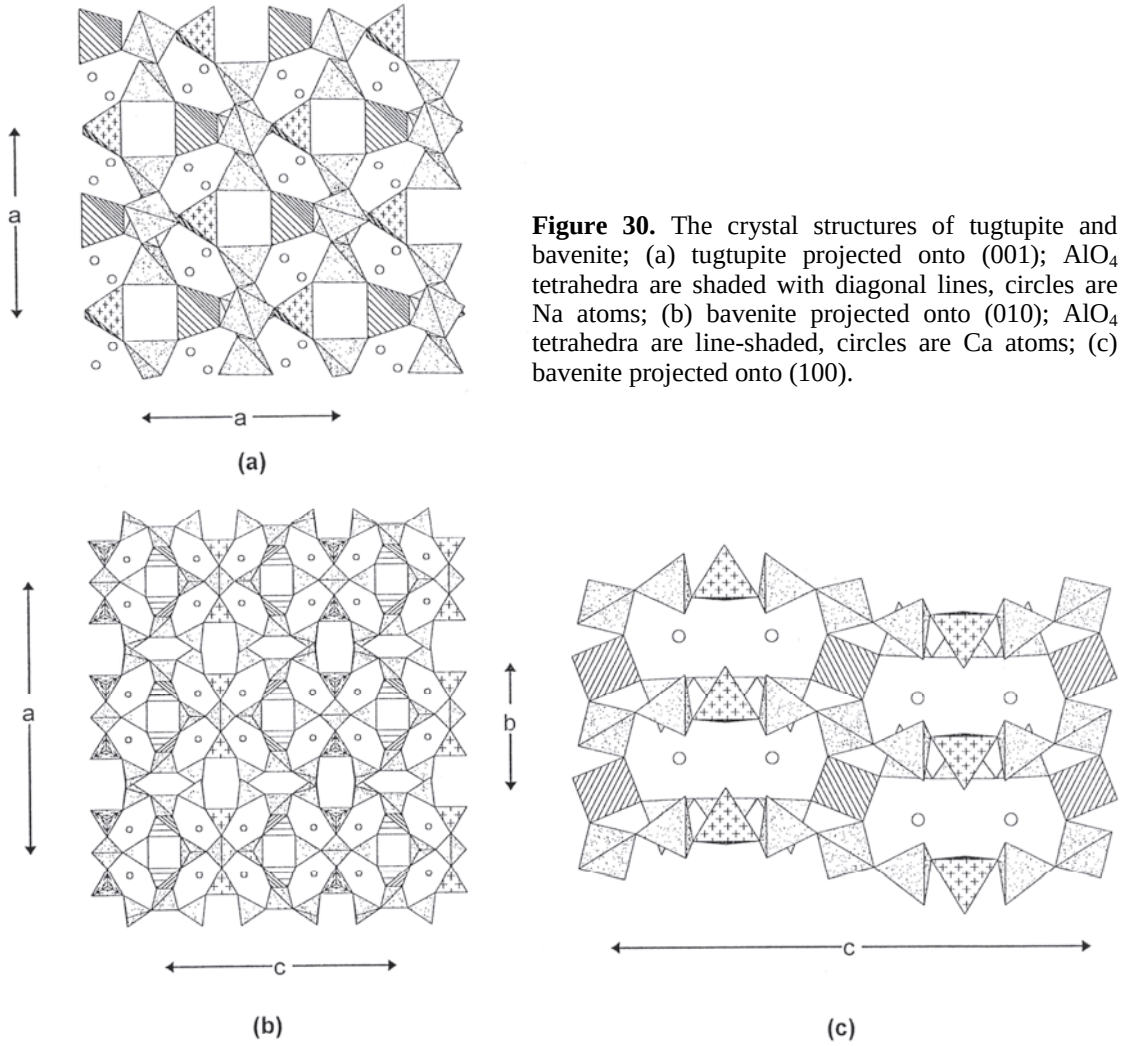

Figure 30. The crystal structures of tugtupite and bavenite; (a) tugtupite projected onto (001); AlO_4 tetrahedra are shaded with diagonal lines, circles are Na atoms; (b) bavenite projected onto (010); AlO_4 tetrahedra are line-shaded, circles are Ca atoms; (c) bavenite projected onto (100).

Ca atoms. In the structure examined by Cannillo et al. (1966), the Be and Al contents of the unit cell are close to integral, and Be and Al are completely ordered in the structure. However, Be ↔ Al substitution is indicated by compositions of bavenite from different localities, and Cannillo et al. (1966) and Kharitonov et al. (1971) suggest that the possible mechanism involves solid solution of Be and Al at one of the tetrahedrally coordinated sites, coupled to local substitution of additional H [as (OH)] into the structure.

Roggianite, $Ca_2[Be(OH)_2Al_2Si_4O_{13}](H_2O)_{2.34}$, is a completely ordered framework in which there seems to be no Be ↔ Al solid-solution. The tetrahedral framework is extremely unusual. It consists of a trellis of tetrahedra (Fig. 31a) with large inter-framework interstices that are filled with H_2O groups. Figure 31b shows that the framework consists of layers of SiO_4 and BeO_4 tetrahedra, parallel to (001), that are linked in the *c*-direction by AlO_4 tetrahedra. Within each layer are four-membered rings of SiO_4 tetrahedra and three-membered rings of BeO_4 and SiO_4 (× 2) tetrahedra (Fig. 31a). The four-membered rings stack on top of each other along the *c*-direction, linked by AlO_4 tetrahedra, and form columns that resemble the four-membered analogue of the linked six-membered rings in the structure of beryl. The smaller interstices in the framework contain [6]-coordinated Ca atoms that neutralize the framework charge.

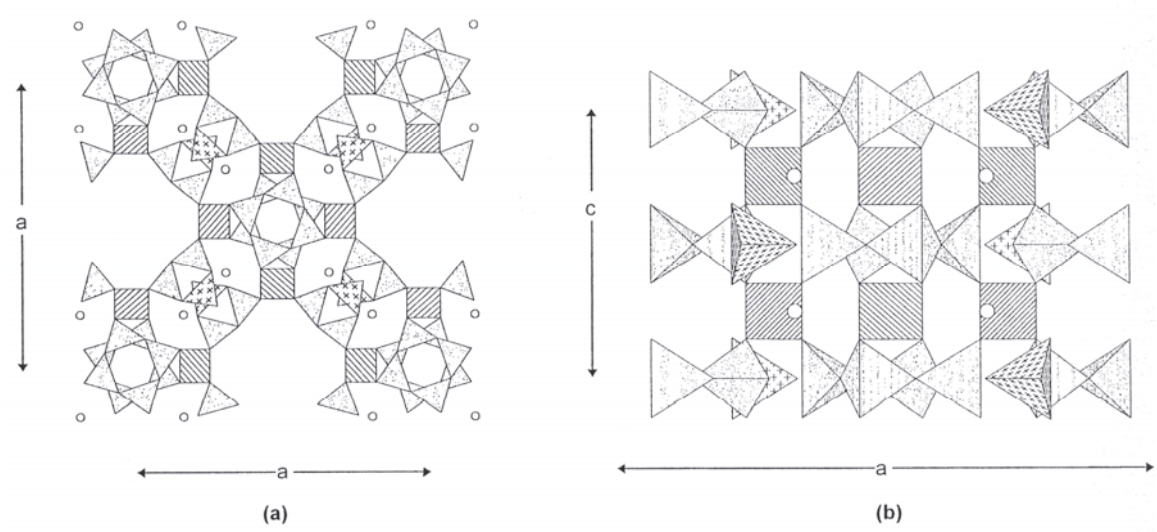

Figure 31. The crystal structure of roggianite; (a) projected onto (001); AlO_4 tetrahedra are line-shaded, circles are Ca atoms; the large interstices are filled with H_2O groups (not shown); (b) projected onto (100).

Frameworks involving Be-Si-Si linkages.

Lovdarite, $K_2Na_6[Be_4Si_{14}O_{36}](H_2O)_9$, has BeO_4 and SiO_4 tetrahedra arranged at the vertices of a 4.8^2 net when viewed in the *a*-direction (Fig. 32a). The four-membered rings consist of three SiO_4 and one BeO_4 tetrahedra, and join through Be-Si linkages along *b* and Si-Si linkages along *c*. These sheets are linked in the *a*-direction through additional SiO_4 tetrahedra (Fig. 32b) involving both Si-Si and Si-Be linkages; this linkage produces three-membered rings in the (010) plane (Fig. 32b) involving one BeO_4 and two SiO_4 tetrahedra. Adjacent sheets are shifted $(b + c)/2$ relative to each other (Fig. 32c) in order to promote intersheet linkage through the additional SiO_4 tetrahedron. The charge on the framework is neutralized by [5]- and [7]-coordinated Na and [9]-coordinated K atoms. Lovdarite shows prominent domain structures (Merlino 1990) that can be interpreted in terms of OD theory (Durovic 1997) and the occurrence of intergrowths of different polytypes.

Bertrandite, $[Be_4Si_2O_7(OH)_2]$, has the general formula $[T_6\varphi_9] = [T\varphi_{1.5}]$, indicating that the anion coordination by framework cations must be greater than 2; moreover, the H-atom must link to a Be-Be bridging anion if the anion bond-valence requirements are to be satisfied: O-Be (2) + O-H 0.5 2 + 1.0 = 2.0 vu. One anion is satisfied *via* an Si-Si linkage, and the remaining anions must be satisfied in the following way: O-Be (2) + O-Si 0.5 2 + 1.0 vu; thus four of the anions of the tetrahedral framework must be [3]-coordinated. The requirement for [3]-coordination of so many anions is satisfied by having the tetrahedra occupy the vertices of a 3^6 net (Fig. 33b). The ordering of chemical species over this net is such that the BeO_4 tetrahedra occupy the vertices of a 6^3 net and the SiO_4 tetrahedra occupy the interstices of this net. These sheets stack in the *a*-direction through Si-Si and Be-Be linkages (Fig. 33a), forming a corrugated 4.6^2 net in which the H atom links to the anion bridging the BeO_4 tetrahedra in the *a*-direction.

Chkalovite, $Na_2[BeSi_2O_6]$, must involve Si-Si linkages as well as Be-Si linkages. The tetrahedra occupy the vertices of a 4^4 net when viewed in the *b*-direction (Fig. 33c).

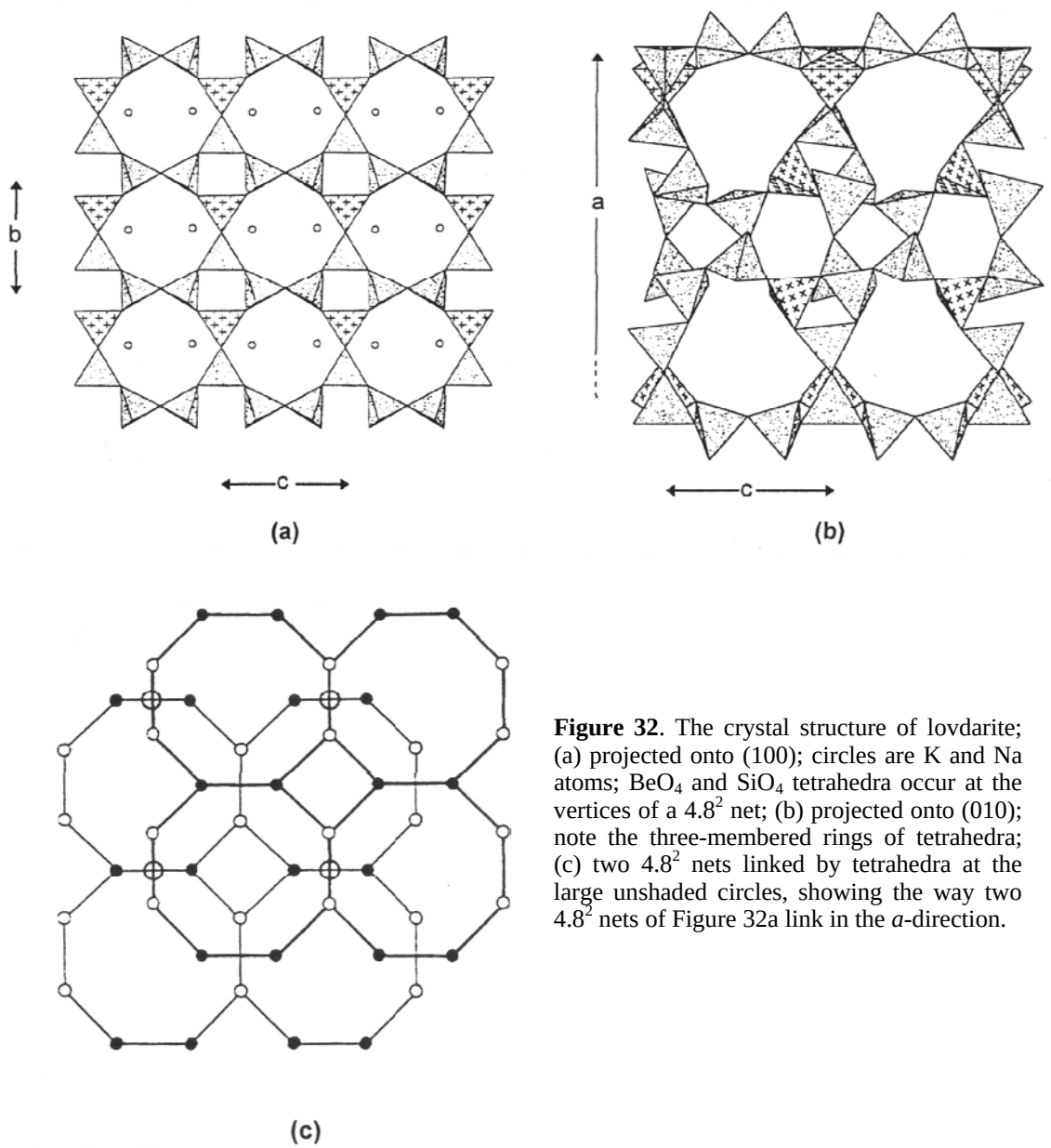

Figure 32. The crystal structure of lovdarite; (a) projected onto (100); circles are K and Na atoms; BeO_4 and SiO_4 tetrahedra occur at the vertices of a 4.8^2 net; (b) projected onto (010); note the three-membered rings of tetrahedra; (c) two 4.8^2 nets linked by tetrahedra at the large unshaded circles, showing the way two 4.8^2 nets of Figure 32a link in the *a*-direction.

There are two distinct types of four-membered ring in this net, one involving an [Si-Be-Si-Be] linkage and the other involving a [Be-Si-Si-Si] linkage. These very corrugated sheets stack in the *b*-direction, forming an 8^3 net (Fig. 33d); note that in this view, the structure also appears as $[SiO_3]$ chains extending along [021] and linked by $[Be_{0.5}\square_{0.5}O_3]$ chains. The framework charge is balanced by the presence of interstitial Na.

Eudidymite, $Na_2[Be_2Si_6O_{15}](H_2O)$, and **epididymite**, $Na_2[Be_2Si_6O_{15}](H_2O)$, are dimorphic. They both contain the $[Be_2Si_6O_{22}]$ cluster that also occurs in sorensenite (Fig. 21c). In eudidymite, these clusters link by sharing vertices of the SiO_4 tetrahedra of adjacent clusters (Fig. 34a) with non-tetrahedral cations in the interstices of the resulting network. Viewed down [010] (Fig. 34b), the structure appears as sheets of linked SiO_4 tetrahedra, joined in the [100] direction by $[Be_2O_6]$ groups. The structure of epididymite is very similar (cf. Figs. 34a and 34d). The silicate sheets contain four-membered rings (Fig. 34c) that join to form sheets which link through $[Be_2O_6]$ groups (Fig. 34e) to form a framework.

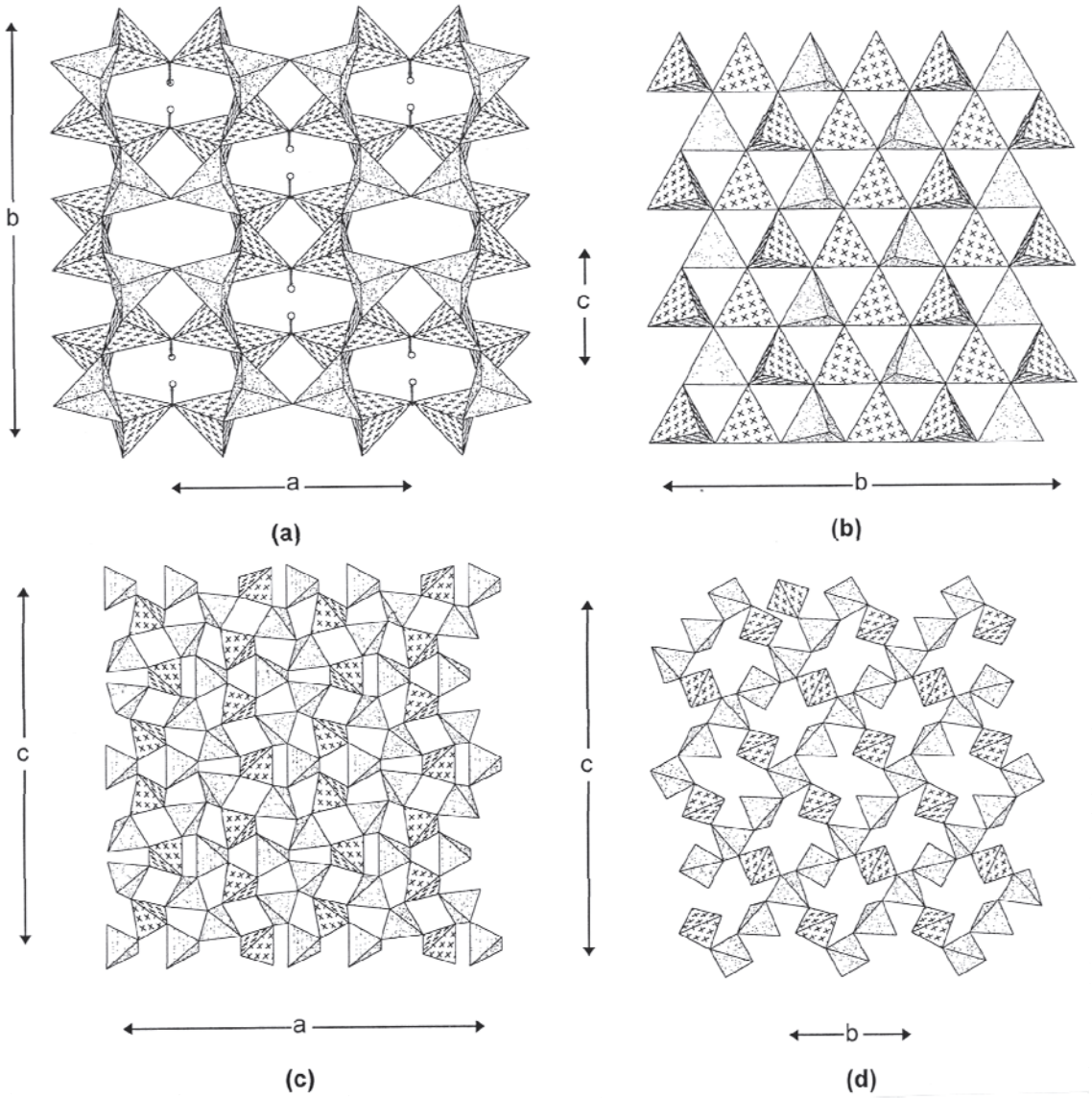

Figure 33. The crystal structures of bertrandite and chkalovite; (a) bertrandite projected onto (001); small circles are H-atoms; (b) bertrandite projected onto (100); tetrahedra occur at the vertices of a 3^6 net in this projection; (c) chkalovite projected onto (010); tetrahedra occur at the vertices of a 4^4 net; (d) chkalovite projected onto (100); tetrahedra occur at the vertices of an 8^4 net; Na atoms are omitted for clarity.

Leifite, $Na_6[Be_2Al_2Si_{16}O_{39}F_2](H_2O)_{1.6}$, has a partly ordered framework structure. There is one distinct $Be\varphi_4$ tetrahedron, but, although Al is ordered at one specific site, this site has mixed occupancy by both Al and Si, whereas the rest of the tetrahedra are SiO_4 only. Projected down the *c*-direction, the tetrahedra occur at the vertices of a very exotic two-dimensional net (Fig. 35a). Six-membered rings of $(Si,Al)O_4$ tetrahedra are linked by $[Si_4O_{11}]$ clusters consisting of an $[Si_2O_7]$ group with two additional tetrahedra sharing corners with both tetrahedra of the $[Si_2O_7]$ group. The six-membered rings occur at the vertices of a plane hexagonal net, and adjacent triplets of hexagonal rings are linked by $[Si_4O_{11}]$ groups (Fig. 35a). BeO_4 tetrahedra occur in large clover-leaf interstices

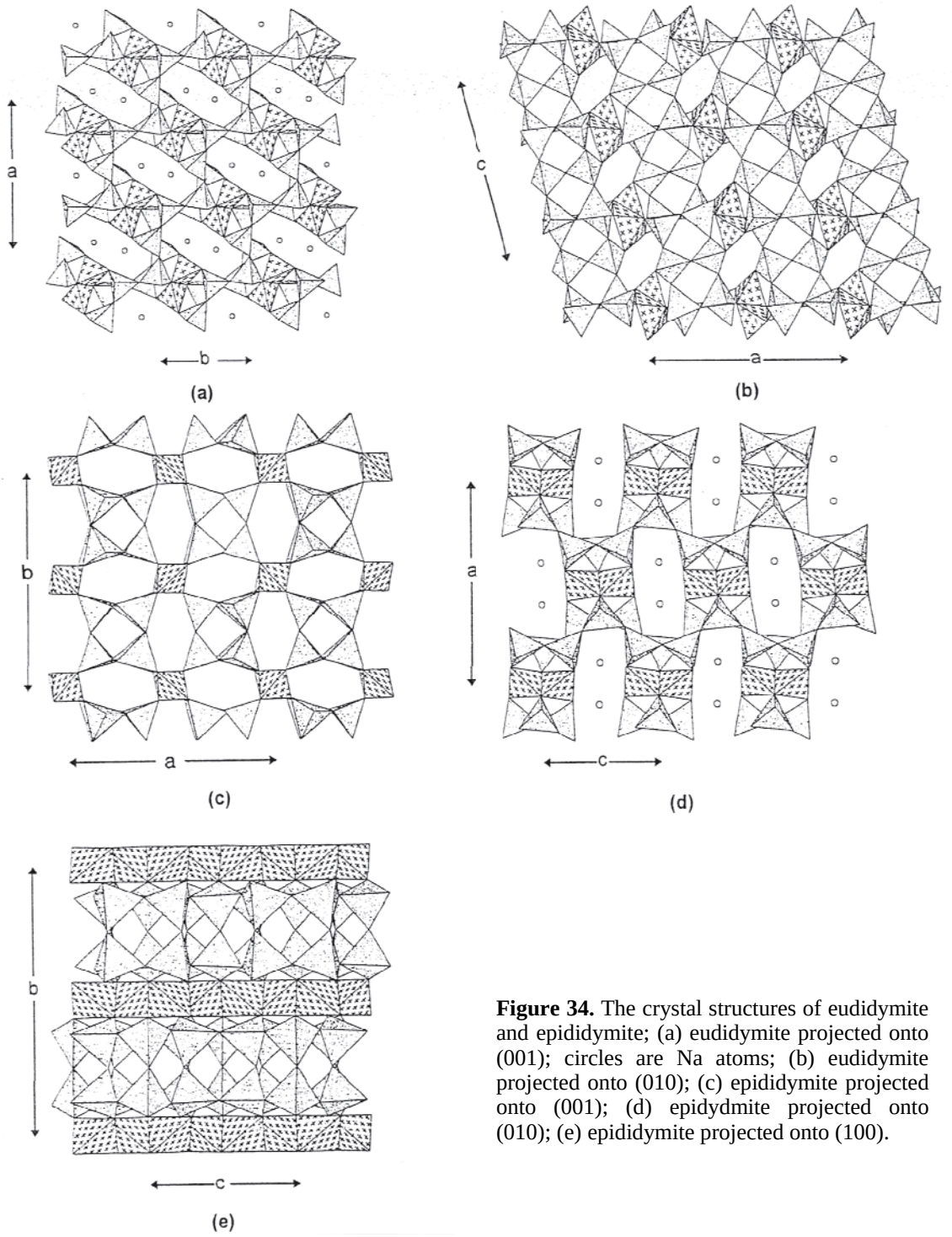

Figure 34. The crystal structures of eudidymite and epididymite; (a) eudidymite projected onto (001); circles are Na atoms; (b) eudidymite projected onto (010); (c) epididymite projected onto (001); (d) epidydmite projected onto (010); (e) epididymite projected onto (100).

of the aluminosilicate net, linking three different $[Si_4O_{11}]$ groups together. These nets stack along the *c*-direction (Fig. 35b), forming prominent $[SiO_3]$ chains. [7]-coordinated Na occurs in the interstices and H_2O groups occur down the channels formed by superposition of the six-membered rings of SiO_4 in the *c*-direction.

Milarite, $KCa_2[Be_2AlSi_{12}O_{30}](H_2O)_x$, is the type structure for a large group of minerals (Hawthorne et al. 1991). Six-membered rings of SiO_4 tetrahedra are arranged at the vertices of a hexagonal plane net (Fig. 35c) and are linked by BeO_4 tetrahedra (similar

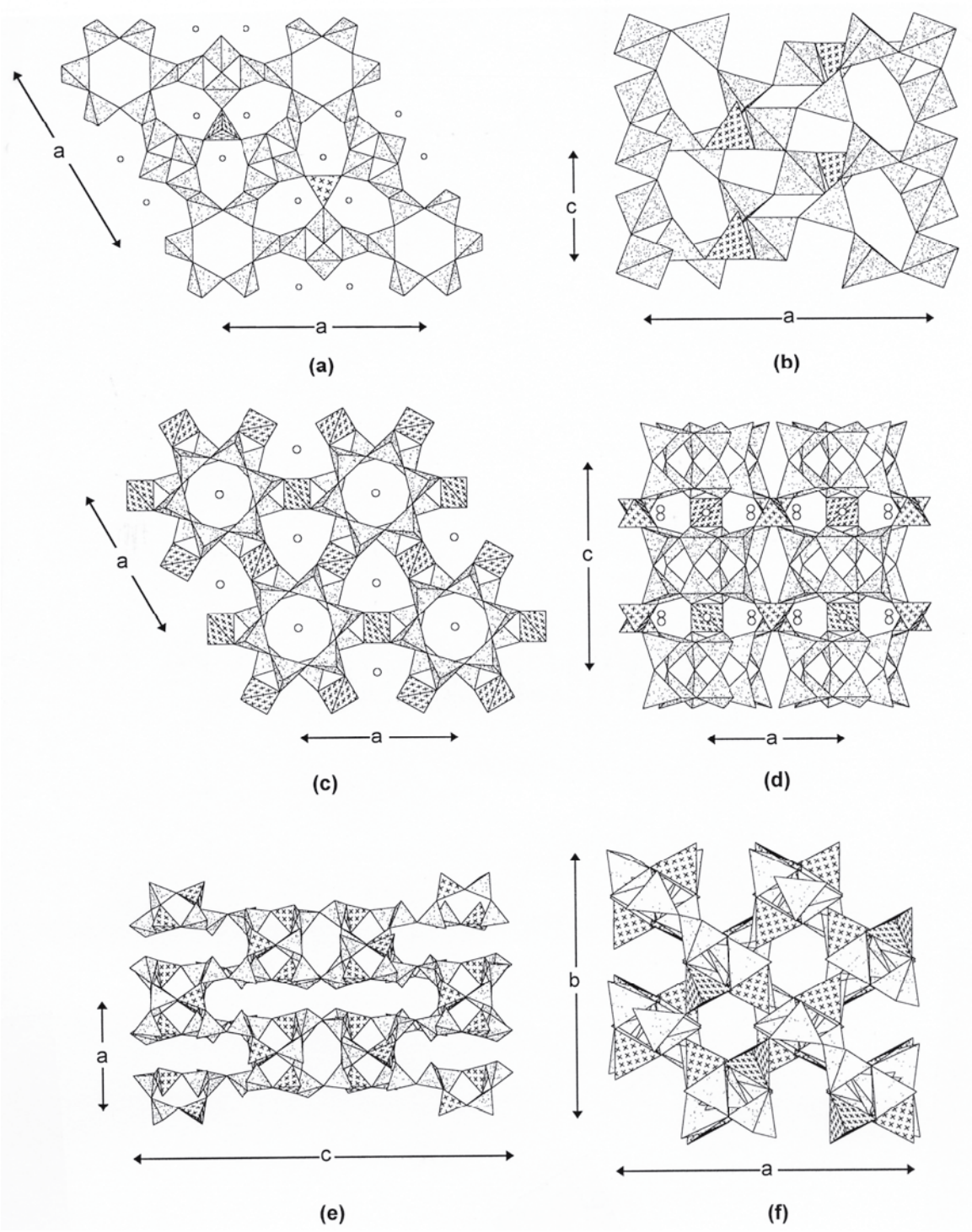

Figure 35. The crystal structures of leifite, milarite and odintsovite; (a) leifite projected onto (001); Na atoms are shown as circles; (b) leifite projected onto (010); (c) milarite projected onto (001); circles are Ca atoms; note the similarity to the structure of beryl (Fig. 36e); (d) milarite projected onto (010); note the $[Si_{12}O_{30}]$ cages; (e) the structural unit in odintsovite projected onto (010); (f) the structural unit in odintsovite projected onto (001); interstitial atoms are omitted for clarity.

to the linkage by $[Si_4O_{11}]$ groups in leifite). Note that there are pairs of six-membered rings at each vertex of the lattice, one rotated by 30° relative to the other such that the BeO_4 tetrahedra also link the two rings in the *c*-direction (Fig. 35c). These sheets then stack along the *c*-direction such that six-membered rings from adjacent sheets link vertices to form an $[Si_{12}O_{30}]$ cage (Fig. 35d). In the interstices of the resulting framework, [6]-coordinated Ca and [12]-coordinated K balance the framework charge.

Odintsovite, $K_2Na_4Ca_3Ti_2O_2[Be_4Si_{12}O_{36}]$, is a very open framework of $Be\varphi_4$ and SiO_4 tetrahedra, the interstices of which are filled with alkali, alkaline earth cations and Ti to form a fairly dense structure. Pairs of three-membered rings (Be-Si-Si) share corners to form a four-membered ring (Be-Si-Be-Si) as shown at the top left of Figure 35e. These groups meld to similar groups along *a* to form rather irregular-looking clusters of the form H. These clusters share corners to link in the *a*- and *c*-directions, forming cavities that are ~21 Å long in the *c*-direction; these cavities are arranged at the vertices of a centered plane net (Fig. 35e). Viewed in the *c*-direction (Fig. 35f), the three-membered rings are prominent. These rings are rotated 180° as they stack down *c*, forming rather irregular-looking square clusters that occur at the vertices of a centered plane lattice; note the prominent hexagonal channels in this view (Fig. 35f).

Barylite, $Ba[Be_2Si_2O_7]$, consists of an ordered framework of BeO_4 and SiO_4 tetrahedra. The ratio of Be:Si (i.e., 1:1) allows alternating BeO_4 and SiO_4 tetrahedra throughout a framework, but this type of arrangement does not occur in barylite. Instead, there are both Si-Si and Be-Be linkages; furthermore, the bond-valence requirements of the anion bridging the Be-Be linkage can also only be satisfied by further linkage to an Si cation, giving three-connected anions in the framework. Viewed in the *c*-direction (Fig. 36a), the structure consists of six-membered rings of BeO_4 and SiO_4 tetrahedra with the linkage [Be-Si-Si-Be-Si-Si]; the $[Si_2O_7]$ groups are shared between six-membered rings adjacent in the ±*a*-directions, thus maintaining ideal stoichiometry. Six-membered rings adjacent in the *b*-direction link to form four-membered rings [Be-Si-Be-Si] and three-membered rings [Be-Be-Si]. These very corrugated sheets stack in the *c*-direction (Fig. 36b); in this view, the three-membered rings and the three-connected anions are easily visible. Barylite was originally refined in the space group *Pnma* (Cannillo et al. 1969). Robinson and Fang (1977) showed barylite to be non-centrosymmetric *via* a positive second-harmonic generation test, but the crystal structure refined in space group $Pn2_1a$ was not significantly different from the structure refined in space group *Pnma*.

Chiavennite, $CaMn^{2+}[Be_2Si_5O_{13}(OH)_2](H_2O)_2$, is an ordered framework of three-connected BeO_4 tetrahedra and four-connected SiO_4 tetrahedra. Four-membered [Be-Si-Be-Si] rings link through common SiO_4 groups (*trans* vertices) to form chains in the *a*-direction (Fig. 36c). Four-membered rings of SiO_4 tetrahedra share *cis* vertices to form a staggered silicate chain. These two types of chain link along the *b*-direction to form an open sheet (Fig. 36c) that stacks in the *c*-direction to produce a very open framework (Fig. 36d). In the interstices of the framework are [6]-coordinated Mn^{2+} and [8]-coordinated Ca, together with H_2O groups that coordinate the interstitial Ca.

Beryl, ideally $Al_2[Be_3Si_6O_{18}]$, consists of an ordered framework of BeO_4 and SiO_4 tetrahedra. Six-membered rings of SiO_4 tetrahedra stack on top of one another in the *c*-direction with a relative rotation of 30° between adjacent rings. These rings are linked in the *c*- and *a*-directions by BeO_4 tetrahedra (Fig. 36e), forming a sheet that is similar in projection to that of milarite (Fig. 30c); these composite sheets stack in the *c*-direction (Fig. 36f). Interstitial [6]-coordinated Al provides further linkage both parallel and perpendicular to the *c*-axis. The resulting structure (Fig. 36f) consists of layers of SiO_4 tetrahedra interleaved with layers of BeO_4 tetrahedra and [6]-coordinated Al (shown as hollow circles in Figs. 36e,f).

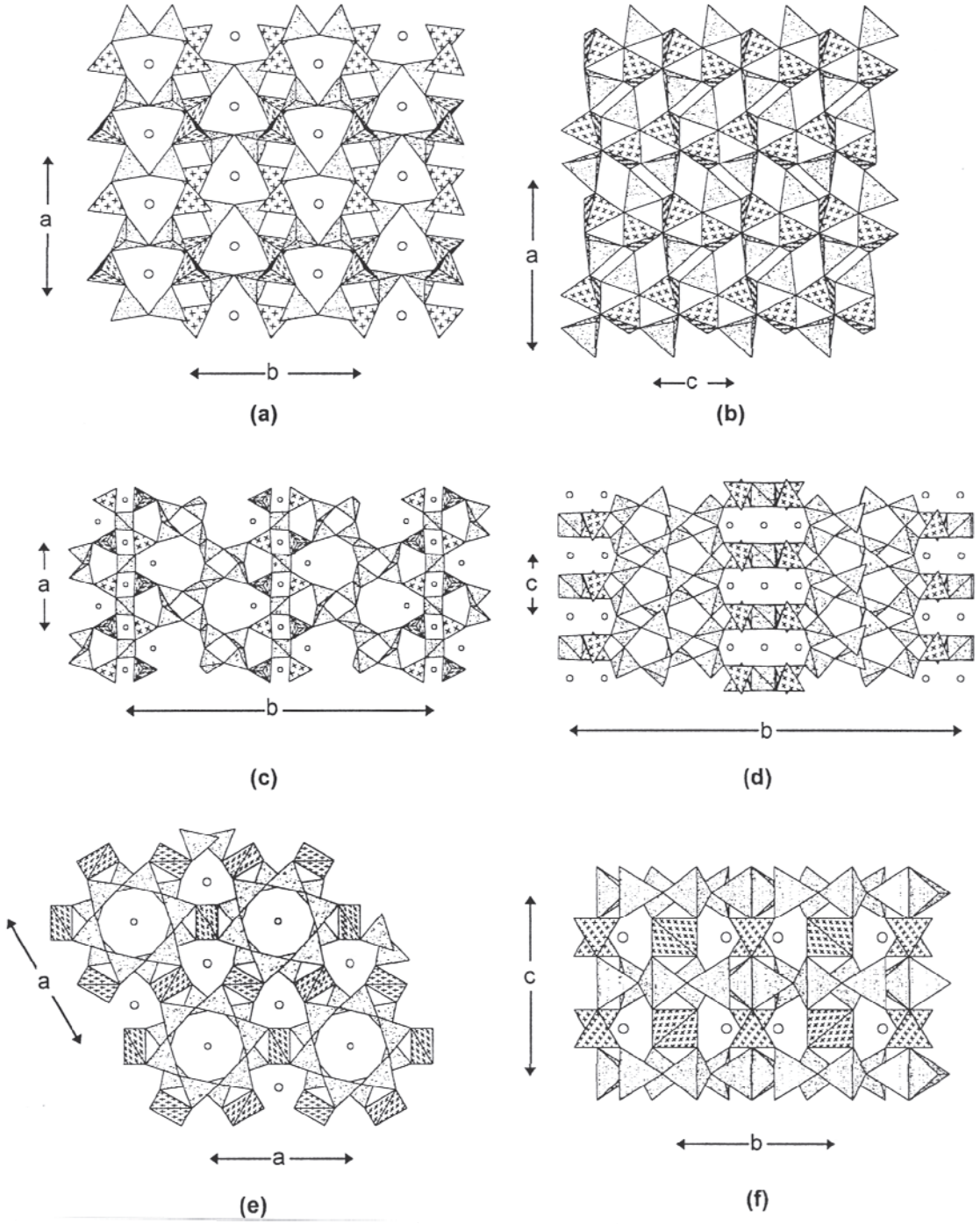

Figure 36. The crystal structures of barylite, chiavennite and beryl; (a) barylite projected onto (001); circles are Ba atoms; tetrahedra form six-membered rings in the (001) plane; (b) barylite projected onto (010); note the three-connected vertices; (c) chiavennite projected onto (001); circles are Ca and Mn atoms; (d) chiavennite projected onto (100); (e) beryl projected onto (001); large circles are Al atoms, small circles are Na, Cs and H_2O groups; note the similarity in this projection with the structure of milarite (Fig. 35c); (f) beryl projected onto (100).

There is extensive incorporation of additional constituents into the beryl structure. In particular, Na, Cs and H_2O are common substituents into the hexagonal channels through the structure (Fig. 36e), and the excess charge is compensated by substitution of Li for Be

and (Mg,Fe^{2+}) for Al (Hawthorne and Čenrý1977; Aurisicchio et al. 1988). Bazzite (Armbruster et al. 1995) is the Sc analogue of beryl, and stoppaniite (Ferraris et al. 1998; Della Ventura et al. 2000) is the Fe^{3+} analogue. Note that the stoppaniite described by Ferraris et al. (1998) lies close to the boundary of stoppaniite with the (as yet, hypothetical) composition $NaFe^{2+}Fe^{3+}[Be_3Si_6O_{18}]$. Č

Structures involving Be-P linkages.

Beryllonite, $Na[Be(PO_4)]$, consists of a well-ordered framework of alternating four-connected BeO_4 and PO_4 tetrahedra arranged at the vertices of a 6^3 net, with BeO_4 and PO_4 tetrahedra pointing in opposing directions along the *b*-axis (Fig. 37b), topologically identical to the tridymite framework. These sheets stack along the *b*-direction and share tetrahedron corners to form four-membered and eight-membered rings (Fig. 37a). The resultant framework has large channels containing [6]- and [9]-coordinated interstitial Na.

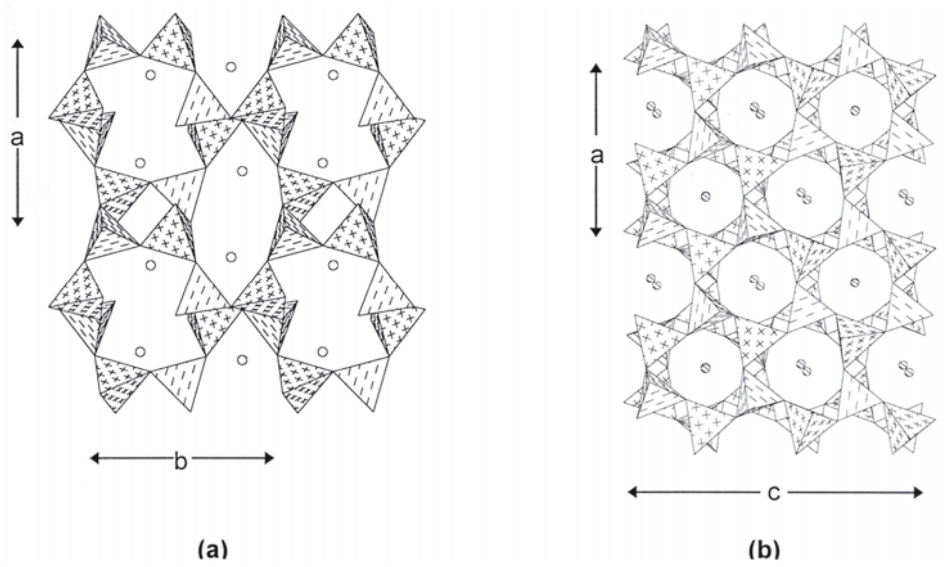

Figure 37. The crystal structure of beryllonite; (a) projected onto (001); circles are Na atoms; (b) projected onto (010); tetrahedra are arranged at the vertices of a 6^3 net.

Tiptopite, $K_2(Li_{2.9}Na_{1.7}Ca_{0.7}\square_{0.7})[Be_6(PO_4)_6](OH)_2(H_2O)_4$, is isotypic with the minerals of the cancrinite group: $Ca_2Na_6[Al_6(SiO_4)_6(CO_3)_2](H_2O)_2$ for the silicate species. The BeO_4 and PO_4 tetrahedra are arranged at the vertices of a two-dimensional net (Fig. 38a) such that all tetrahedra are three-connected when viewed down [001]. Prominent twelve-membered rings are arranged at the vertices of a 3^6 net such that they two-connect four-membered rings and three-connect through six-membered rings. These sheets link in the *c*-direction such that all tetrahedra are four-connected and, projected down the *b*-direction, form a two-dimensional net of four- and six-membered rings (Fig. 38b). The latter can be considered as a 6^3 net in which every third row of hexagons have a linear defect corresponding to an *a*-glide operation along *c*, i.e., double chains of hexagons extending in the *c*-direction and interleaved by single ladders of edge-sharing squares. Details of the rather complex relations between the interstitial species are discussed by Peacor et al. (1987).

Pahasapaite, $Ca_8Li_8[Be_{24}P_{24}O_{96}](H_2O)_{38}$, has an ordered array of BeO_4 and PO_4 tetrahedra arranged in a zeolite-rho framework, topologically similar to the minerals of the faujasite group and related to the synthetic aluminophosphate zeolite-like frameworks. Viewed along any crystallographic axis, the structure consists of prominent

eight-membered rings of alternating BeO_4 and PO_4 tetrahedra (Fig. 38c) in an I-centered (F-centered in projection) array; they are connected along the axial directions by linear triplets of four-membered rings, and to nearest-neighbor eight-membered rings through six-membered rings. All tetrahedra are four-connected; BeO_4 tetrahedra link only to PO_4 tetrahedra, and vice versa. The structure has large cages (Rouse et al. 1989) and prominent intersecting channels (Fig. 38c) that contain interstitial Li, [7]-coordinated Ca and strongly disordered H_2O groups.

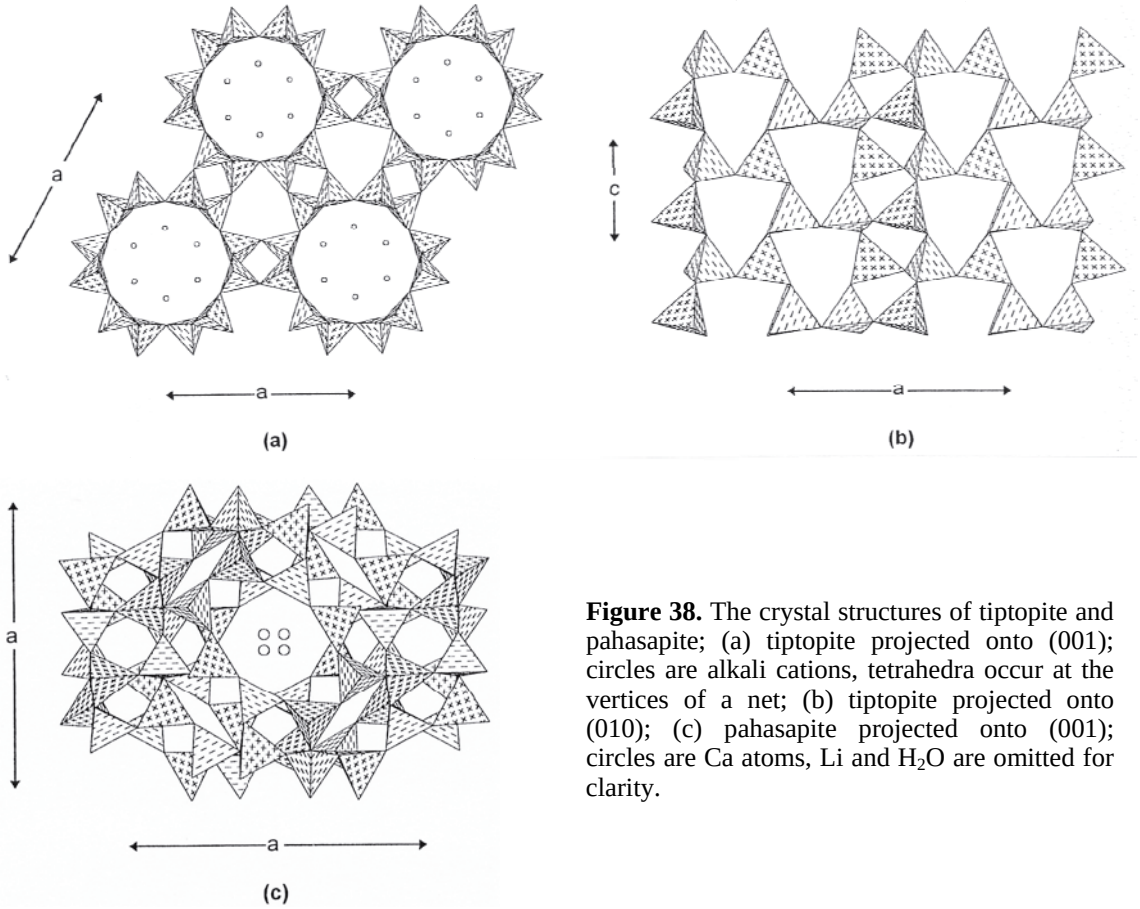

Figure 38. The crystal structures of tiptopite and pahasapite; (a) tiptopite projected onto (001); circles are alkali cations, tetrahedra occur at the vertices of a net; (b) tiptopite projected onto (010); (c) pahasapite projected onto (001); circles are Ca atoms, Li and H_2O are omitted for clarity.

Weinebeneite, $Ca[Be_3(PO_4)_2(OH)_2](H_2O)_4$, contains an ordered framework of BeO_4 and PO_4 tetrahedra; the PO_4 tetrahedra connect only to BeO_4 tetrahedra, but the BeO_4 tetrahedra connect to both PO_4 and BeO_4 tetrahedra, the Be-Be linkages occurring through the OH groups of the framework. Viewed down [100], the structure consists of alternating BeO_4 and PO_4 tetrahedra at the vertices of a 4.8^2 net (view not shown; however, cf. lovdarite, Fig. 32a); sheets superimposed in the [100] direction are offset by $(0\,\frac{1}{2}\,\frac{1}{2})$ and linked through BeO_4 tetrahedra, similar to the arrangement in lovdarite (Fig. 32c). Projected onto (001) (Fig. 39a) and viewed down [010] (Fig. 39b), the 4.8^2 sheets stack in the [100] direction and link together through additional (non-sheet) BeO_4 tetrahedra. Interstitial [7]-coordinated Ca is situated to one side of the large channels thus formed, with channel H_2O also bonded to the Ca.

Hurlbutite, $Ca[Be_2(PO_4)_2]$, consists of an ordered array of BeO_4 and PO_4 tetrahedra in which all tetrahedra are four-connected and there is alternation of BeO_4 and PO_4 tetrahedra in the structure. Viewed down [001] (Fig. 39c), the tetrahedra are arranged at the vertices of a 4.8^2 net with [7]-coordinated Ca occupying the interstices; these sheets

link along the [001] direction by vertex-sharing (Fig. 39d). The structure is very similar to that of danburite, $Ca[B_2(SiO_4)_2]$, but has a different ordering scheme (and space group).

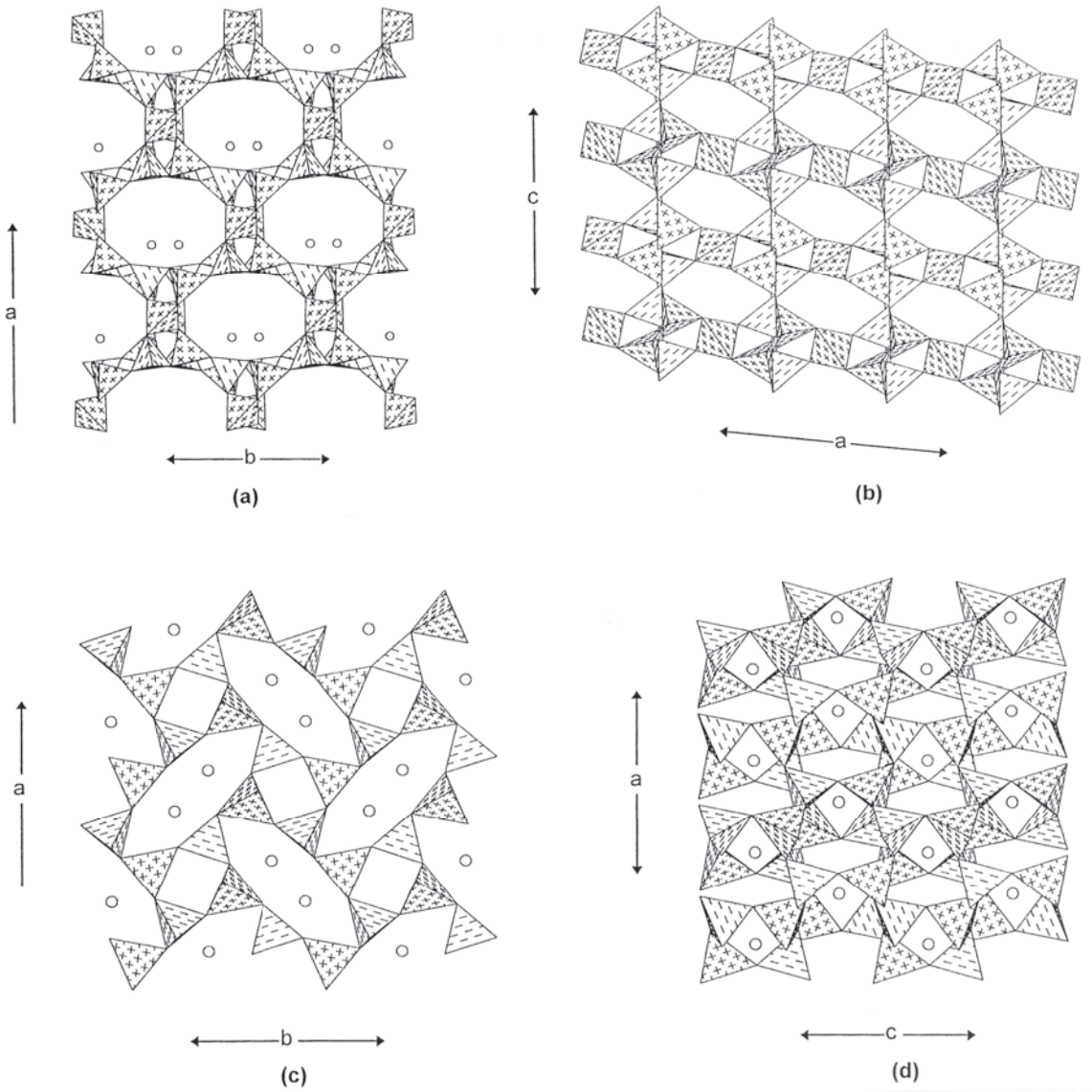

Figure 39. The crystal structures of weinebeneite and hurlbutite; (a) weinebeneite projected onto (001); circles are Ca atoms; (b) weinebeneite projected onto (010); in both (a) and (b), 4.8^2 nets of tetrahedra link in the *a*-direction through an additional BeO_4 group, (H_2O) groups are omitted for clarity; (c) hurlbutite projected onto (001); circles are Ca atoms; tetrahedra occupy the vertices of a net; (d) hurlbutite projected onto (010).

Babefphite, $Ba[Be(PO_4)F]$, is a rather unusual mineral; it is an ordered framework of PO_4 and BeO_3F tetrahedra. Projected down the *c*-direction, tetrahedra are arranged at the vertices of a 6^3 net (Fig. 40a) with the tetrahedra pointing (uuuddd). Projected down the *a*-direction, again the tetrahedra occur at the vertices of a 6^3 net (Fig. 40b) but the tetrahedra point (uuuuuu). Both the $Be\varphi_4$ and the PO_4 tetrahedra are three-connected, and the F anions are the non-*T*-bridging species in the $Be\varphi_4$ tetrahedra. The interstices of the framework are occupied by [9]-coordinated Ba.

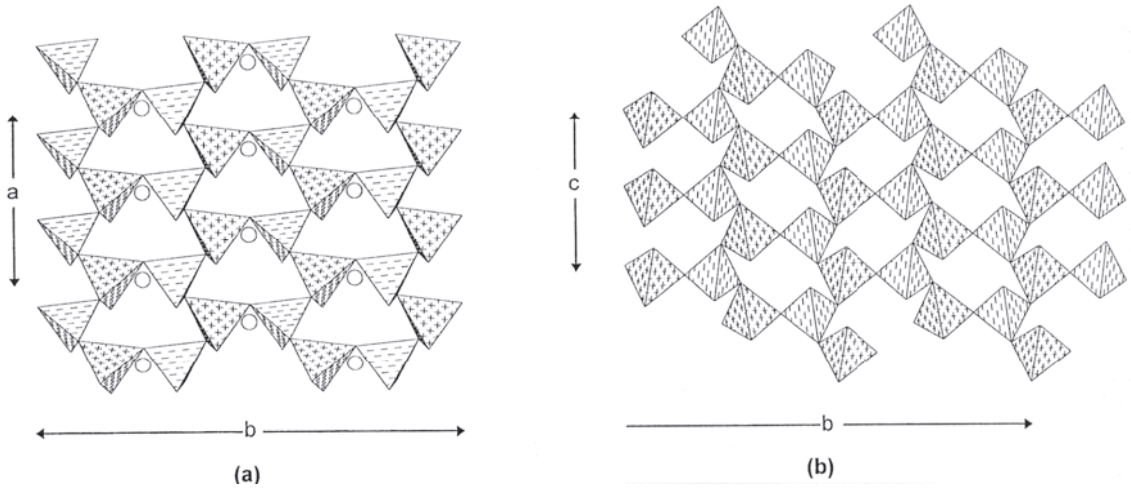

Figure 40. The crystal structure of babefphite; (a) projected onto (001); circles are Ba atoms; tetrahedra occur at the vertices of a 6^3 net; (b) projected onto (100); tetrahedra occur at the vertices of a 6^3 net.

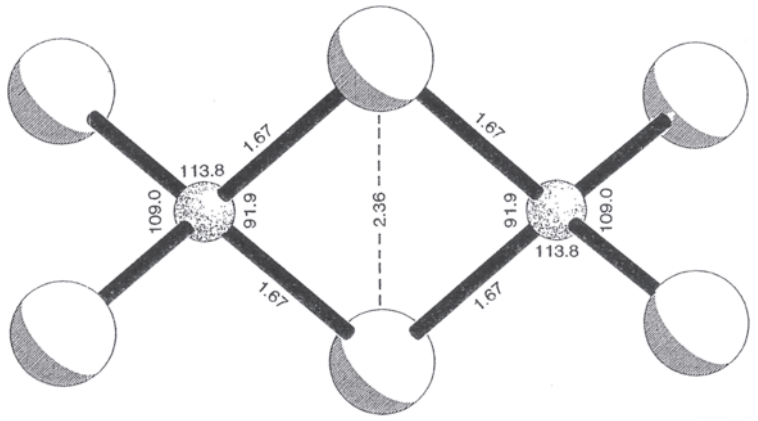

Figure 41. The $[Be_2O_6]$ group of edge-sharing BeO_4 tetrahedra:
Be, random-dot-shaded circles
O, highlighted circles.
Interatomic distances are the mean values from the structures of sorensenite, eudidymite and epididymite.

THE $[Be_2O_6]$ GROUP

An unusual stereochemical feature of a few of the Be minerals is the presence of the $[Be_2O_6]$ group (Fig. 41), a pair of edge-sharing tetrahedra. Of the oxyanion minerals, only the Be-bearing commonly show this feature; the sulfates, phosphates, silicates, aluminosilicates, etc., do not show edge-sharing tetrahedra involving their principal cations, although synthetic materials with edge-sharing LiO_4 tetrahedra are known. Pauling's third rule (Pauling 1929) predicts that high-valence low- coordination-number cations should not share coordination-polyhedra edges or faces because of the ensuing destabilization caused by strong cation-cation interactions; thus we normally do not expect tetrahedral oxyanions to share edges or faces. However, low-valence high-coordination-number cations frequently share coordination-polyhedra edges and faces, and hence the issue here is the position of the boundary between these two types of cations. Of interest in this regard is the corundum structure: This has octahedrally coordinated Al, and the octahedra share both edges and faces. Although this arrangement of face-sharing AlO_6 octahedra is unusual, it does occur in other structures besides corundum. In corundum, the mean bond-valences are 0.50 vu, similar to the mean bond-valence in BeO_4 tetrahedra. The Al-Al approach is ~2.2 Å without distortion, whereas the

Be-Be approach is ~1.9 Å without distortion; however, the formal charges are higher for Al compared with Be. Thus it seems that $^{[6]}$Al and $^{[4]}$Be are where Pauling's third rule begins to lose its applicability.

The $[Be_2O_6]$ group occurs in the structures of sorensenite (Figs. 21c,d, Table 6), eudidymite (Figs. 34a,b; Table 7) and epididymite (Figs. 34c,d,e; Table 7). Figure 41 shows the average geometry of the $[Be_2O_6]$ group from these structures. It is immediately apparent that the two tetrahedra are significantly relaxed (i.e., distorted) relative to the holosymmetric arrangement. The bonds to the anions defining the shared edge are much longer than the mean bond-length (1.629 Å), the shared edge itself is much shorter than the mean edge-length (3.07 Å), and the angle subtended by the shared edge at the cation is much less than the holosymmetric value of 109.47°. All of these relaxations serve to increase the Be-Be distance (2.33 Å) relative to the separation of 1.88 Å for a holosymmetric arrangement, presumably stabilizing this type of linkage.

SOLID SOLUTION OF BERYLLIUM WITH OTHER CATIONS IN MINERALS: CRYSTAL CHEMISTRY

Beryllium may form distinct crystal structures of minerals in five different ways:

(1) formation of a structure that is unrelated to any non-Be-bearing structure, and in which Be occupies completely one or more distinct sites;
(2) formation of a structure that is topologically similar to other non-Be-bearing structures, and in which Be occupies completely one or more distinct sites;
(3) formation of a structure that is unrelated to any non-Be-bearing structure, but in which Be shows solid solution with other cations;
(4) formation of a structure that is topologically similar to other non-Be-bearing structures, but in which Be shows solid solution with other cations;
(5) formation of a structure that is topologically similar to a non-Be-bearing structure, but in which Be occupies a site not occupied in the Be-absent structure.

Most of the minerals of Appendix A fall into category (1). A few minerals fall into category (2); here, Be completely replaces another cation at one (or more) of a set of sites, lowering the symmetry of the atomic arrangement. An excellent example of this is the amphibole joesmithite (Fig. 11d) in which Be replaces Si completely at two of the four *T*(2) sites of the $[T_8O_{22}]$ chain, thereby breaking the mirror symmetry of the tetrahedral chain to produce a symmetrically (but not topologically) distinct site. Categories (1) and (2) are the most frequent for Be minerals. However, categories (3) and (4) involve solid solution and give rise to more common and flexible structures, and the details of the types of solid solution are of interest.

Beryl

The prototype mineral of the beryl group is beryl itself: $Al[Be_3Si_6O_{18}]$. Beryl may incorporate significant Li and Na (+ Cs, Rb) into its structure [i.e., is of category (4) above]. Belov (1958) proposed direct substitution of Be by Li: Li $\leftrightarrow$ Be, and this was supported by the results of a partial refinement of a Cs-Li-enriched beryl by Bakakin et al. (1969). Conversely, Beus (1960) proposed a coupled substitution of the form $^{[6]}$Li + $^{[4]}$Al $\leftrightarrow$ $^{[6]}$Al + $^{[4]}$Be which was supported by a preliminary refinement of a Cs-rich beryl by Evans and Mrose (1966). Hawthorne and Čenrý (1977) refined the crystal structure of a (Cs,Li)-rich beryl and showed definitively that Li substitutes directly for Be at the *Be* (tetrahedrally coordinated) site, i.e., ^{Be}Be. Figure 42a shows the variation in <*Be*-O> distance as a function of Be content; as $^{[4]}$Be (r = 0.27 Å) is smaller than $^{[4]}$Li (r = 0.59 Å, Shannon 1976), the <*Be*-O> distance increases with decreasing Be occupancy (and increasing Li occupancy). Moreover, the slope of the relation in Figure 42a is in accord

with that expected for a hard-sphere model.

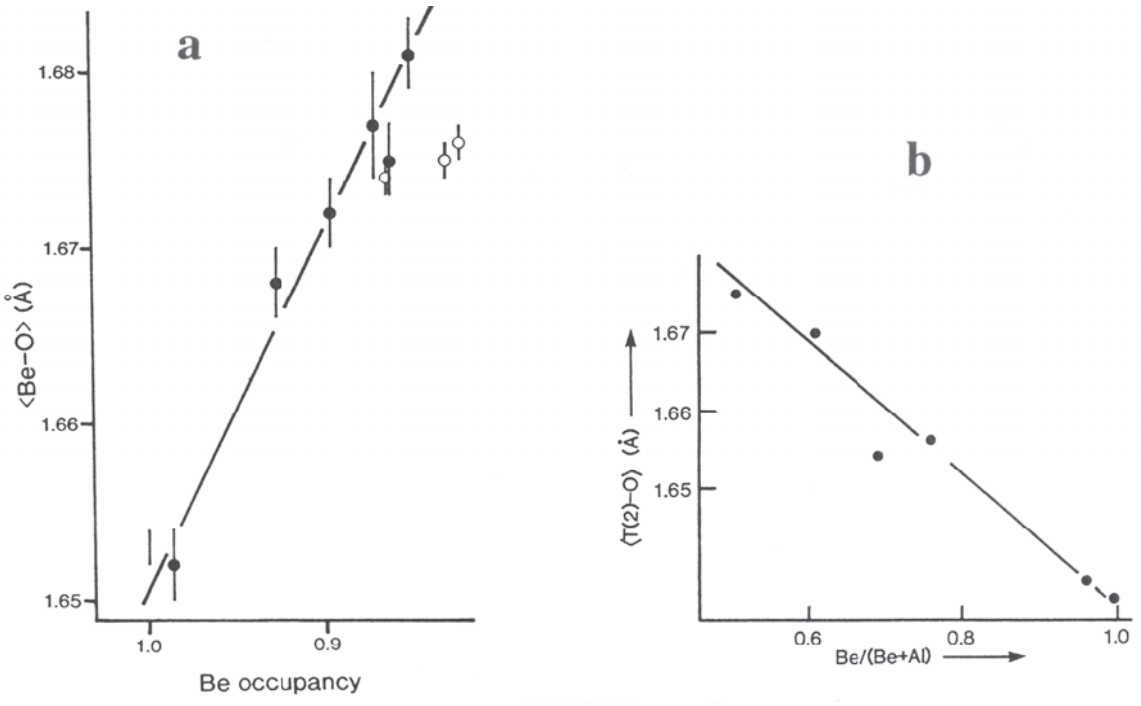

Figure 42. (a) Variation in <*Be*-O> distance as a function of Be content of the *Be* site (= Be + Li) in alkali-bearing beryl; solid circles, Sherriff et al. 1991; Hawthorne and Cerny 1977; Brown and Mills 1986; hollow circles (not included in regression), Aurisicchio et al. 1988; vertical dash is the mean value for synthetic alkali-free beryl. (b) Variation in <*T*(2)-O> distance as a function of Be/(Be + Al) ratio at the *T*(2) site in milarite (after Hawthorne et al. 1991).

In end-member beryl, the ideal bond-valence sum at the O(2) anion is 2.00 vu. Local replacement of Be by Li reduces the sum as follows: 2 - 0.50 + 0.17 = 1.67 vu; how is this discrepancy compensated? To some extent, this can be done as proposed by Hawthorne and Cerny (1977): The structure adjusts by shortening the Si-O(2) bond and lengthening both Si-O(1) and Si-O(1)a bonds, the resultant deficiency at O(1) being compensated by bonding from the channel alkali atoms that are part of the ^{Be}Li + ^{C}(Na,Cs) ↔ ^{Be}Be + $^{C}\square$ mechanism of substitution. Figure 43 shows this to be the case for continuous substitution; Si-O(1) and Si−O(1)a gradually lengthen with decreasing Be, and Si-O(2) decreases. The additional contribution of bond valence from Li (at the *Be* site) to O(2) results in satisfaction of the local short-range bond-valence requirements. However, the replacement of Be by Li leads to a net charge deficiency that is balanced by substitution of alkali cations, specifically Na and Cs, into the channel of the beryl structure. The resultant mechanism of incorporation of Li and (Na,Cs) into the beryl structure may be written as ^{Be}Li + ^{C}(Na,Cs) → ^{Be}Be + $^{C}\square$, where *C* denotes the channel sites.

Milarite

The prototype mineral of the milarite group is milarite: $KCa_2[AlBe_2Si_{12}O_{30}](H_2O)$, but many minerals of this group [e.g., brannockite: $KSn_2[Li_3Si_{12}O_{30}]$ and poudrettite: $KNa_2[B_3Si_{12}O_{30}]$ do not contain Be, and milarite shows extensive solid solution, with Al substituting for Be at the *T*(2) site [i.e., is of category (4) above]. Hawthorne et al. (1991)

showed that the <*T*(2)-O> distance decreases with increasing Be/(Be+Al) ratio (Fig. 42b); the slope of the relation in Figure 42b is in accord with a hard-sphere model for solid solution between Be ($^{[4]}$r = 0.27 Å) and Al ($^{[4]}$r = 0.39 Å).

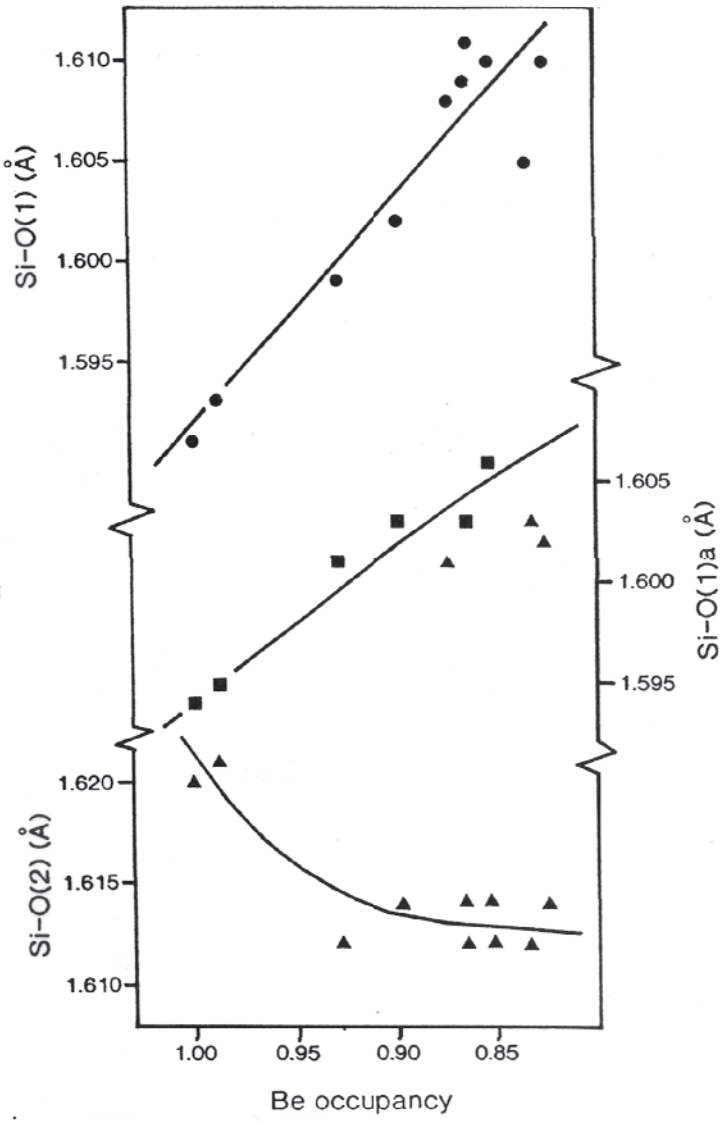

Figure 43. Variation in Si-O distances with Be occupancy of the *Be* site in the beryl structure (after Sherriff et al. 1991).

Beryllium-bearing cordierite

Cordierite has an ideal end-member formula that is usually written as $Mg_2Al_4Si_5O_{18}$. However, cordierite has a structure that is topologically identical to that of beryl (Fig. 36e), and hence it is more informative if we write their formulae as $Al_2[Be_3Si_6O_{18}]$ and $Mg_2[Al_4Si_5O_{18}]$, with the structural unit in square brackets representing the tetrahedral framework. Beryl has $[Si_6O_{18}]$ rings arranged parallel to {001} and linked into columns by BeO_4 tetrahedra, whereas cordierite has analogous $[Al_2Si_4O_{18}]$ rings linked by (AlO_4) and (SiO_4) tetrahedra. In cordierite, there is prominent long-range ordering of Al and Si in the $[T_6O_{18}]$ rings, causing cordierite to be orthorhombic (rather than hexagonal, as is beryl) (Gibbs 1966; Cohen et al. 1977).

Beryllium has been reported in cordierite by many authors. Cerny and Povondra (1966) reported up to 1.94 wt % Be in cordierite, and proposed that Be was incorporated into the structure of cordierite via the substitution (Na,K) + Be ↔ □ + Al. This mechan-

ism has been since confirmed by many authors (e.g., Povondra and Langer 1971; Schreyer et al. 1979; Armbruster and Irouschek 1983). Beryllium could potentially replace Al in the six-membered rings or in the four-membered rings. By analogy with the Na + Li → □ + Be substitution in beryl, Be should replace Al in the four-membered rings, linking the $[Al_2Si_4O_{18}]$ rings together; Armbruster (1986) has shown this to be the case.

Hölscher and Schreyer (1989) synthesized a hexagonal cordierite-like phase with the composition $Mg_2[(Al_2Be)Si_6O_{18}]$, i.e., Be is incorporated into the cordierite (indialite) structure via the substitution Be + Si ↔ Al + Al. However, as noted by Hölscher and Schreyer (1989), this substitution has not been identified as yet in cordierite: There is always sufficient Na present to accommodate the substitution (Na,K) + Be ↔ □ + Al of Cerny and Povondra (1966).

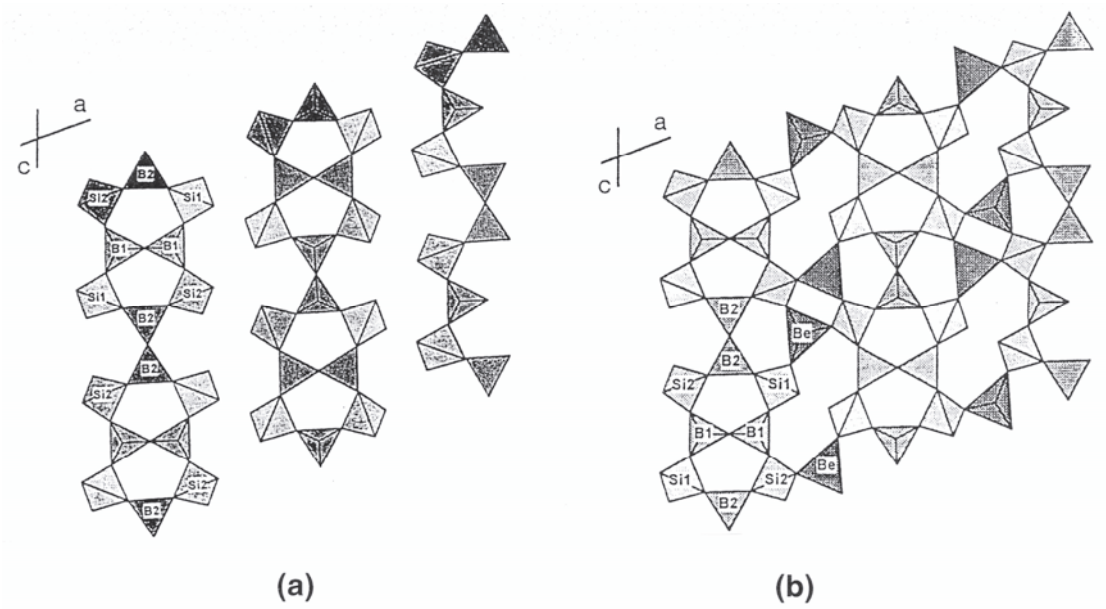

Figure 44. (a) The borosilicate chains in the structure of hellandite; (b) the *Be* sites in Be-bearing hellandite linking the borosilicate chains to form a sheet (after Oberti et al. 1999).

Beryllium-bearing hellandite

Hellandite is a borosilicate mineral with the end-member formula $Ca_5YAl[B_4Si_4O_{20}](OH)$ (Hawthorne et al. 1996). Oberti et al. (1999) refined the crystal structure of a Be-bearing hellandite and showed that Be occupies a site that is vacant in Be-absent hellandite [i.e, this Be-bearing hellandite is of category (5) above]. The borosilicate structural unit of hellandite is shown in Figure 44a; it consists of pentagonal borosilicate rings that link to form complex chains extending along the *c*-axis. In Be-bearing hellandite (Fig. 44b), Be (partly) occupies tetrahedrally coordinated sites that link the borosilicate chains into a berylloborosilicate sheet. In the crystal examined by Oberti et al. (1999), the *Be* site is also partly occupied by Li. Both the refined site-scattering values and the results of SIMS analysis suggest that occupancy of the *Be* site by Be (and Li) is locally associated with F, forming a BeO_3F group.

Oberti et al. (2002) have reported variable Be (and Li) in a suite of hellandites with Be varying between 0.02 and 1.18 apfu. The Be and Li occur at the new site (denoted *T*) of Oberti et al. (1999), and the resultant tetrahedron shows a regular variation in mean

bond-length as a function of the scattering at the *T* site (Fig. 45). It is apparent from Figure 45 that there is continuous variation of Be and Li at the *T* site in beryllian hellandite. Oberti et al. (2002) identify several distinct end-member compositions with the hellandite structure (Table 8). Two of these are potential Be minerals in which the *T* site is filled with Be. Moreover, one of the compositions listed by Oberti et al. (2002) has Be > 1.0 apfu and falls within the composition field of end-member (7).

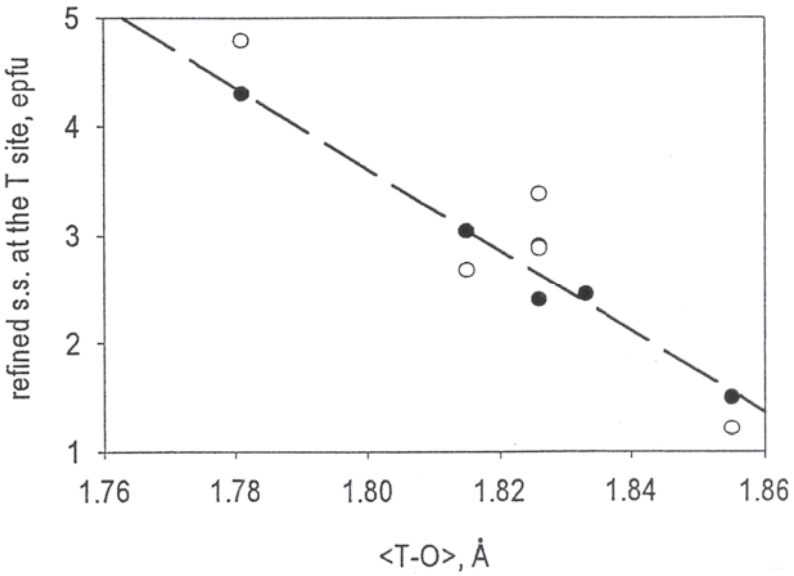

Figure 45. Variation in the site scattering at the *T* site as a function of <*T*–O> in Be-bearing hellandite structures; solid circles are SREF data, hollow circles are SIMS data. Used by permission of the Mineralogical Society of America, from Oberti et al. (2002), *American Mineralogist*, Vol. 87.

Table 8. Possible end-member compositions for hellandite-group minerals*.

	X **	*Y* **	*Z*	*T*		*W*
(1)	Ca_3Y	Y_2	Al	$\square_2$	$[B_4Si_4O_{22}]$	$(OH)_2$
(2)	Ca_4	Y_2	Ti	$\square_2$	$[B_4Si_4O_{22}]$	$(OH)_2$
(3)	Ca_4	ThY	Al	$\square_2$	$[B_4Si_4O_{22}]$	$(OH)_2$
(4)	Ca_4	Y_2	Ti	Li_2	$[B_4Si_4O_{22}]$	$O^{2-}{}_2$
(5)	Ca_3Y	Y_2	Al	Li_2	$[B_4Si_4O_{22}]$	$O^{2-}{}_2$
(6)	Ca_4	ThY	Al	Li_2	$[B_4Si_4O_{22}]$	$O^{2-}{}_2$
(7)	Ca_4	CaY	Al	Be_2	$[B_4Si_4O_{22}]$	$O^{2-}{}_2$
(8)	Ca_4	Ca_2	Ti	Be_2	$[B_4Si_4O_{22}]$	$O^{2-}{}_2$

* from Oberti et al. (2002)

** $Y = (Y^{3+} + REE^{3+})$; $Al = (Al^{3+} + Mn^{3+} + Fe^{3+})$; $OH = (OH^- + F^-)$

Rhodizite

Rhodizite is a berylloborate structure with the ideal end-member composition $KAl_4[Be_4(B_{11}Be)O_{28}]$. The structure is a framework (Figs. 27c,d) of BeO_4 and BO_4 tetrahedra arranged in a checker-board pattern. There is one *Be* site with a rank of 4 and a <*Be*-O> distance of 1.604 Å, and there is one *B* site with a rank of 12 and a <*B*-O>

distance of 1.492 Å. Pring et al. (1986) proposed a model with the *Be* site filled with Be and the *B* site occupied by 11.35 B + 0.50 Be, although this was not a truly least-squares solution. The <Be-O> and <B-O> distances are in reasonable accord with this model. However the observed <Be-O> distance of 1.604 Å is much less than the grand <Be-O> distance of 1.633 Å shown in Figure 1a, raising the possibility of a small amount of B being incorporated at this site [thereby accounting for the small <*Be*-O> distance]. The observed <*B*-O> distance of 1.492 Å is somewhat longer than the grand <B-O> distance of 1.476 Å reported by Hawthorne et al. (1996). This is in accord with the incorporation of some Be at this site. Thus rhodizite could possibly be slightly less ordered than suggested by Pring et al. (1986), although there is definite substitution of both Be and B at the same site in rhodizite.

Hyalotekite

Hyalotekite (Moore et al. 1982) is a complex framework of BO_4 and SiO_4 tetrahedra. One of the tetrahedral sites with *T*-O distances fairly typical of Si-O [*Si*(1)] showed lower than expected scattering, and Moore et al. (1982) assigned Be to this site. Thus Be and Si occur at the *Si*(1) site. Another possible arrangement can be suggested. The <*Si*(1)-O> distance is 1.597 Å, which is very short for a <Si-O> distance; the other <Si-O> distances in hyalotekite are 1.613, 1.610 and 1.613 Å. Now Be ($^{[4]}r$ = 0.27 Å) is marginally larger than Si ($^{[4]}r$ = 0.26 Å), and substitution of Be cannot account for the small <*Si*(1)-O> distance. However, if Be were to substitute for B at the *B* site and the displaced B were to substitute for Si at the *Si*(1) site, then the <*Si*(1)-O> distance would be shorter than the distance characteristic of <Si-O>, and the <B-O> distance should be longer than the distance characteristic of <B-O> (= 1.476 Å, Hawthorne et al. 1996). Moreover, Be substitutes for B and B substitutes for Si, as is observed in many other structures, rather than Be substituting for Si, which tends not to occur. Christy et al. (1998) re-refined the data of Moore et al. (1982) and came to this same conclusion.

Let us examine the possible end-member compositions of hyalotekite from the viewpoint of the above discussion of the site occupancies of Be, B and Si. Christy et al. (1998) write the general formula of hyalotekite as

$(Ba,Pb,K)_4\ (Ca,Y)_2\ Si_8\ (Be,B)_2\ (Si,B)_2\ O_{28}\ F$

Their chemical data show that Ba is often dominant over Pb^{2+}, and Ca is dominant over Y, and hence let us write a simplified formula as

$Ba_4Ca_2\ Si_8\ (Be,B)_2\ (Si,B)_2\ O_{28}\ F$

This is not an end-member formula as there is disorder at more than one site in the structure. This formula can be resolved into two simpler components

(1) $Ba_4\ Ca_2\ Si_8\ (BeB)\ (Si)_2\ O_{28}\ F$

(2) $Ba_4\ Ca_2\ Si_8\ (B_2)\ (SiB)\ O_{28}\ F$

These are true end-members in that neither can be resolved into more simple compositions that retain the hyalotekite structure and remain neutral.

Christy et al. (1998) provide chemical data for a range of compositions of hyalotekite. Figure 46a examines this data from the perspective of the above two end-members. The data extend between the two end-member compositions, in accord with the above discussion. Moreover, the displacement of the data from the ideal line correlates closely with the amount of K substituting for Ca, indicating the presence of a significant additional substitution. Let us next examine the character of this substitution. There are three possible ways to incorporate K into the hyalotekite structure if we ignore replacement of Ca by Y: (1) Ba + Be ↔ K + B; (2) 2Ba + Be ↔ K + Si; (3) Ba + B ↔ K + Si. The directions of these three substitutions relative to the axes of Figure 46a are

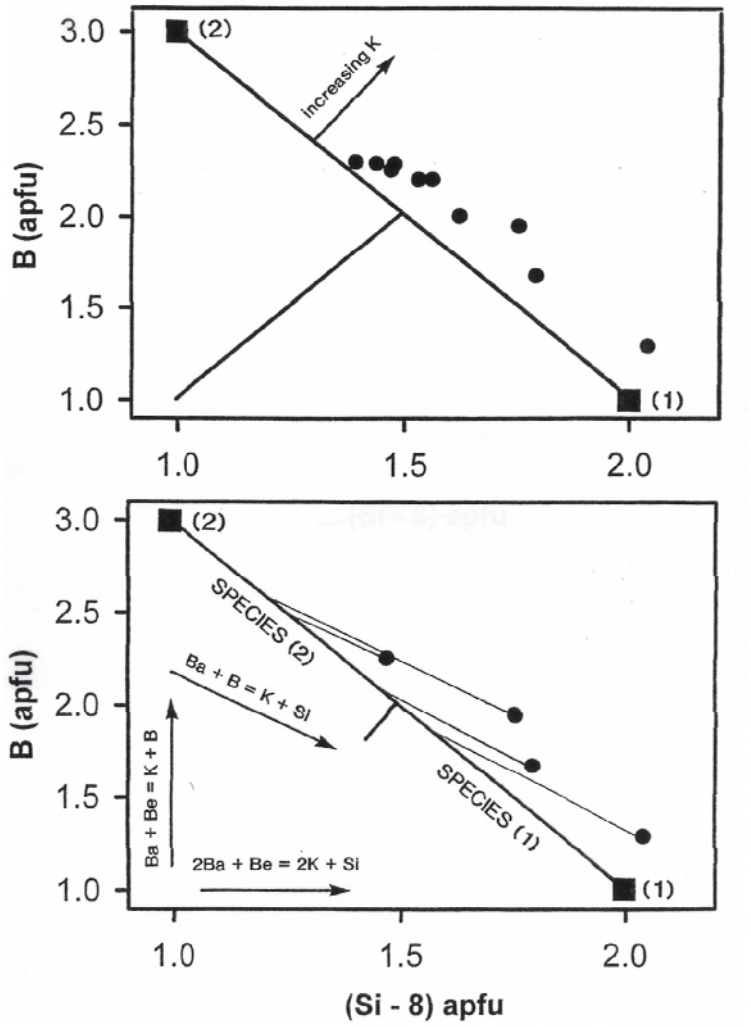

Figure 46. Variation in the chemical composition of hyalotekite; (a) B vs. [8-Si]; the compositions (1) $Ba_4Ca_2Si_8(BeB)(Si_2)O_{28}F$ and (2) $Ba_4Ca_2Si_8(B_2)(SiB)O_{28}F$ are marked by filled squares and are joined by a line representing the substitution B + B ↔ Be + Si; data from Christy et al. (1998) are shown as filled circles; (b) B vs. [8-Si]; the arrows represent the directions of the substitutions involving K, the lines join selected datapoints to points on the (1)-(2) line with the same Be content; note that these lines are parallel to the substitution Ba + B ↔ K + Si.

shown in Figure 46b. Now, if the data were to lie exactly along the line between compositions (1) and (2) in Figure 46a, the Be content should vary along this line from 1.0 apfu at composition (1) to 0.0 apfu at composition (2). Let us join the data points to the corresponding measured Be contents along the line between compositions (1) and (2) (Fig. 46b). For clarity, not all data are shown in Figure 46b. However, what is apparent is that the lines joining the observed data points with their Be content along the (1)-(2) join are all sub-parallel to the substitution direction defined by Ba + B ↔ K + Si, indicating that this is the substitution whereby K is incorporated into the hyalotekite structure.

Another important feature of Figure 46b is that is shows that *both* species (1) and (2) are represented in the compositional data of Christy et al. (1998). We may summarize the situation for hyalotekite as follows: There are two distinct end-members (1) and (2) (see above), and that compositions fall into both compositional fields. Thus there are two distinct 'hyalotekite minerals,' one of which [composition (1)] contains essential Be, and

the other of which [composition (2)] does not contain essential Be. In this regard, kapitsaite-(Y) is Be-free and isostructural with hyalotekite. Sokolova et al. (2000) wrote the formula as

$(Ba_{3.68}K_{0.12}Pb^{2+}_{0.20})\ (Y_{1.00}Ca_{0.66}REE_{0.34})\ Si_8\ B_2\ (B_{1.7}Si_{0.3})\ O_{28}\ F$.

Thus the end-member composition may be written as

$Ba_4\ (YCa)\ Si_8\ (B_2)\ (B_2)\ O_{28}\ F$

following the scheme used above for hyalotekite, and is related to the Be-free end-member of the hyalotekite series by the substitution $Y + B \leftrightarrow Ca + Si$.

"Makarochkinite"

"Makarochkinite" is a non-accredited Be-bearing aenigmatite-like phase. The structure (Fig. 10) consists of decorated chains of BeO_4, SiO_4 and $(Si,Al)O_4$ tetrahedra extending along the *a*-axis (Fig. 10a) and forming layers of tetrahedra orthogonal to [011] (Fig. 10b). Two of the tetrahedra show disorder of Si and Be: *T*1 and *T*4. The <*T*-O> distances and the isotropic-displacement factors seem in accord with this assignment. However, it must be noted that multiple occupancy of sites by Be and Si is quite unusual.

It is of interest to examine the compositional relations between these minerals, as Grauch et al. (1994) state that "makarochkinite" is the same as høgtuvaite. Details of the structure of aenigmatite are given by Cannillo et al. (1971). It is triclinic, space group $P\bar{1}$, with six [4]-coordinated sites, designated *T*(1) to *T*(6), seven [6]-coordinated sites designated *M*(1) to *M*(7), and two [8]-coordinated sites designated *Na*(1) and *Na*(2). Two of the *M* sites, *M*(1) and *M*(2), occur at centers of symmetry, and thus one can write the resulting structural formula as $Na_2M_6T_6O_{22}$. In aenigmatite (Cannillo et al. 1971), Ti is strongly ordered at the *M*(7) site and Fe^{2+} occurs at the other M*(1)* to M(6) sites to give the end-member formula $Na_2(Fe^{2+}_5Ti)Si_6O_{20}$. We may ignore homovalent substitutions in the present case, and focus on "makarochkinite" and høgtuvaite, the chemical compositions and formulae of which are shown in Table 9. Following aenigmatite, we assume that Ti is ordered at the *M*(7) site. In "makarochkinite," Ti > 0.50 apfu and hence the *M*(7) site is dominated by Ti, i.e., Ti is an essential constituent of "makarochkinite." In høgtuvaite, Ti < 0.50 apfu and hence does not predominate at the *M*(7) site, i.e., Ti is *not* an essential constituent of høgtuvaite. Are "makarochkinite" and høgtuvaite distinct? Yes, according to the data currently available, as Ti is an essential constituent of "makarochkinite" and is *not* an essential constituent of høgtuvaite. The problem is most easily resolved by writing the end-member formula of each of these species, following what we have discussed above. The *T* content of each are very close (Table 9), but fall on either side of the boundary between two distinct arrangements: (Si_4BeAl) in "makarochkinite" and (Si_5Be) in høgtuvaite. The *M* content of each may be written as follows: ($Fe^{2+}_4Fe^{3+}Ti$) for "makarochkinite" (where $Fe^{2+} \equiv Fe^{2+} + Mg + Mn$) and ($Fe^{2+}_4Fe^{3+}_2$) for høgtuvaite (where $Fe^{2+} \equiv Fe^{2+} + Mg + Mn$). Thus we may write the end-member formulae as follows:

"makarochkinite"	Ca_2	$(Fe^{2+}_4Fe^{3+}Ti)$	(Si_4BeAl)	O_{20}
høgtuvaite	Ca_2	$(Fe^{2+}_4Fe^{3+}_2)$	(Si_5Be)	O_{20}

Hence these are distinct species, and the statement of Grauch et al. (1994) that the "informally proposed new mineral" (*viz.* "makarochkinite") "is the same as høgtuvaite" is not correct according to the published data, although we do note that the formula for "makarochkinite" is unsatisfactory from the excess amount of (Ca + Na + K) (Table 8).

Very recently, Barbier et al. (2001) report a refined crystal structure of "makarochkinite". Although full details of the structure are not yet available, they state that Ti is dominant at *M*(7) and Be is disordered over two *T* sites, but do not report site populations

Table 9. Chemical composition (wt %)* and unit formula (apfu) for "makarochkinite" (M) and høgtuvaite (H).

	M		*H*
SiO_2	30.09		31.60
Al_2O_3	3.55		2.64
BeO	2.32		2.65
TiO_2	6.02		2.77
Fe_2O_3	11.12		19.03
FeO	26.91		28.06
MnO	1.26		0.27
MgO	2.74		0.42
CaO	13.38		10.44
Na_2O	1.35		1.52
K_2O	0.30	SnO_2	0.53
	99.04		99.93
Si	4.39		4.60
Al	0.61		0.45
Be	0.81		0.93
ΣT	5.81		5.98
Fe^{3+}	1.22		2.09
Fe^{2+}	3.28		3.42
Mn	0.16		0.03
Mg	0.60		0.09
Ti	0.66		0.30
ΣM	5.92		**5.96
Ca	2.09		1.63
Na	0.38		0.43
K	0.06		-
Σ	2.53		2.06

* Data from Yakubovich et al. (1990) and Grauch et al. (1994)** including 0.03 Sn.

for *M*(1)-*M*(6). Moreover, the Al content is slightly less than that reported by Yakubovich et al. (1990); however, the Ca (1.77) and Na (0.20 apfu) contents of the [7]-coordinated sites are much more satisfactory than the previously reported values. Thus the "makarochkinite" reported by Barbier et al. (2001) is almost exactly half-way between the compositions

(1) Ca_2 $(Fe^{2+}_4Fe^{3+}Ti)$ (Si_4BeAl) O_{20}

(2) Ca_2 (Fe^{2+}_5Ti) (Si_5Be) O_{20}

Composition (1) corresponds to that above that we derived for the "makarochkinite" of Yakubovich et al. (1990) and composition (2) is new. Both compositions (1) and (2) are *bona-fide* end-member compositions of the aenigmatite structure, provided they show ordered cation distribution at the *M*(1)-*M*(6) and/or *T*(1)-*T*(6) sites.

Table 10 summarizes the end-member compositions for aenigmatite and some Be-bearing compositions. Moore (1978) gives the end-member composition as welshite (1) (Table 10). This seems the most reasonable end-member, although the chemical composition leads to an empirical formula with only 5.5 tetrahedrally coordinated cations pfu. Grew et al. (2001) give a new empirical composition for welshite:

$Ca_2(Mg_{3.8}Mn^{2+}_{0.6}Fe^{2+}_{0.1}Sb^{5+}_{1.5})O_2[Si_{2.8}$-
$Be_{1.7}Fe^{3+}_{0.65}Al_{0.7}As_{0.17}O_{18}]$

Combining Mg, Mn^{2+} and Fe^{2+} and expressing the result as Mg, combining Si and As and expressing the result as Si, and combining Al and Fe^{3+} and expressing the result as Al, we get the following:

Ca_2 $(Mg_{4.5}Sb^{5+}_{1.5})O_2$ $[Si_{3.0}Be_{1.7}Al_{1.3}O_{18}]$

This formula has an excess negative charge of 0.2. Now there are two possibilities for the octahedrally coordinated cations in an end member: $(Mg_4Sb^{5+}_2)$ and (Mg_5Sb^{5+}). These require the charge at the tetrahedrally coordinated sites to be 18^+ and 21^+, respectively. For a charge of 18^+, the possible tetrahedrally coordinated cations are $[Al_6]$, $[SiBeAl_4]$, $[Si_2Be_2Al_2]$ and $[Si_3Be_3]$; comparison with the above empirical formula indicates that the first two are inappropriate. For a charge of 21^+, the possible tetrahedrally coordinated cations are $[Si_3Al_3]$ and $[Si_4BeAl]$. Thus we end up with four possible end-members:

(1) Ca_2 (Mg_4Sb_2) O_2 $[Si_2Be_2Al_2O_{18}]$

(2) Ca_2 (Mg_4Sb_2) O_2 $[Si_3Be_3O_{18}]$

(3) Ca_2 (Mg_5Sb) O_2 $[Si_3Al_3O_{18}]$

(4) Ca_2 (Mg_5Sb) O_2 $[Si_4BeAlO_{18}]$

Table 10. Beryllium minerals of the aenigmatite group: comparison with aenigmatite.

Aenigmatite	Na_2	Fe^{2+}_4	Fe^{2+}	Ti^{4+}	O_2	$[Si_6O_{18}]$
"Makarochkinite"(1)	Ca_2	Fe^{2+}_4	Fe^{3+}	Ti^{4+}	O_2	$[BeAlSi_4O_{18}]$
"Makarochkinite"(2)	Ca_2	Fe^{2+}_5		Ti^{4+}	O_2	$[BeSi_5O_{18}]$
Høgtuvaite	Ca_2	Fe^{2+}_4	Fe^{3+}	Fe^{3+}	O_2	$[BeSi_5O_{18}]$
Welshite (1)	Ca_2	Mg_4	Fe^{3+}	Sb^{5+}	O_2	$[Be_2Si_4O_{18}]$
Welshite (2)	Ca_2	Mg_4		Sb^{5+}_2	O_2	$[Be_3Si_3O_{18}]$

Taking compositions exactly intermediate between (2) and (3), and (1) and (4), gives the same composition:

$$Ca_2 \quad (Mg_{4.5}Sb_{1.5}) \quad O_2 \quad [Si_3Be_{1.5}Al_{1.5}O_{18}]$$

This is extremely close to the simplified composition for welshite given above. However, combining end-members (2) and (3) can produce different values of Be and Al, whereas combining end-members (1) and (4) must produce equal amounts of Be and Al. Hence combining end-members (2) and (3) in the proportions 0.57 and 0.43, respectively, produces the composition

$$Ca_2 \quad (Mg_{4.43}Sb_{1.57}) \; O_2 \quad [Si_{3.00}Be_{1.70}Al_{1.30}O_{18}]$$

which is extremely close to the composition of welshite given by Grew et al. (2001). Hence the most appropriate end-member for this sample of welshite is (2), and the sample has extensive solid-solution toward end-member (3).

Sapphirine-related structures

Khmaralite, $Mg_7Al_9O_4[Al_6Be_{1.5}Si_{4.5}O_{36}]$, and surinamite, $Mg_3Al_3O[AlBeSi_3O_{15}]$, are structurally related to sapphirine, $Mg_7Al_9[Al_9Si_3O_{40}]$, where the formulae given here are the Mg-Al end-members. All three structures consist of the basic sapphirine arrangement (Moore 1969) in which different composition and ordering schemes produce different superstructures. Sapphirine itself shows extensive polytypism and disorder in the form of planar and line defects (Christy and Putnis 1988). Moreover, it can incorporate variable amounts of Be (Grew 1981; Christy 1988; Grew et al. 2000). Grew (1981) showed that sapphirine can contain variable Be (0.5-1.0 wt % BeO), and proposed the substitution Be + Si Al + Al. Grew et al. (2000) provided additional data, extended the known range of this substitution (1.1-2.5 wt % BeO), and showed that there is a continuous correlation between Be and Si from sapphirine through to khmaralite (Fig. 47) following the substitution proposed by Grew (1981). In both surinamite and khmaralite, Be occupies the three-connected tetrahedra in the branched chains, but details of the stereochemical variations with varying Be/Si contents are not available over the range of compositions represented in Figure 47.

Be-bearing micas

Details of the structure of bityite, ideally $Ca(LiAl_2)(BaAlSi_2)O_{10}(OH)_2$, are not available, but Lin and Guggenheim (1983) refined the structure of a (Li,Be)-rich brittle mica intermediate in composition between bityite and margarite, ideally $Ca(Al_2)(Al_2Si_2)O_{10}(OH)_2$. The *T*-site populations given by Lin and Guggenheim are as follows: *T*(1) = 0.24 Be + 0.71 Al + 0.05 Si, *T*(11) = 0.04 Be + 0.15 Al + 0.81 Si, *T*(2) = 0.12 Al + 0.88 Si, *T*(22) = 0.30 Be + 0.70 Al. We may adjust these to bring them into accord with the

chemical composition of this mica to give $T(1) = 0.32$ Be + 0.68 Al, $T(11) = 1.00$ Si, $T(2) = 1.00$ Si, $T(22) = 0.32$ Be + 0.68 Al. It is very apparent here that Be substitutes for Al and does not substitute for Si.

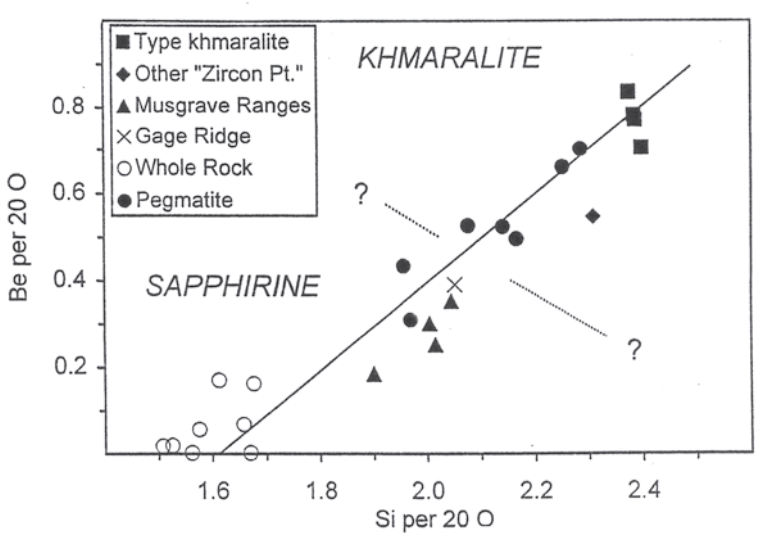

Figure 47. Variation in Be as a function of Si in sapphirine and khamaralite; the line designates the substitution Be + Si ↔ Al + Al; after Grew et al. (2000).

General observations on solid-solution relations involving beryllium

There are two issues involved in solid-solution relations involving Be: (1) at what specific sites does Be occur in the crystal structure, and (2) what cation(s) is Be replacing at its constituent sites. Huminicki and Hawthorne (2001b) have examined the first issue for Be minerals whose structural units are sheets. They represented the sheets as two-dimensional nets and looked at the local topology of the net vertices that represent Be sites in the structures. Although none of the minerals examined display solid solution between Be and other tetrahedrally coordinated cations, their work addresses the issue of the effect of network topology on the occupancy of tetrahedrally coordinated sites by Be. Huminicki and Hawthorne (2001b) note that Be has a strong preference for three-connected sites in sheet minerals.

Table 11 summarizes the substitutions involving Be for minerals in which there is solid solution involving Be. The majority of substitutions involve replacement of a cation differing from Be by one formal charge (i.e., Li^{+}, B^{3+} and Al^{3+}). With the exception of beryllian hellandite (for which there is a paucity of data), these solid solutions are extensive and fairly common. The effective radii of these cations in tetrahedral coordination are as follows: Li: 0.59 Å, Be: 0.27 Å, B: 0.11 Å. The differences between these radii are greatly in excess of the oft-quoted 15%, but no serious crystal chemist has considered this figure appropriate for decades. The key generalization is that *solid solutions tend to involve cations that differ in formal charge by one valence unit, and that can adopt the same coordination number.* It is also notable that all of these substitutions occur at 4-connected tetrahedra; this point is seemingly contradictory to the observation by Huminicki and Hawthorne (2001b) that Be prefers tetrahedrally coordinated sites that are 3-connected in sheet structures. A more general examination of this issue seems justified.

There are two substitutions that are not in accord with our general rule of substituents involving cations with a difference in formal charge of one valence unit. In beryllian hellandite, we have Be and Li substituting for a □, so the charge difference is

2^+. In "makarochkinite," Be substitutes for Si, again a charge difference of 2^+. Inspection of Table 11 shows that these substitutions in which there is a charge difference of 2^+ occur at tetrahedra with a connectivity of 3, whereas substitutions in which there is a charge difference of 1^+ occur at tetrahedra with a connectivity of 4. In khmaralite, Barbier et al. (1999) report Be at five tetrahedrally coordinated sites. However, the site occupancies for Be at two sites (T4 and T8) are low (≤0.05) and hence cannot be considered as significant. Thus Be occurs at three sites, together with Al and Si, and hence it is not apparent whether Be is substituting for Al or Si. In surinamite, refinement of the structure indicates a site occupancy of 0.97 Be + 0.03 Si; the occupancy of this site by Si is probably not statistically significant.

Thus there seems to be some regularities in the occurrence of Be as a constituent of solid solutions (as summarized in Table 11), but the number of examples of this (as distinct from Al ↔ Si substitution, for example) is too small to be certain that these regularities will hold for other, as yet uncharacterized, solid solutions involving Be.

Table 11. Minerals with solid solutions involving Be, the principal substituents, and the connectivity of the site at which the solid solution occurs.

Mineral	*Substituents*	*Connectivity*
Beryl	Be ↔ Li	4
Milarite	Be ↔ Al	4
Beryllian cordierite	Be ↔ Al	4
(Li,Be)-mica	Be ↔ Al	3
Beryllian hellandite	Be ↔ G	3
Rhodizite	Be ↔ B	4
Hyalotekite	Be ↔ B	4
"Makarochkinite"	Be ↔ Si	3
Khmaralite	Be ↔ (Al,Si)	3

ACKNOWLEDGMENTS

We thank Sergey Krivovichev, Vanessa Gale and Editor Ed Grew for detailed reviews of this chapter. This work was supported by Natural Sciences and Engineering Research Council of Canada grants to FCH.

APPENDIX A

&

APPENDIX B

on the following four pages.

Appendix A. End-member formulae and crystallographic data for Be minerals of known structure.

Name	End-member formula	*a* (Å)	*b* (Å)	*c* (Å)	β (°)	Sp. Gr.	Ref.
aminoffite	$Ca_3[Be_2Si_3O_{10}(OH)_2]$	9.864(2)	*a*	9.930(2)	–	$P4_2/n$	(1)
asbecasite	$Ca_3Ti^{4+}[As_6Be_2S_2O_{20}]$	8.318(1)	*a*	15.264(2)	–	$P\bar{3}c1$	(2)
babefphite[1]	$Ba[BePO_4F]$	6.889(3)	16.814(7)	6.902(3)	90.3(1)	$F1$	(3)
barylite	$Ba[Be_2Si_2O_7]$	9.820(10)	11.670(10)	4.690(10)	–	$Pnma$	(4)
bavenite	$Ca_4[Be_2Al_2Si_9O_{26}(OH)_2]$	23.190(20)	5.005(9)	19.390(20)	–	$Cmcm$	(5)
bazzite	$Sc_2[Be_3Si_6O_{18}]$	9.510	*a*	9.110	–	$P6/mcc$	(6)
bearsite	$[Be_2AsO_4(OH)](H_2O)_4$	7.235(1)	12.686(2)	8.655(1)	98.4(0)	$P2_1/a$	(7)
behoite	$[Be(OH)_2]$	4.530(2)	4.621(2)	7.038(2)	–	$P2_12_12_1$	(8)
berborite-2*H*	$[Be_2BO_3(OH)](H_2O)$	4.433(2)	*a*	10.638(5)	–	$P6_3$	(9)
berborite-1*T*	$[Be_2BO_3(OH)](H_2O)$	4.434(1)	*a*	5.334(2)	–	$P3$	(9)
berborite-2*T*	$[Be_2BO_3(OH)](H_2O)$	4.431(1)	*a*	10.663(3)	–	$P3/c1$	(9)
bergslagite	$Ca[BeAsO_4(OH)]$	4.882(1)	7.809(1)	10.127(1)	90.2(0)	$P2_1/c$	(10)
bertrandite	$[Be_4Si_2O_7(OH)_2]$	8.716(3)	15.255(3)	4.565(1)		$Cmc2_1$	(11)
beryl	$Al_2[Be_3Si_6O_{18}]$	9.278(2)	*a*	9.195(2)		$P6/mcc$	(12)
beryllonite	$Na[BePO_4]$	8.178(3)	7.818(2)	14.114(6)	90.0(0)	$P2_1/n$	(13)
bityite	$CaLiAl_2[BeAlSi_2O_{10}](OH)_2$	5.058(1)	8.763(3)	19.111(7)	95.39(2)	Cc	(14)
bromellite	$[BeO]$	2.718(1)	*a*	4.408(1)	–	$P6_3mc$	(15)
“calcybeborosilite”	$CaY\square[BeBSi_2O_8(OH)_2]$	9.846(4)	7.600(2)	4.766(2)	90.1(0)	$P2_1/a$	(16)
chiavennite	$CaMn^{2+}[Be_2Si_5O_{13}(OH)_2](H_2O)_2$	8.729(5)	31.326(11)	4.903(2)	–	$Pnab$	(17)
chkalovite	$Na_2[BeSi_2O_6]$	21.129(5)	6.881(2)	21.188(5)	–	$Fdd2$	(18)
chrysoberyl	$Al_2[BeO_4]$	9.402(1)	5.475(0)	4.426(0)	–	$Pnma$	(19)
clinobehoite	$[Be(OH)_2]$	11.020(8)	4.746(6)	8.646(9)	98.9(1)	$P2_1$	(20)
danalite	$Fe^{2+}_8[Be_6Si_6O_{24}]S_2$	8.218(0)	*a*	*a*	–	$P\bar{4}3n$	(21)
ehrleite[2]	$Ca_2[ZnBe(PO_4)_2(PO_3OH)](H_2O)_4$	7.130(4)	7.430(4)	12.479(9)	102.1(0)	$P\bar{1}$	(22)
epididymite	$Na_2[Be_2Si_6O_{15}](H_2O)$	12.74(1)	13.63(1)	7.33(1)	–	$Pnma$	(23)
euclase	$Al[BeSiO_4OH]$	4.746(1)	14.189(11)	4.599(1)	100.2(0)	$P2_1/a$	(24)
eudidymite	$Na_2[Be_2Si_6O_{15}](H_2O)$	12.630(10)	7.380(10)	14.020(10)	103.7(1)	$C2/c$	(25)

Appendix A. cont.

Name	End-member formula	*a* (Å)	*b* (Å)	*c* (Å)	β (°)	Sp. Gr.	Ref.
fransoletite	$Ca_3[Be_2(PO_4)_2(PO_3\{OH\})_2](H_2O)_4$	7.348(1)	15.052(3)	7.068(1)	96.52(1)	$P2_1/a$	(26)
gadolinite-(Ce)	$Ce_2Fe^{2+}[Be_2Si_2O_{10}]$	4.82(2)	7.58(2)	10.01(3)	90.5(3)	$P2_1/c$	(27)
gadolinite-(*Y*)	$Y_2Fe^{2+}[Be_2Si_2O_{10}]$	4.747(1)	7.544(1)	9.931(1)	90.5(0)	$P2_1/c$	(28)
gainesite	$NaKZr_2[BeP_4O_{16}](H_2O)_{1.5}$	6.567(3)	*a*	17.119(5)	–	$I4_1/amd$	(29)
genthelvite	$Zn_8[Be_6Si_6O_{24}]S_2$	8.109(0)	*a*	8.109(0)	–	$P\bar{4}3n$	(21)
gugiaite	$Ca_2[BeSi_2O_7]$	7.419(1)	*a*	4.988(1)	–	$P\bar{4}2_1m$	(30)
hambergite	$[Be_2BO_3(OH)]$	9.754(2)	12.231(2)	4.434(1)	–	*Pbca*	(31)
harstigite	$Ca_6Mn^{2+}[Be_4Si_6O_{22}(OH)_2]$	9.793(2)	13.636(3)	13.830(3)	–	*Pnam*	(32)
helvite	$Mn^{2+}{}_8[Be_6Si_6O_{24}]S_2$	8.291(1)	*a*	*a*	–	$P\bar{4}3n$	(21)
herderite	$Ca[BePO_4F]$	–	–	–	–	–	(–)
“hingganite-(Y)”	$Y[BeSiO_4(OH)]$	9.930(6)	7.676(7)	4.768(3)	90.28(–)	$P2_1/a$	(33)
hingganite-(Yb)	$Yb[BeSiO_4(OH)]$	9.888(5)	7.607(3)	4.740(2)	90.4(0)	$P2_1/a$	(34)
høgtuvaite[3]	$Ca_2(Fe^{2+}{}_4Fe^{3+}{}_2)O_2[BeSi_5O_{18}]$	10.317(1)	10.724(1)	8.855(1)	92.21(1)	$P\bar{1}$	(35)
hsianghualite	$Ca_3Li_2[Be_3Si_3O_{12}]F_2$	12.864(2)	*a*	*a*	–	$I2_13$	(36)
hurlbutite	$Ca[Be_2P_2O_8]$	8.306(1)	8.790(1)	7.804(1)	89.5(0)	$P2_1/a$	(37)
hyalotekite[4]	$(Pb,Ba)_4Ca_2[(B,Be)_2(Si,B)_2Si_8O_{28}]F$	11.310(2)	10.955(2)	10.317(3)	90.02	$I\bar{1}$	(38)
hydroxylherderite	$Ca[BePO_4OH]$	9.789(2)	7.661(1)	4.804(1)	90.0(0)	$P2_1/a$	(39)
joesmithite	$Pb^{2+}Ca_2(Mg_3Fe^{3+}{}_2)[Be_2Si_6O_{22}](OH)_2$	9.915(2)	17.951(4)	5.243(1)	105.9(0)	*P*2/*a*	(40)
khmaralite	$Mg_7Al_9O_4[Al_6Be_{1.5}Si_{4.5}O_{36}]$	19.800(1)	14.371(1)	11.254(1)	125.53(1)	$P2_1/c$	(41)
leifite	$Na_6[Be_2Al_2Si_{16}O_{39}(OH)_2](H_2O)_{1.5}$	14.352(3)	*a*	4.852(3)	–	$P\bar{3}m1$	(42)
leucophanite	$CaNa[BeSi_2O_6F]$	7.401(2)	7.412(2)	9.990(2)	–	$P2_12_12_1$	(43)
liberite	$Li_2[BeSiO_4]$	4.680(20)	4.950(30)	6.130(20)	90.3(1)	*Pn*	(44)
londonite	$CsAl_4[Be_4(B_{11}Be)O_{28}]$	7.321(1)	*a*	*a*	–	$P\bar{4}3m$	(45)
lovdarite	$K_2Na_6[Be_4Si_{14}O_{36}](H_2O)_9$	39.756(1)	6.931(0)	7.153(0)	–	*Pma*2	(46)
“makarochkinite”[5]	$Ca_2(Fe^{2+}{}_4Fe^{3+}Ti^{4+})O_2[BeAlSi_4O_{18}]$	10.352(5)	10.744(3)	8.864(4)	96.2(0)	$P\bar{1}$	(47)
mccrillisite	$NaCs[BeZr_2(PO_4)_4](H_2O)_{1–2}$	6.573(2)	*a*	17.28(2)	–	$I4_1/amd$	(48)
meliphanite	$CaNa[BeSi_2O_6F]$	10.516(2)	*a*	9.887(2)	–	$I\bar{4}$	(49)

Appendix A. cont.

Name	End-member formula	*a* (Å)	*b* (Å)	*c* (Å)	β (°)	Sp. Gr.	Ref.
milarite	$KCa_2[Be_2AlSi_{12}O_{30}](H_2O)$	10.340(1)	*a*	13.758(2)	–	*P*6/*mcc*	(50)
minasgeraisite	$CaY_2[Be_2Si_2O_{10}]$	4.702(1)	7.562(1)	9.833(2)	90.46(6)	$P2_1/c$	(51)
moraesite	$[Be_2PO_4(OH)](H_2O)_4$	8.553(6)	12.319(6)	7.155(8)	97.9(1)	*C*2/*c*	(52)
magnesiotaaffeite-6*N*′3*S* *	$MgAl_5[BeMgAlO_{12}]$	5.682(1)	*a*	41.150(10)	–	$R\bar{3}m$	(53)
odintsovite	$K_2Na_4Ca_3Ti^{4+}{}_2O_2[Be_4Si_{12}O_{36}]$	14.243(3)	13.045(4)	33.484(6)	–	*Fddd*	(54)
pahasapaite	$Ca_8Li_8[Be_{24}P_{24}O_{96}](H_2O)_{38}$	13.783(1)	*a*	*a*	–	*I*23	(55)
parafransoletite[6]	$Ca_3[Be_2(PO_4)_2(PO_3\{OH\})_2](H_2O)_4$	7.327(1)	7.696(1)	7.061(1)	96.82(1)	$P\bar{1}$	(26)
ferrotaaffeite-6*N*′3*S* *	$Fe^{2+}Al_5[BeFe^{2+}AlO_{12}]$	5.70	*a*	41.16	–	$R\bar{3}m$	(56)
phenakite	$[Be_2SiO_4]$	12.485(3)	*a*	8.264(3)	–	$R\bar{3}$	(57)
rhodizite	$KAl_4[Be_4(B_{11}Be)O_{28}]$	7.319(1)	*a*	7.319(1)	–	$P\bar{4}3m$	(58)
roggianite	$Ca_2[Be(OH)_2Al_2Si_4O_{13}](H_2O)_{2.34}$	18.330(20)	*a*	9.160(10)	–	*I*4/*mcm*	(59)
roscherite	$Ca_2Mn^{2+}{}_5[Be_4P_6O_{24}(OH)_4](H_2O)_6$	15.88(4)	11.90(3)	6.66(3)	94.7(3)	*C*2/*c*	(60)
samfowlerite	$Ca_{14}Mn^{2+}{}_3[(Be_7Zn)Zn_2Si_{14}O_{52}(OH)_6]$	9.068(2)	17.992(2)	14.586(2)	104.9(0)	$P2_1/c$	(61)
selwynite	$NaK[BeZr_2(PO_4)_4](H_2O)_2$	6.570(3)	*a*	17.142(6)	–	$I4_1/amd$	(62)
semenovite	$(RE)_2Fe^{2+}Na_{0-2}(Ca,Na)_8[Be_6Si_{14}O_{40}(OH)_4F_4]$	13.879(5)	13.835(5)	9.942(6)	–	*Pmnn*	(63)
sorensenite	$Na_4Sn^{4+}[Be_2Si_6O_{18}](H_2O)_2$	20.698(17)	7.442(5)	12.037(11)	117.3(1)	*C*2/*c*	(64)
stoppaniite	$Fe^{3+}{}_2[Be_3Si_6O_{18}](H_2O)_2$	9.397(1)	*a*	9.202(2)	–	*P*6/*mcc*	(65)
surinamite	$Mg_3Al_3O[AlBeSi_3O_{15}]$	9.916(1)	11.384(1)	9.631(1)	109.3(0)	*P*2/*n*	(66)
sverigeite	$NaMn^{2+}{}_2Sn^{4+}[Be_2Si_3O_{12}(OH)]$	10.815(8)	13.273(8)	6.818(6)	–	*Imma*	(67)
swedenborgite	$NaSb^{5+}[Be_4O_7]$	5.470	*a*	8.920	–	$P6_3mc$	(68)
magnesiotaaffeite-2*N*′2*S* *	$MgAl_7[BeMg_2AlO_{16}]$	5.687(1)	*a*	18.337(3)	–	$P6_3mc$	(53)
tiptopite	$K_2Li_3Na_3[Be_6P_6O_{24}(OH)_2](H_2O)_4$	11.655(5)	*a*	4.692(2)	–	$P6_3$	(69)
trimerite	$CaMn^{2+}{}_2[BeSiO_4]_3$	8.098	7.613	14.065	90.0(0)	$P2_1/n$	(70)
tugtupite	$Na_8[BeAlSi_4O_{12}]_2Cl_2$	8.769	*a*	8.976	–	$I\bar{4}$	(71)
uralolite	$Ca_2[Be_4P_3O_{12}(OH)_3](H_2O)_5$	6.550(1)	16.005(3)	15.969(4)	101.6(0)	$P2_1/n$	(72)
väyrynenite	$Mn^{2+}[BePO_4(OH)]$	5.411(5)	14.490(20)	4.730(50)	102.8(1)	$P2_1/a$	(73)

Appendix A. cont.

Name	End-member formula	*a* (Å)	*b* (Å)	*c* (Å)	β (°)	Sp. Gr.	Ref.
weinebeneite	$Ca[Be_3P_2O_8(OH)_2](H_2O)_4$	11.897(2)	9.707(1)	9.633(1)	95.8(0)	*Cc*	(74)
welshite[7]	$Ca_2(Mg_4Sb^{5+}{}_2)O_2[Be_3Si_3O_{18}]$	10.381(1)	10.766(2)	8.881(1)	96.33(1)	$P\bar{1}$	(75)
zanazziite[8]	$Ca_2Mg_5[Be_4P_6O_{24}(OH)_4](H_2O)_6$	15.921(5)	11.965(4)	6.741(1)	94.3(1)	$C\bar{1}$	(76)

[1] α = 90.0, γ = 90.0°; [2] α = 94.3(0), γ = 82.7(0)°; [3] α = 105.77(1), γ = 124.77(1)°; [4] α = 90.43(2), γ = 90.16°;
[5] α = 105.7(0), γ = 124.9(0)°; [6] α = 94.90(1), γ = 101.87(1)°, [7] α = 105.92(1), γ = 124.97(1), [8] α = 91.1(1), γ = 90.0(1)°

* New nomenclature: magnesiotaaffeite-6*N′*3*S* ≡ musgravite-18*R*; ferrotaaffeite-6*N′*3*S* ≡ pehrmanite-18*R*; magnesiotaaffeite-2*N′*2*S* ≡ taaffeite-8*H*

References: (1) Coda et al. (1967), Huminicki and Hawthorne (2001b); (2) Sacerdoti et al. (1993); (3) Simonov et al. (1980);
(4) Robinson and Fang (1977); (5) Cannillo et al. (1966), Kharitonov et al. (1971); (6) Armbruster et al. (1995); (7) Harrison et al. (1993); (8) Seitz et al. (1950), Stahl et al. (1998); (9) Giuseppetti et al. (1990); (10) Hansen et al. (1984); (11) Giuseppetti et al. (1992); (12) Artioli et al. (1995); (13) Giuseppetti and Tadini (1973); (14) Lin and Guggenheim (1983); (15) Hazen and Finger (1986);
(16) Rastsvetaeva et al. (1996); (17) Tazzoli et al. (1995); (18) Simonov et al. (1975); (19) Pilati et al. (1993); (20) Nadezhina et al. (1989); (21) Hassan and Grundy (1985); (22) Hawthorne and Grice (1987); (23) Robinson and Fang (1970); (24) Hazen et al. (1986); (25) Fang et al. (1972); (26) Kampf (1992); (27) Segalstad and Larsen (1978); (28) Demartin et al. (1993); (29) Moore et al. (1983); (30) Kimata and Ohashi (1982); (31) Burns et al. (1995); (32) Hesse and Stuempel (1986); (33) Ximen and Peng (1985);
(34) Yakubovich et al. (1983); (35) Grauch et al. (1994); (36) Rastsvetaeva et al. (1991); (37) Bakakin et al. (1974); (38) Christy et al. (1998); (39) Lager and Gibbs (1974); (40) Moore et al. (1993); (41) Barbier et al. (1999); (42) Coda et al. (1974); (43) Cannillo et al. (1967), Grice and Hawthorne (1989); (44) Chang (1966); (45) Simmons et al. (2001); (46) Merlino (1990); (47) Yakubovich et al. (1990); (48) Foord et al. (1994); (49) Dal Negro et al. (1967); (50) Hawthorne et al. (1991); (51) Foord et al. (1986); (52) Merlino and Pasero (1992); (53) Nuber and Schmetzer (1983); (54) Rastsvetsaeva et al. (1995); (55) Corbin et al. (1991); (56) Burke and Lustenhouwer (1981); (57) Tsirel'son et al. (1986); (58) Taxer and Buerger (1967), Pring et al. (1986); (59) Giuseppetti et al. (1991); (60) Fanfani et al. (1975, 1977); (61) Rouse et al. (1994); (62) Birch et al. (1995); (63) Mazzi et al. (1979); (64) Metcalf and Gronbaek (1977); (65) Ferraris et al. (1998); (66) Moore and Araki (1983); (67) Rouse et al. (1989); (68) Pauling et al. (1935), Huminicki and Hawthone (2001a); (69) Peacor et al. (1987); (70) Klaska and Jarchow (1977); (71) Hassan and Grundy (1991); (72) Mereiter et al. (1994); (73) Mrose and Appleman (1962), Huminicki and Hawthorne (2000); (74) Walter (1992); (75) Moore (1978), Grew et al. (2001); (76) Fanfani et al. (1977), Leavens et al. (1990).

Appendix B. End-member formulae and crystallographic data for Be minerals of unknown structure.

Name	Formula	*a* (Å)	*b* (Å)	*c* (Å)	β (°)	Sp.Gr.	Ref.
Faheyite	$(Mn,Mg,Na)[Be_2(PO_4)_4](H_2O)_6$	9.42(2)	9.42(2)	15.98(3)	–	$P6_422$	(1)
Jeffreyite	$Ca_2[BeSi_2O_7]$	14.90(1)	14.90(1)	40.41(8)	–	$C222_1$	(2)
Tvedalite	$(Ca,Mn)_4Be_3Si_6O_{17}(OH)_4(H_2O)_3$	8.724(6)	23.14(1)	4.923(4)	–	*C****	(3)
Wawayandaite	$Ca_{12}Mn_4B_2Be_{18}Si_{12}O_{46}(OH,Cl)_3$	15.59(2)	4.87(1)	18.69(4)	101.8(2)	*P*2/*c*	(4)

(1) Lindberg (1964); (2) Grice and Robinson (1984); (3) Larsen et al. (1992); (4) Dunn et al. (1990)

REFERENCES

Arguello CA, Rousseau DL, Porto SPS (1969) First-order Raman effect in wurtzite-type crystals. Phys Rev 181:1351-1363

Armbruster T (1986) Role of Na in the structure of low-cordierite: A single-crystal X-ray study. Am Mineral 71:746-757

Armbruster T (2002) Revised nomenclature of högbomite, nigerite and taaffeite minerals. Eur J Mineral (submitted)

Armbruster T, Irouschek A (1983) Cordierites from the Lepontine Alps: Na + Be → Al substitution, gas content, cell parameters, and optics. Contrib Mineral Petrol 82:389-396

Armbruster T, Libowitsky E, Diamond L, Auernhammer M, Bauerhansl P, Hoffmann C, Irran E, Kurka A, Rosenstingl H (1995) Crystal chemistry and optics of bazzite from Furkabasistunnel (Switzerland). Mineral Petrol 52:113-126

Artioli G, Rinaldi R, Wilson CC, Zanazzi PF (1995) Single-crystal pulsed neutron diffraction of a highly hydrous beryl. Acta Crystallogr B51:733-737

Aurisicchio C, Fioravanti G, Grubessi O, Zanazzi PF (1988) Reappraisal of the crystal chemistry of beryl. Am Mineral 73:826-837

Bakakin VV, Rylov GM, Belov NV (1969) Crystal structure of a lithium-bearing beryl. Dokl Acad Nauk SSSR 188:659-662 (in Russian)

Bakakin VV, Rylov GM, Alekseev VI (1974) Refinement of the crystal structure of hurlbutite $CaBe_2P_2O_8$. Kristallografiya 19:1283-1285 (in Russian)

Barbier J, Grew ES, Moore PB, Shu S-C (1999) Khmaralite, a new beryllium-bearing mineral related to sapphirine: A superstructure resulting from partial ordering of Be, Al, and Si on tetrahedral sites. Am Mineral 84:1650-1660

Barbier J, Grew ES, Yates MG (2001) Beryllium minerals related to aenigmatite. Geol Assoc Canada, Mineral Assoc Canada, Joint Ann Meet, Abstr 26:7

Baur WH (1977) Computer simulation of crystal structures. Phys Chem Minerals 2:3-20

Belov NV (1958) Essays on structural mineralogy IX. Mineral Sbornik Geol Soc Lvov 12:15-42 (in Russian)

Bentle GG (1966) Elastic constants of single-crystal BeO at room temperature. J Am Ceram Soc 49: 125-128

Beus AA (1960) Geochemistry of Beryllium and Genetic Types of Beryllium Deposits. Publ House Acad Sci, Moscow

Birch WD, Pring A, Foord EE (1995) Selwynite, $NaK(Be,Al)Zr_2(PO_4)_4 \cdot 2H_2O$, a new gainesite-like mineral from Wycheproof, Victoria, Australia. Can Mineral 33:55-58

Bowen NL (1928) The Evolution of Igneous Rocks. Princeton University Press, Princeton, New Jersey

Boyer LL, Mehl MJ, Feldman JL, Hardy JR, Flocken JW, Fong CY (1985) Beyond the rigid ion approximation with spherically symmetric ions. Phys Rev Lett 54:1940-1943

Bragg WL (1930) The structure of silicates. Z Kristallogr 74:237-305

Brown GE Jr, Mills BA (1986) High-temperature structure and crystal chemistry of hydrous alkali-rich beryl from the Harding pegmatite, Taos County, New Mexico. Am Mineral 71:547-556

Brown ID (1981) The bond-valence method: An empirical approach to chemical structure and bonding. *In* O'Keeffe M, Navrotsky A (eds) Structure and Bonding in Crystals. Academic Press, New York, 2:1-30

Brown ID, Shannon RD (1973) Empirical bond strength-bond length curves for oxides. Acta Crystallogr A29:266-282

Burdett JK, Hawthorne FC (1993) An orbital approach to the theory of bond valence. Am Mineral 78: 884-892

Burke EAJ, Lustenhouwer WJ (1981) Pehrmanite, a new beryllium mineral from Rosendal pegmatite, Kemiö Island, southwestern Finland. Can Mineral 19:311-314

Burns PC, Novak M, Hawthorne FC (1995) Fluorine-hydroxyl variation in hambergite: A crystal structure study. Can Mineral 22:1205-1213

Cannillo E, Coda A, Fagnani G (1966) The crystal structure of bavenite. Acta Crystallogr 20:301-309

Cannillo E, Giuseppetti G, Tazzoli V (1967) The crystal structure of leucophanite. Acta Crystallogr 23: 255-259

Cannillo E, Dal Negro A, Rossi G (1969) On the crystal structure of barylite. Rend Soc Ital Mineral Petrol 26:2-12

Cannillo E, Mazzi F, Fang JH, Robinson PD, Ohya Y (1971) The crystal structure of aenigmatite. Am Mineral 56:427-446

Cannillo E, Giuseppetti G, Mazzi F, Tazzoli V (1992) The crystal structure of a rare earth bearing leucophanite: $(Ca,RE)CaNa_2Be_2Si_4O_{12}(F,O)_2$. Z Kristallogr 202:71-79

Cerny P, Povondra P (1966) Beryllian cordierite from Vezná: (Na,K) + Be → Al. N Jahrb Mineral Monatsh 1966:36-44

Chang HC (1966) Structural analysis of liberite. Acta Geol Sinica 46:76-86
Christy AG (1988) A new 2*c* superstructure in beryllian sapphirine from Casey Bay, Enderby Land, Antarctica. Am Mineral 73:1134-1137
Christy AG, Putnis A (1988) Planar and line defects in the sapphirine polytypes. Phys Chem Minerals 15:548-558
Christy AG, Grew ES, Mayo SC, Yates MG, Belakovskiy DI (1998) Hyalotekite, $(Ba,Pb,K)_4(Ca,Y)_2Si_8(B,Be)_2(Si,B)_2O_{28}F$, a tectosilicate related to scapolite: New structure refinement, phase transitions and a short-range ordered 3*b* superstructure. Mineral Mag 62:77-92
Cline CF, Dunegan HL, Henderson GW (1967) Elastic constants of hexagonal BeO, ZnS and CdSc. J Appl Phys 38:1944-1948
Coda A, Rossi G, Ungaretti L, Carobbi SG (1967) The crystal structure of aminoffite. Accademia Nazionale dei Lincei, Rend Classe Sci Fis, Mat Nat 43:225-232
Coda A, Ungaretti L, Guista AD (1974) The crystal structure of leifite, $Na_6Si_{16}Al_2(BeOH)_2O_{39}(H_2O)_{1.5}$. Acta Crystallogr B30:396-401
Cohen AJ, Gordon RG (1976) Modified electron-gas study of the stability, elastic properties and high-pressure and high-pressure behavior of MgO and CaO crystals. Phys Rev B14:4593-4605
Cohen JP, Ross FK, Gibbs GV (1977) An X-ray and neutron diffraction study of hydrous low cordierite. Am Mineral 62:67-78
Cohen RE, Boyer LL, Mehl MJ (1987) Theoretical studies of charge relaxation effects on the statics and dynamics of oxides. Phys Chem Minerals 14:294-302.
Corbin DR, Abrams L, Jones GA, Harlow RL, Dunn PJ (1991) Flexibility of the zeolite RHO framework: Effect of dehydration on the crystal structure of the beryllophosphate mineral, pahasapaite. Zeolites 11:364-367
Dal Negro A, Rossi G, Ungaretti L (1967) The crystal structure of meliphanite. Acta Crystallogr 23:260-264
Della Ventura G, Rossi P, Parodi GC, Mottana A, Raudsepp M, Prencipe M (2000) Stoppaniite, $(Fe,Al,Mg)_4(Be_6Si_{12}O_{36})\cdot(H_2O)_2(Na,\square)$, a new mineral of the beryl group from Latium (Italy). Eur J Mineral 12:121-127
Demartin F, Pilati T, Diella V, Gentile P, Gramaccioli CM (1993) A crystal-chemical investigation of alpine gadolinite. Can Mineral 30:127-136
Dempsey MJ, Strens RGJ (1976) Modelling crystal structures. *In* Strens RGJ (ed) Physics and Chemistry of Rocks and Minerals. Wiley, New York.
Downs JW, Gibbs GV (1981) The role of the BeOSi bond in the structures of beryllosilicate minerals. Am Mineral 66:819-826
Downs JW, Gibbs GV (1987) An exploratory examination of the electron density and electrostatic potential of phenakite. Am Mineral 72:769-777
Dunn PJ, Peacor DR, Grice JD, Wicks FJ, Chi PH (1990) Wawayandaite, a new calcium manganese beryllium boron silicate from Franklin, New Jersey. Am Mineral 75:405-408
Durovic S (1997) Fundamentals of the OD theory. Eur Mineral Union Notes in Mineralogy 1:3-28
Evans HT Jr, Mrose ME (1966) Crystal chemical studies of cesium beryl. Abstracts for 1966, Geol Soc Am Spec Paper 101:63
Fanfani L, Nunzi A, Zanazzi PF, Zanzari AR (1975) The crystal structure of roscherite. Tschermaks mineral petrol Mitt 22:266-277
Fanfani L, Zanazzi PF, Zanzari AR (1977) The crystal structure of a triclinic roscherite. Tschermaks mineral petrogr Mitt 24:169-178
Fang JH, Robinson PD, Ohya Y (1972) Redetermination of the crystal structure of eudidymite and its dimorphic relationship to epididymite. Am Mineral 57:1345-1354
Ferraris G, Principe M, Rossi P (1998) Stoppaniite, a new member of the beryl group: Crystal structure and crystal-chemical implications. Eur J Mineral 10:491-496
Foord EE, Gaines RV, Crock JG, Simmons WB Jr, Barbosa CP (1986) Minasgeraisite, a new member of the gadolinite group from Minas Gerais, Brazil. Am Mineral 71:603-607
Foord EE, Brownfield ME, Lichte FE, Davis AM, Sutley SJ (1994) McCrillsite, $NaCs(Be,Li)Zr_2[PO_4]_4\cdot 1\text{-}2\ H_2O$, a new mineral species from Mount Mica, Oxford County, Maine, and new data for gainesite. Can Mineral 32:839-842
Ganguli D (1979) Variabilities in interatomic distances and angles involving BeO_4 tetrahedra. Acta Crystallogr B35:1013-1015
Garber JA, Granato AV (1975a) Theory of the temperature dependence of second-order elastic constants in cubic materials. Phys Rev B 11:3990-3997
Garber JA, Granato AV (1975b) Fourth-order elastic constants and the temperature dependence of second-order elastic constants in cubic materials. Phys Rev B 11:3998-4007

Geisinger KL, Gibbs GV, Navrotsky A (1985) A molecular orbital study of bond length and angle variations in framework silicates. Phys Chem Minerals 11:266-283

Gibbs GV (1966) The polymorphism of cordierite: I. The crystal structure of low cordierite. Am Mineral 51:1068-1087

Gibbs GV (1982) Molecules as models for bonding in solids. Am Mineral 67:421-450

Gibbs GV, Breck DW, Meagher EP (1968) Structural refinement of hydrous and anhydrous synthetic beryl, $Al_2(Be_3Si_6)O_{18}$ and emerald $Al_{1.9}Cr_{0.1}(Be_3Si_6)O_{18}$. Lithos 1:275-285

Giuseppetti G, Tadini C (1973) Refinement of the crystal structure of beryllonite, $NaBePO_4$. Tschermaks mineral petrogr Mitt 20:1-12

Giuseppetti G, Mazzi F, Tadini C, Larsen AO, Asheim A, Raade G (1990) Berborite polytypes. N Jahrb Mineral Abh 162:101-116

Giuseppetti G, Mazzi F, Tadini C, Galli E (1991) The revised crystal structure of roggianite: $Ca_2[Be(OH)_2Al_2Si_4O_{13}]\cdot 2.5H_2O$. N Jahrb Mineral Monatsh 1991:307-314

Giuseppetti G, Tadini C, Mattioli V (1992) Bertrandite, $Be_4Si_2O_7(OH)_2$, from Val Vigezzo (NO) Italy: The X-ray structural refinement. N Jahrb Mineral Monatsh 1992:13-19

Gordon RG, Kim YS (1972) Theory for the forces between closed-shell atoms and molecules. J Chem Phys 56:3122-3133

Grauch RI, Lindahl I, Evans HT Jr, Burt DM, Fitzpatrick JJ, Foord EE, Graff P-R, Hysingjord J (1994) Høgtuvaite, a new beryllian member of the aenigmatite group from Norway, with new X-ray data on aenigmatite. Can Mineral 32:439-448

Grew ES (1981) Surinamite, taaffeite, and beryllian sapphirine from pegmatites in granulite-facies rocks of Casey Bay, Enderby Land, Antarctica. Am Mineral 66:1022-1033

Grew ES, Yates MG, Barbier J, Shearer CK, Sheraton JW, Shirashi K, Motoyoshi Y (2000) Granulite-facies beryllium pegmatites in the Napier complex in Khmara and Amundsen Bays, Western Enderby Land, East Antarctica. Polar Geosci 13:1-40

Grew ES, Hålenius U, Kritikos M, Shearer CK (2001) New data on welshite, e.g., $Ca_2Mg_{3.8}Mn^{2+}_{0.6}Fe^{2+}_{0.1}Sb^{5+}_{1.5}O_2[Si_{2.8}Be_{1.75}Fe^{3+}_{0.65}Al_{0.7}As_{0.17}O_{18}]$, an aenigmatite-group mineral. Mineral Mag 65:665-674

Grice JD, Hawthorne FC (1989) Refinement of the crystal structure of leucophanite. Can Mineral 27: 193-197

Grice JD, Robinson GW (1984) Jeffreyite, $(Ca,Na)_2(Be,Al)Si_2(O,OH)_7$, a new mineral species and its relation to the melilite group. Can Mineral 22:443-446

Griffen DT, Ribbe PH (1979) Distortions in the tetrahedral oxyanions of crystalline substances. N Jahrb Mineral Abh 137:54-73

Gupta A, Swanson DK, Tossell JA, Gibbs GV (1981) Calculation of bond distances, one-electron energies and electron density distributions in first-row tetrahedral hydroxy and oxyanions. Am Mineral 66: 601-609

Hansen S, Faelth L, Johnson O (1984) Bergslagite, a mineral with tetrahedral berylloarsenate sheet anions. Z Kristallogr 166:73-80

Harris LA, Yakel HL (1966) The crystal structure of calcium beryllate $Ca_{12}Be_{17}O_{29}$. Acta Crystallogr 20:296-301

Harris LA, Yakel HL (1967) The crystal structure of Y_2BeO_4. Acta Crystallogr 22:354-360

Harris LA, Yakel HL (1969) The crystal structure of $SrBe_3O_4$. Acta Crystallogr B25:1647-1651

Harrison WTA, Nenoff TM, Gier TE, Stucky GD (1993) Tetrahedral-atom 3-ring groupings in 1-dimensional inorganic chains: $Be_2AsO_4OH\cdot 4H_2O$ and $Na_2ZnPO_4OH\cdot 7H_2O$. Inorg Chem 32: 2437-2441

Hassan I, Grundy HD (1985) The crystal structure of helvite group minerals, $(Mn,Fe,Zn)_8(Be_6Si_6O_{24})S_2$. Am Mineral 70:186-192

Hassan I, Grundy HD (1991) The crystal structure and thermal expansion of tugtupite, $Na_8(Al_2Be_2Si_8O_{24})Cl_2$. Can Mineral 29:385-390

Hawthorne FC (1983a) Enumeration of polyhedral clusters. Acta Crystallogr A39:724-736

Hawthorne FC (1983b) The crystal chemistry of the amphiboles. Can Mineral 21:173-480

Hawthorne FC (1984) The crystal structure of stenonite and the classification of the aluminofluoride minerals. Can Mineral 22:245-251

Hawthorne FC (1985) Towards a structural classification of minerals: The $^{vi}M^{iv}T_2O_n$ minerals. Am Mineral 70:455-473

Hawthorne FC (1994) Structural aspects of oxide and oxysalt crystals. Acta Crystallogr B50:481-510

Hawthorne FC (1997) Short-range order in amphiboles: A bond-valence approach. Can Mineral 35: 201-216

Hawthorne FC, Cerny P (1977) The alkali-metal positions in Cs-Li beryl. Can Mineral 15:414-421

Hawthorne FC, Grice JD (1987) The crystal structure of ehrleite, a tetrahedral sheet structure. Can Mineral 25:767-774

Hawthorne FC, Groat LA, Raudsepp M, Ercit TS (1987) Kieserite, a titanite-group mineral. N Jahrb Mineral Abh 157:121-132

Hawthorne FC, Kimata M, Cerny P, Ball N, Rossman GR, Grice JD (1991) The crystal chemistry of the milarite-group minerals. Am Mineral 76:1836-1856

Hawthorne FC, Burns PC, Grice JD (1996) The crystal chemistry of boron. Rev Mineral 33:41-115.

Hazen RM, Finger LW (1986) High-pressure and high-temperature crystal chemistry of beryllium oxide. J Appl Phys 59:3728-3733

Hazen RM, Au AY, Finger LW (1986) High-pressure crystal chemistry of beryl ($Be_3Al_2Si_6O_{18}$) and euclase ($BeAlSiO_4OH$). Am Mineral 71:977-984

Hesse K-F, Stuempel G (1986) Crystal structure of harstigite, $MnCa_6Be_4(SiO_4)_2(Si_2O_7)_2(OH)_2$. Z Kristallogr 177:143-148

Hölscher A, Schreyer W (1989) A new synthetic hexagonal BeMg-cordierite, $Mg_2[Al_2BeSi_6O_{18}]$, and its relationship to Mg-cordierite. Eur J Mineral 1:21-37

Huminicki DMC, Hawthorne FC (2000) Refinement of the crystal structure of väyrynenite. Can Mineral 38:1425-1432

Huminicki DMC, Hawthorne FC (2001a) Refinement of the crystal structure of swedenborgite. Can Mineral 39:153-158

Huminicki DMC, Hawthorne FC (2001b) The crystal structure of aminoffite. Can Mineral (accepted)

Jephcoat AP, Hemley RJ, Hazen RM (1986) Bromellite: Raman spectroscopy to 40 Gpa. (abstr) EOS Trans Am Geophys Union 67:361

Kampf AR (1992) Beryllophosphate chains in the structures of fransoletite, parafransoletite, and ehrleite and some general comments on beryllophosphate linkages. Am Mineral 77:848-856

Kharitonov YuA, Kuz'min EA, Ilyukhin VV, Belov NV (1971) The crystal structure of bavenite. Zh Struktur Khimii 12:87-93 (in Russian)

Kimata M, Ohashi H (1982) The crystal structure of synthetic gugiaite, $Ca_2BeSi_2O_7$. N Jahrb Mineral Abh 143:210-222

Klaska KH, Jarchow O (1977) Die Bestimmung der Kristallstruktur von Trimerit $CaMn_2(BeSiO_4)_3$ und das Trimeritgesetz der Verzwillingung. Z Kristallogr 145:46-65

Koster AS (1971) Influence of the chemical bond on the K emission spectrum of oxygen and fluorine. J Phys Chem Solids 32:2685-2692

Lager GA, Gibbs GV (1974) A refinement of the crystal structure of herderite, $CaBePO_4OH$. Am Mineral 59:919-925

Larsen AO, Åsheim A, Raade G, Taftø J (1992) Tvedalite, $(Ca,Mn)_4Be_3Si_6O_{17}(OH)_4 \cdot 3H_2O$, a new mineral from syenite pegmatite in the Oslo Region, Norway. Am Mineral 77:438-443

Leavens PB, White JS, Nelen JA (1990) Zanazziite, a new mineral from Minas Gerais, Brazil. Mineral Rec 21:413-417

Lichanot A, Rerat M (1993) Elastic properties in BeO. An ab initio Hartree-Fock calculation. Chem Phys Lett 211:249-254

Lichanot A, Chaillet M, Larrieu C, Dovesi R, Pisani C (1992) Ab initio Hartree-Fock study of solid beryllium oxide: Structure and electronic properties. Chem Phys 164:383-394

Liebau F (1985) Structural Chemistry of Silicates. Springer-Verlag, Berlin

Liefeld RJ, Hanzely S, Kirby TB, Mott D (1970) X-ray spectrometric properties of potassium acid pthalate crystals. Adv X-ray Anal 13:373-381

Lin J-C, Guggenheim S (1983) The crystal structure of a Li,Be-rich brittle mica: A dioctahedral-trioctahedral intermediate. Am Mineral 68:130-142

Lindberg ML (1958) The beryllium content of roscherite from the Sapucaia pegmatite mine, Minas Gerais, Brazil, and from other localities. Am Mineral 43:824-838

Lindberg ML (1964) Crystallography of faheyite, Sapucaia pegmatite mine, Minas Gerais, Brazil. Am Mineral 49:395-398

Mazzi F, Galli E (1978) Is each analcime different? Am Mineral 63:448-460

Mazzi F, Ungaretti L, Dal Negro A, Petersen OV, Rönsbo JG (1979) The crystal structure of semenovite. Am Mineral 64:202-210

Mereiter K, Niedermayr G, Walter F (1994) Uralolite, $Ca_2Be_4(PO_4)_3(OH) \cdot 3.5(H_2O)$: New data and crystal structure. Eur J Mineral 6:887-896

Merlino S (1990) Lovdarite, $K_4Na_{12}(Be_8Si_{28}O_{72}) \cdot 18(H_2O)$, a zeolite-like mineral: Structural features and OD character. Eur J Mineral 2:809-817

Merlino S, Pasero M (1992) Crystal chemistry of beryllophosphates: The crystal structure of moraesite, $Be_2(PO_4)(OH) \cdot 4H_2O$. Z Kristallogr 201:253-262

Metcalf Johansen J, Gronbaek Hazell R (1976) Crystal structure of sorensenite, $Na_4SnBe_2(Si_3O_9)_2(H_2O)_2$. Acta Crystallogr B32:2553-2556

Moore PB (1965) A structural classification of Fe-Mn-orthophosphate hydrates. Am Mineral 50: 2052-2062

Moore PB (1969) The crystal structure of sapphirine. Am Mineral 54:31-49

Moore PB (1973) Pegmatite phosphates. Descriptive mineralogy and crystal chemistry. Mineral Rec 4: 103-130

Moore, PB (1978) Welshite, $Ca_2Mg_4Fe^{3+}Sb^{5+}O_2[Si_4Be_2O_{18}]$, a new member of the aenigmatite group. Mineral Mag 42:129-132

Moore PB, Araki T (1983) Surinamite, ca. $Mg_3Al_4Si_3BeO_{16}$: Its crystal structure and relation to sapphirine, ca. $Mg_{2.8}Al_{7.2}Si_{1.2}O_{16}$. Am Mineral 68:8804-8810

Moore PB, Araki T, Ghose S (1982) Hyalotekite, a complex lead borosilicate: Its crystal structure and the lone-pair effect of $Pb_{(II)}$. Am Mineral 67:1012-1020

Moore PB, Araki T, Steele IM, Swihart GH (1983) Gainesite, sodium zirconium beryllophosphate: A new mineral and its crystal structure. Am Mineral 68:1022-1028

Moore PB, Davis AM, Van Derveer DG, Sen Gupta PK (1993) Joesmithite, a plumbous amphibole revisited and comments on bond valences. Mineral Petrol 48:97-113

Mrose ME, Appleman DE (1962) The crystal structures and crystal chemistry of väyrynenite, $(Mn,Fe)Be(PO_4)(OH)$, and euclase, $AlBe(SiO_4)(OH)$. Z Kristallogr 117:16-36

Nadezhina TN, Pushcharovskii DY, Rastsvetaeva RK, Voloshin AV, Burshtein IF (1989) Crystal structure of a new natural form of $Be(OH)_2$. Dokl Akad Nauk SSSR 305:95-98 (in Russian)

Nuber B, Schmetzer K (1983) Crystal structures of ternary Be-Mg-Al oxides: Taaffeite, $BeMg_3Al_8O_{16}$, and musgravite, $BeMg_2Al_6O_{12}$. N Jahrb Mineral Monatsh 1983:393-402

Oberti R, Ottolini L, Camara F, Della Ventura G (1999) Crystal structure of non-metamict Th-rich hellandite-(Ce) from Latium (Italy) and crystal chemistry of the hellandite-group minerals. Am Mineral 84:913-921

Oberti, R, Della Ventura G, Ottolini L, Bonazzi P, Hawthorne FC (2002) Re-definition of hellandite based on recent single-crystal structure refinements, electron- and ion-microprobe analyses, and FTIR spectroscopy: A new unit-formula and nomenclature. Am Mineral (in press)

O'Keeffe M (1981) Some aspects of the ionic model of crystals. *In* O'Keeffe M, Navrotsky A (eds) Structure and Bonding in Crystals. Academic Press, New York, 1:299-322

Pauling LS (1929) The principles determining the structure of complex ionic crystals. J Am Chem Soc 51:1010-1026

Pauling L, Klug HP, Winchell AN (1935) The crystal structure of swedenborgite, $NaBe_4SbO_7$. Am Mineral 20:492-501

Peacor DR, Rouse RC, Ahn J-H (1987) Crystal structure of tiptopite, a framework beryllophosphate isotypic with basic cancrinite. Am Mineral 72:816-820

Petersen OV, Ronsbo JG, Leonardsen ES (1994) Hingganite-(Y) from Zomba-Malosa complex, Malawi. N Jahrb Mineral Monatsh 1994:185-192

Pilati T, Demartin F, Cariati F, Bruni S, Gramaccioli CM (1993) Atomic thermal parameters and thermodynamic functions for chrysoberyl ($BeAl_2O_4$) from vibrational spectra and transfer of empirical force fields. Acta Crystallogr B49:216-222

Povondra P, Langer K (1971) Synthesis and some properties of sodium-beryllium bearing cordierite, $Na_xMg_2(Al_{4-x}Be_xSi_5O_{18})$. N Jahrb Mineral Abh 116:1-19

Pring A, Din VK, Jefferson DA, Thomas JM (1986) The crystal chemistry of rhodizite: A re-examination. Mineral Mag 50:163-172

Rastsvetaeva RK, Rekhlova O Yu, Andrianov VI, Malinovskii Yu A (1991) Crystal structure of hsianghualite. Dokl Akad Nauk SSSR 316:624-628 (in Russian)

Rastsvetaeva RK, Evsyunin VG, Kashaev AA (1995) Crystal structure of a new natural K,Na,Ca-titanoberyllosilicate. Kristallografiya 40:253-257 (in Russian)

Rastsvetaeva RK, Pushcharovskii D Yu, Pekov IV, Voloshin AV (1996) Crystal structure of calcybeborosilite and its place in the datolite-gadolinite isomorphous series. Kristallografiya 41:235-239 (in Russian)

Robinson PD, Fang JH (1970) The crystal structure of epididymite. Am Mineral 55:1541-1549

Robinson PD, Fang JH (1977) Barylite, $BaBe_2Si_2O_7$: Its space group and crystal structure. Am Mineral 62: 167-169

Rouse RC, Peacor DR, Metz GW (1989) Sverigeite, a structure containing planar NaO_4 groups and chains of 3- and 4-membered beryllosilicate rings. Am Mineral 74:1343-1350

Rouse RC, Peacor DR, Dunn PJ, Su S-C, Chi PH, Yeates H (1994) Samfowlerite, a new CaMnZn beryllosilicate mineral from Franklin, New Jersey: Its characterization and crystal structure. Can Mineral 32:43-53

Sacerdoti M, Parodi GC, Mottana A, Maras A, Della Ventura G (1993) Asbecasite: Crystal structure refinement and crystal chemistry. Mineral Mag 57:315-322

Schlenker JL, Griffen DT, Phillips MW, Gibbs GV (1978) A population analysis for Be and B oxyanions. Contrib Mineral Petrol 65:347-350

Schreyer W, Gordillo CR, Werding G (1979) A new sodian-beryllian cordierite from Soto, Argentina, and the relationship between distortion index, Be content, and state of hydration. Contrib Mineral Petrol 70:421-428

Segalstad TV, Larsen AO (1978) Gadolinite-(Ce) from Skien, southwestern Oslo region, Norway. Am Mineral 63:188-195

Seitz A, Roesler U, Schubert K (1950) Kristallstruktur von $Be(OH)_2$-beta. Z Anorg Allgem Chem 261: 94-105

Shannon RD (1976) Revised effective ionic radii and systematic studies of interatomic distances in halides and chalcogenides. Acta Crystallogr A32:751-767

Sherriff BL, Grundy HD, Hartman JS, Hawthorne FC, Cerny P (1991) The incorporation of alkalis in beryl: Multi-nuclear MAS NMR and crystal-structure study. Can Mineral 29:271-285

Simmons WB, Pezzotta F, Falster AU, Webber KL (2001) Londonite, a new mineral: The Cs-dominant analogue of rhodizite from the Antandrokomby granitic pegmatite, Madagascar. Can Mineral (accepted)

Simonov MA, Egorov-Tismenko YK, Belov NV (1975) Refined crystal structure of chkalovite $Na_2Be(Si_2O_6)$. Dokl Akad Nauk SSSR 225:1319-1322 (in Russian)

Simonov MA, Egorov-Tismenko YK, Belov NV (1980) Use of modern X-ray equipment to solve fine problems of structural mineralogy by the example of the crystal RE of structure of babefphite $BaBe(PO_4)F$. Kristallografiya 25:55-59 (in Russian)

Sirota NN, Kuz'mina AM, Orlova NS (1992) Debye-Waller factors and elastic constants for beryllium oxide at temperatures between 10 and 720 K. I. Anisotropy of ionic mean-square displacements. Crystallogr Res Techn 27:703-709

Slavík F (1914) Neue Phosphate vom Greifenstein bei Ehrenfriedersdorf. Ak Ceská, Bull – Bull intern ac sc Bohême 19:108-123

Sokolova EV, Ferraris G, Ivaldi G, Pautov LA, Khvorov PV (2000) Crystal structure of kapitsaite-(Y), a new borosilicate isotypic with hyalotekite—Crystal chemistry of the related isomorphous series. N Jahrb Mineral Monatsh 2000:74-84

Stahl R, Jung C, Lutz HD, Kockelmann W, Jacobs H (1998) Kristallstrukturen und Wasserstoffbrücken bindungen bei β-$Be(OH)_2$ und ε-$Zn(OH)_2$. Z anorg allg Chem 624:1130-1136

Taxer KJ, Buerger MJ (1967) The crystal structure of rhodizite. Z Kristallogr 125:423-436

Tazzoli V, Domeneghetti MC, Mazzi F, Cannillo E (1995) The crystal structure of chiavennite. Eur J Mineral 7:1339-1344

Tossell JA (1980) Calculation of bond distances and heats of formation for BeO, MgO, SiO_2, TiO_2, FeO and ZnO using the ionic model. Am Mineral 65:163-173

Tossell JA, Gibbs GV (1978) The use of molecular-orbital calculations on model systems for the prediction of bridging-bond-angle variations in siloxanes, silicates, silicon nitrides and silicon sulfides. Acta Crystallogr A34:463-472

Tossell JA, Vaughan DJ (1992) Theoretical Geochemistry. Oxford University Press, New York

Tsirel'son VG, Sokolova YV, Urusov VS (1986) An X-ray diffraction study of the electron-density distribution and electrostatic potential in phenakite Be_2SiO_4. Geokhimiya 8:1170-1180 (in Russian)

Vaughan DJ, Tossell JA (1973) Molecular orbital calculations on beryllium and boron oxyanions: Interpretation of X-ray emission, ESCA, and NQR spectra and of the geochemistry of beryllium and boron. Am Mineral 58:765-770

Walter F (1992) Weinebenite, $CaBe_3(PO_4)_2(OH)_2 \cdot 4H_2O$, a new mineral species: Mineral data and crystal structure. Eur J Mineral 4:1275-1283

Watson RE (1958) Analytic Hartree-Fock solutions for $O^=$. Phys Rev 111:1108-1110

Ximen L, Peng Z (1985) Crystal structure of hingganite. Acta Mineral Sinica 5:289-293 (in Chinese) [Am Mineral 73:441-442]

Yakubovich OV, Matvienko EN, Voloshin AV, Simonov MA (1983) The crystal structure of hingganite-(Yb), $(Y_{0.51}Ln_{0.36}Ca_{0.13})Fe_{0.065}Be(SiO_4)(OH)$. Kristallografiya 28:457-460 (in Russian)

Yakubovich OV, Malinovskii Yu A, Polyakov VO (1990) Crystal structure of makarochkinite. Kristallografiya 35:1388-1394 (in Russian)

Zoltai T (1960) Classification of silicates and other minerals with tetrahedral structures. Am Mineral 45: 960-973